



HAL
open science

Coagulation d'un latex de caoutchouc naturel - noir de carbone / silice : suivi de l'évolution nanostructurale d'une suspension colloïdale à un composite d'élastomère

Gianluca Cattinari

► To cite this version:

Gianluca Cattinari. Coagulation d'un latex de caoutchouc naturel - noir de carbone / silice : suivi de l'évolution nanostructurale d'une suspension colloïdale à un composite d'élastomère. Material chemistry. Université Paris-Saclay, 2020. English. NNT : 2020UPASF009 . tel-03104598v2

HAL Id: tel-03104598

<https://theses.hal.science/tel-03104598v2>

Submitted on 12 Jun 2021

HAL is a multi-disciplinary open access archive for the deposit and dissemination of scientific research documents, whether they are published or not. The documents may come from teaching and research institutions in France or abroad, or from public or private research centers.

L'archive ouverte pluridisciplinaire **HAL**, est destinée au dépôt et à la diffusion de documents scientifiques de niveau recherche, publiés ou non, émanant des établissements d'enseignement et de recherche français ou étrangers, des laboratoires publics ou privés.

Natural rubber latex-carbon black/silica
coagulation: following the
nanostructure evolution from a
colloidal suspension to an elastomeric
composite

Thèse de doctorat de l'université Paris-Saclay

École doctorale n° 571, Sciences chimiques : Molécules, Matériaux, Instrumentation et
Biosystèmes (2MIB)
Spécialité de doctorat : Chimie
Unité de recherche : Université Paris-Saclay, CNRS, Institut des Sciences Moléculaires
d'Orsay, 91405, Orsay, France.
Référent : Faculté des sciences d'Orsay

**Thèse présentée et soutenue à Orsay, le 25/09/2020, par
Gianluca CATTINARI**

Composition du Jury

Bertrand POUMELLEC Directeur de recherche (HDR), CNRS, Université Paris-Saclay	Président
Karim BENZERARA Directeur de recherche (HDR), CNRS, Sorbonne Université	Rapporteur & Examineur
Julian OBERDISSE Directeur de recherche (HDR), CNRS, Laboratoire Charles Coulomb	Rapporteur & Examineur
Michel CLOITRE Directeur de recherche (HDR), CNRS, ESPCI	Examineur
Catherine GAUTHIER Professeur, INSA de Lyon, Michelin R&D	Examinatrice
Marie-Pierre FONTAINE-AUPART Directeur de recherche, CNRS, U. Paris-Saclay	Directrice de thèse
Karine STENKEESTE Maitre de conférences, U. Paris-Saclay	Co-Encadrante
Marc COUTY Michelin R&D	Co-Encadrant
Matthieu GALLOPIN Michelin R&D	Co-Encadrant

Acknowledgments

First of all, it is a real pleasure to thank all the people directly involved in this project.

I will start by expressing my deepest gratitude to Dr. Fontaine-Aupart, my PhD supervisor, for always being there and for always trying to understand. Discussion has been constant from the beginning till the end and I have really appreciated it.

I would also like to thank the Michelin coordinators of the project: Dr. Mattheiu Gallopin for his positive attitude during discussions and for his creativity which pushed me to perform more and more experiments, and Dr. Marc Couty for his general supervision and guidance.

I would like to thank Dr. Karine Steenkeste for returning in moments of need and for having checked very carefully every scientific documents I sent her.

My deepest gratitude goes also to Alexis Canette for his skills in electron microscopy and his sixth-sense when it comes down to create new protocols. Thank you for the time spent in front of the microscope!

Healthful thanks goes to Dr. Ludivine Houel Renault, for the support in the CPBM chemistry room and for listening to me during numerous coffee breaks.

I would also like to express my gratitude to all the collaborators which enrich my work with their significance contribution. The group of Sandrine Leveque-Fort and his students, comprising Dr. Clement Cabriel, Pierre Jouchet, and Adrien Mau for helping me through all my endless super-resolution fluorescence experiments. A thank goes also to the Abbelight team for their quick optical and informatics development that facilitated some of my experiments. Many thanks go to Dr. Ariane Deniset for her expertise in AFM-IR, for her help during data treatment and for her cooperation. Another big thanks goes to Catherine le Bris for her engineering skills and her willingness to help.

A huge thank goes to my lab-mates and friends Seray Ural and Joanna Christodoulou for their dose of fun and good vibes during endless days spent in the laboratory.

These acknowledgements would not be complete without thanking the closest people with whom I shared the struggles and joys during this experience: Dr. Luca Polacchi, Dr. Ricardo Garcia de Castro and Dr. Ivan Pacheco Bubi.

List of abbreviations

AFM	Atomic Force Microscopy
AFM-IR	Atomic Force Microscopy coupled InfraRed spectroscopy
BSE	BackScattered Electrons
CB	Carbon Black
CLSM	Confocal Laser Scanning Microscopy
DBSCAN	Density Based Spatial Clustering of Application with Noise
DONALD	Direct Optical Nanoscopy with Axial Localized Detection
DPNR	DeProteinized Natural Rubber
d-STORM	Direct Stochastic Optical Reconstruction Microscopy
EM	Electron Microscopy
E-SBR	Emulsion Styrene Butadiene Rubber
FESEM	Field Emission Scanning Electron Microscopy
FTIR	Fourier Transformed InfraRed spectroscopy
Hilo	Highly Inclines Laminated Optical sheets
IC	Internal Conversion
IR	InfraRed
ISC	InterSystem Crossing
LRPs	Large Rubber Particles
NMR	Nuclear Magnetic Resonance
NR	Natural Rubber
PAINT	Points Accumulation for Imaging in Nanoscale Topography
PALM	Photo-Activated Localization luorescence Microscopy
PM	Photonic Microscopy
PSF	Point Spread Function
REF	Rubber Elongation Factor
SE	Secondary Electrons
SEM	Scanning Electron Microscopy
Si	Silica
SIM	Structured Illumination Microscopy
SMLM	Single Molecule Localization Microscopy
SPM	Scanning Probe Microscopy
SRPs	Small Rubber Particles
SRPP	Small Rubber Particle protein
S-SBR	Solution Styrene Butadiene Rubber
SR	Synthetic Rubber

STED	Stimulated Emission Depletion
TEDPNR	TransEsterified Deproteinized Natural Rubber
TEM	Transmission Electron Microscopy
TIRF	Total Internal Reflection Fluorescence

Table of contents

General Introduction to the manuscript.....	1
Chapter 1: Introduction to natural rubber and its association with fillers.....	3
Chapter 2: Imaging methods for structural characterization of polymer composites: focus on FESEM, d-STOR and AFMIR.....	41
Chapter 3: Natural rubber – carbon black coagulation: following the nanostructure evolution from a colloidal suspension to an elastomeric composite.....	83
Chapter 4: Natural rubber-silica coagulation: structural characterization and evolution towards an elastomeric composite.....	109
Conclusions and Perspectives.....	165

General introduction to the manuscript

Natural rubber (NR) latex extracted from *Hevea brasiliensis* is known to be used for the preparation of a variety of materials, showing some advantages in comparison to its synthetic counterpart. In addition to the rubber, reinforcing fillers are considered essential for every formulation, to increase mechanical properties of a polymer matrix. Several strategies have been proposed to mix NR and fillers. Among the different methods, the liquid mixing process is central for MICHELIN innovation strategy. This method first consists of mixing an aqueous suspension of fillers (silica or carbon black) with elastomers in the form of latex to obtain a coagulum, which is subsequently dried. If the technological process parameters are under control at the engineering level, the fundamental knowledge of the hetero-aggregation mechanism as well as the structural characterization and evolution of the coagulum along drying are unknown. The context of the study as well as its novel character are better discussed and detailed throughout **chapter 1**, where a state of the art on composite material made of NR and fillers is first introduced.

The fillers used for the study are both silica (Si) and carbon black (CB). Each of them were separately mixed with NR latex to obtain a binary colloidal suspension and its resulting coagulum. For both, we investigated on (i) the formation and the structural evolution dynamic of the obtained NR-CB or NR-Si coagulum, as well as (ii) the role of external physical stress (shear and/or sonication). Additionally, in case of NR-Si system, the spatial distribution of proteins and lipids of NR at different stages of the process, and their localization in respect to Si fillers was also explored. For this purpose, a multimodal microscopy approach was developed combining Field Emission Scanning Electron Microscopy (FESEM), direct stochastic optical reconstruction microscopy (d-STORM) as super resolution fluorescent microscopy technique and Atomic Force Microscopy coupled to Infra-Red spectroscopy (AFM-IR). These techniques and their original application to our study are reviewed in **chapter 2**.

The obtained results and related discussions are presented in the form of scientific publications inserted in the manuscript. **Chapter 3** is devoted to the study concerning NR latex-CB mixing, while **chapter 4** refers to the investigation on NR latex-Si system. In both cases our work is a substantial contribution in the understanding of an elastomeric composite formation obtained via hetero-aggregation of a binary NR-filler colloidal suspension. We believe that our investigation might open up new ways to exploit and improve the liquid mixing process as discussed in **Conclusions and Perspectives** of this manuscript.

CHAPTER 1: Introduction to natural rubber and its
association with fillers

Natural rubber (NR) is a bio-based product largely used in the production of a variety of materials. In most applications, NR is coupled with fillers, to improve the mechanical response of the obtained composite or nanocomposite. This chapter aims first at giving a very brief introduction to the field of elastomer-based nanocomposite. Subsequently, we specifically focused on NR, which is the main raw material used in this study. Its mixing with particulate fillers such as carbon black (CB) and silica (Si) is also described. Lastly, the knowledge gap and main objective of our study are also reported.

1. A world of nanocomposites: focus on elastomer based composites

Historically, the development and advancement of societies have been intimately related to materials and their innovations. In fact, many technologies that make people's life more comfortable are closely related to materials.

The twenty-first century has witnessed a tremendous upsurge in the field of nanomaterials and nanotechnology. By the use of nanotechnology, we can obtain structures with new characteristics attributable to their nanometer dimensions. One of the most growing fields in this domain concerns the nanocomposite research and production¹. By definition, a *nanocomposite* is a matrix to which nano-objects have been added to improve particular properties of the material. The matrix is a continuous phase and it includes metals, inorganic non-metallic matrices and polymer matrices. The term nano-object refers to a discontinuous phase made up of particles, sheets (e.g. exfoliated clay stacks) or fibers having at least one dimension in the nanometer range. These nano-scale objects are also known by the term of *fillers*. The properties of nanocomposites have caused researchers and companies to consider using these materials in several fields, ranging from consumer's electronics to automotive industry, packaging and so on²⁻⁴.

In addition to being of technological importance, the subject of nanocomposite is a fascinating area of interdisciplinary research. As a matter of facts nanocomposites possess unique physical, chemical, optical, mechanical, magnetic and electrical properties. Thus, research in the field of nanocomposite material spreads over a wide range of scientific subjects. While industry is seeking materials to meet difficult challenges with unique properties, there is no "rule of mixture" to identify how to mix multiple nanomaterials in the matrix to achieve all the required properties.

Among the different types of nanocomposite, a particular class refers to elastomer based nanocomposite. This type of materials are a complex multicomponent systems whose properties depend on the type of elastomer (or mixtures of elastomers) as well as on the type of fillers⁵. The word "elastomer" derives from two words, elastic (describing the ability of a material to extend and return to its original shape when a load is removed) and mer (from polymer, in which poly means many and mer means part). Therefore, an elastomer is a polymer with the property of "elasticity," generally having notably low Young's modulus⁶. Elastomers are one of the most applicable materials in science

and technology, due to their the high level of flexibility, mechanical strength etc.⁷. The most common example of elastomers refers to rubber-like materials, with their ability to return to their original configuration when a certain stress is removed. In fact, the term “elastomer” is often used interchangeably with the word “rubber”. Thus, the association of rubber polymers with a discontinuous phase of fillers gives rise to an elastomeric-based composite material. Over the past two decades, with the development and introduction of fillers in polymer systems, elastomer-based composites are entering a new era of nanostructured polymeric systems. To classify an elastomer-based composite as nanostructured, at least one of its phase should be in nanosized regions. Obviously, in the case of elastomer-based composites this phase is the filler. Carbon based nano-fillers like carbon nanotubes, graphene and graphitic derivatives, inorganic fillers like nanosilica, nanometal particles and nanoclays, bio-nanofillers such as cellulose, starch and chitin etc. are a few of the fillers having nano dimension imparting reinforcement for the elastomer based systems⁷. Please note that those are just a few of the fillers used in combination with elastomers, we will further focus on the ones specifically used in this study (subsection 3.2).

In terms of use, the principal commercial elastomers are listed in Table 1, together with their related application field. Tyre manufacturing is the most significant application of elastomeric based nanocomposite materials. Other applications include the railway industry and numerous mechanical, civil, electronics sectors. Furthermore, the production of rubber goods has also great importance: various belts, pipes, hoses and so forth. The development of conductive rubbers obtained by formation of interconnected charge carried paths in the dielectric rubber matrix by loading it with conductive filler significantly widens the applicability of elastomers nanocomposites extending it to sensor based materials, transducers, electromagnetic shielding and so on⁸.

Table 1.1. *Principal commercial elastomers, related properties and applications⁷.*

Polymer type	Glass transition temperature (°C)	Melting temperature(°C)	Applications
Natural Rubber (NR)	-70	/	Tires, gloves, adhesives
(cis)-Polyisoprene	-70	35	Tires, springs, shoes, adhesives
Styrene-butadiene	-60	/	Tire treads, adhesives, belts
(cis)-Polybutadiene	-100	5	Tire treads, shoes, conveyor belts

Acrylonitrile-butadiene (nitrile rubber)	-50 to -25	/	Fuel hoses, gaskets, rollers
Isobutylene-isoprene (butyl rubber)	-70	-5	Window strips
Ethylene-propylene monomer (EPM), ethylene-propylene diene (EPDM)	-55	/	Electrical insulation
Polychloprene (neoprene)	-50	25	Hoses, belts, springs, wetsuit and aquatic sports equipment
Polysulfide (Thiokol)	-50	/	Seal, gaskets, rocket propellants
Polydimethyl siloxane (silicone)	-125	-50	Seal, gaskets, surgical implants
Polyethylene	-70	/	O-rings, seal, gaskets
Styrene-butadiene-styrene (SBS)	-60	/	Automotive parts, shoes, adhesives
Fluoroelastomer	-10	/	O-rings, seal, gaskets
Polyacrylate	-15 to -40	/	Hoses, belts, seals, coated fabric

Natural Rubber (NR) is a particular type of elastomer, and it distinguishes itself by the other polymer types which refer to Synthetic form of Rubber (SR). NR is an elastomer of natural origin derived from a milky colloidal suspension obtained from the sap of particular botanical families of some plants (Euphorbiaceae, Apocynaceae, Asclepiadaceae, Asteraceae, Moraceae, Papaveraceae and Sapotaceae⁹). Such colloidal suspension is called NR latex. On the other hand, the production of SRs is prompted by cheap and relatively constant supplies of petrochemical feedstock. Based on technological properties, both NR and SR, which have their own merits, will be used continuously by the rubber industries. Inevitably, oil and gas resources are depleting, thus biofeedstocks for synthesis of SRs or substitution of SRs by NR, or chemically modified NR with equivalent properties may be the future direction of the research and development highlighting the importance of studies on NR. This particular elastomer constitutes the polymer matrix for our study. Therefore, the following sections are devoted to an introduction to the origin and characteristics of NR.

2. Natural rubber

2.1. An overview of natural rubber

NR is one of the most important raw material of biological origin. *Hevea brasiliensis* commonly called “rubber tree” is the most economically important latex source for the NR industry. The plant was originally discovered in Amazonia, but nowadays the NR plantations are mainly concentrated all over Southeast Asia. As a matter of facts, the global production of NR amounted to 13,7 million tons in 2018, and the quantity produced in Asia is over 88%, with Thailand and Indonesia being the two first world producers (Figure 1.1).

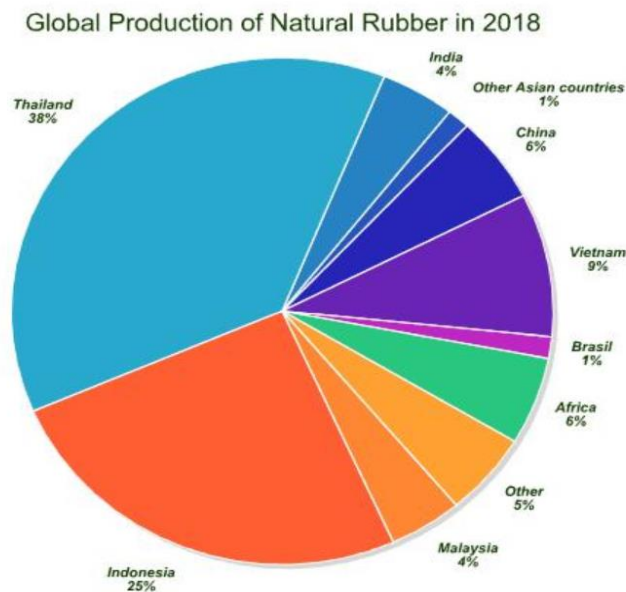


Figure 1.1. World NR production in 2018, source SIPH (Société Internationale de Plantations d'Hévéas).

After five or six years from plantation the rubber tree is normally ready to produce the NR latex. The process of extraction of NR is called tapping, and it consists of wounding the bark of the *Hevea* tree. When the bark is cut, a milky liquid exudes from the wound: this product is commonly named NR latex or field NR latex. It is known that this product accumulates in the laticifers cells, but its role in the plant is not well understood. It is likely to play a role in the defense mechanisms since it also accumulates high levels of transcripts from plant defense – or stress related genes and hydrolytic enzymes¹⁰.

In terms of composition, the out-coming field NR latex is a complex colloidal dispersion, with density varying between 0.97 and 0.98 g * cm⁻³, and it contains particles ranging from several nm to several microns dispersed in a cytoplasmic serum (C-serum). It is constituted by NR globules (also called NR particles) ranging from 100 nm to 1000 nm, luteoids with size from 2 to 5 µm, and Frey –Wysling

particles of 5-6 μm (Figure 1.2)¹¹. Rubber globules are spherical or pear-shaped core-shell particles containing cis-1,4 polyisoprene surrounded by a bio-membrane, while lutoids are complex lysosomal vacuoles. In terms of composition, NR latex mostly comprises cis-1,4 polyisoprene (~30-35 wt%) contained in the core of rubber globules, and non-polymeric substances such as proteins, lipids, sugars, minerals (~ 5 wt%), and water (~ 60%). It is difficult to summarize an exact composition of a freshly extracted latex since it depends on the season of the year for the extraction and age of the tree, but a typical composition is displayed in Table 1.2

Table 1.2. Composition of freshly tapped NR Latex¹¹. These are only approximate values and are dependent on the clone, season and physiological status of the tree.

Compound	wt%
Rubber (polyisoprene)	36,0
Proteins and nitrogen related molecules	1,7
Lipids	1,6
Ashes	0,5
Inositol and carbohydrates	1,6
Water	58,6

Once extracted, NR latex can be kept in the liquid state or transformed in solid NR. The solid state is obtained either by controlled coagulation or by natural coagulation (the latex coagulates naturally in the cup). The first one is made by addition of a weak acid such acetic acid or formic acid. On the other hand, the natural coagulation results from the action of microbial communities present in the latex. Micro-organisms in fresh latex of *H. brasiliensis* have been mainly studied from 1930 to 1975, and their activities during latex coagulation were indeed rapidly linked with evolutions of the physical properties of the latex. To avoid the natural aggregation and to allow collection and storage of NR latex in its liquid state, addition of ammonia (NH_3) is necessary in order to rise the pH of the suspension (pH~10). The addition of ammonia inhibits bacterial growth and influences the composition of the latex by hydrolyzing a part of the proteins and lipids. Such hydrolysis process increases the stability of the product¹².

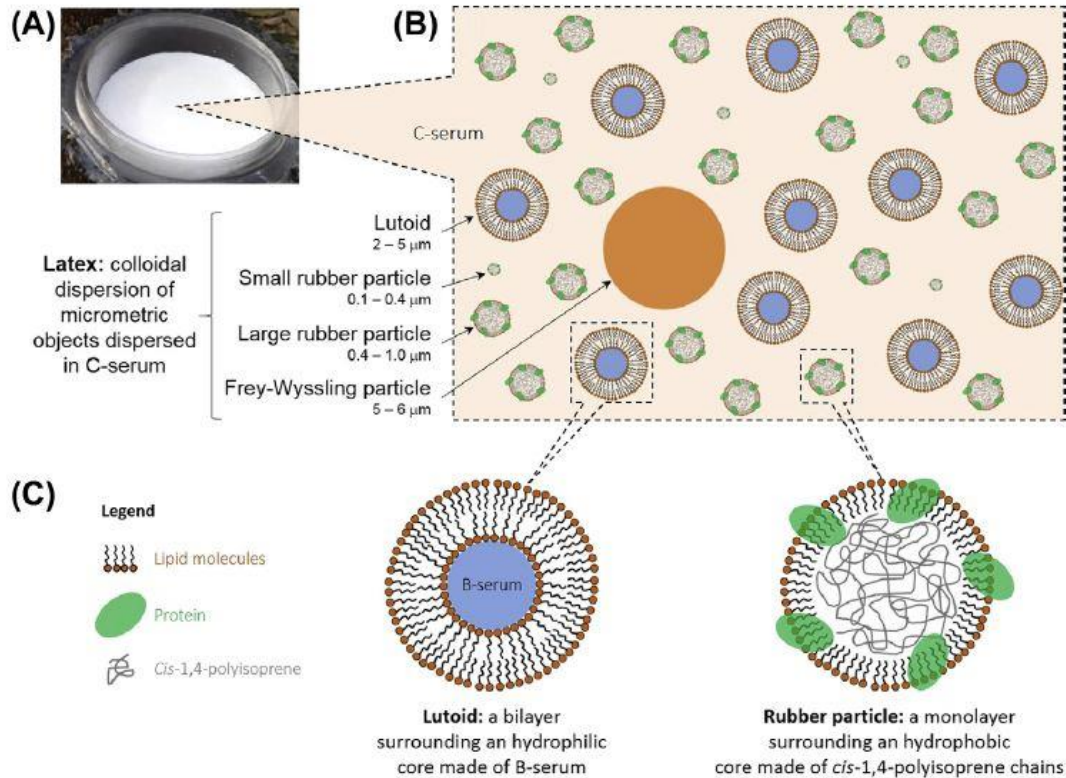


Figure 1.2. Particles contained in NR latex. (A) Picture of a cup of freshly extracted NR latex. (B) Schematic view of the latex at the mesoscale showing lutoids, rubber particles and Frey-Wyssling particles dispersed in the aqueous serum. (C) Schematic views of the major constituents of latex at the microscale: a lutoid and a rubber particle¹¹.

It is uneconomical to transport the preserved field NR latex over long distances. The normal procedure is to concentrate it to about 60% in *cis*-1,4 polyisoprene. The mainly used concentration processes are centrifugation, creaming, evaporation, and electrodecantation methods. Among these, the centrifugation is the most popular one. When field NR latex is subjected to centrifugation, it separates into four main fractions based on their densities: an upper layer which is a milky colloidal suspension constituted of only NR globules, a thin yellowish layer containing Frey-Wyssling particles, an aqueous phase called serum or C-serum and a bottom fraction composed of sediments of lutoid particles. Thus, keeping only the uppermost fraction, the NR globules are isolated from other components and the latex is concentrated: it is then commonly called high ammoniated NR latex or concentrated NR latex. A comparison of the composition of field NR latex with high ammoniated NR latex is displayed in Table 1.3.

Table 1.3. Comparison of field NR latex and high ammoniated (concentrated) latex obtained from centrifugation¹³. These are only approximate values and are dependent on the clone, season and physiological status of the tree.

Component	Field NR latex (%w/w)	High ammoniated NR latex (%w/w)
Rubber (polyisoprene)	~33-35%	60%
Water	60%	38%
Proteins, amino acids	1,5%	1%
Lipids	1,5%	1%
Other components (metals, carbohydrates, etc.)	1-2%	/

To simplify the system involved in our study, we chose to eliminate non-NR globule components from field NR latex. Thus, we mainly used high ammoniated NR latex for our experiments.

2.2. Natural rubber globules

In this subchapter we will discuss some general aspects concerning the overall microstructure and size of NR globules.

Interestingly, NR globules exhibit a bimodal size distribution, differentiating between Small Rubber Particles (SRPs) and Large Rubber Particle (LRPs)^{14,15}. SRPs have diameter ranging from 100 nm to 500 nm, while LRPs have diameters comprised between 500 nm and 1000 nm. The detailed size distribution of the NR latex used for our experiments will be presented in chapter 4.

Rubber particles are of a core-shell type. The core consists in polyisoprene chains while the shell is a complex biomembrane made of lipids and proteins. 1839 different types of proteins were identified in rubber particles, with a range in relative molecular mass of 3.9–194.2 kDa and in isoelectric point values ranging between 4.0–11.2¹⁶. Two of these proteins are present in major quantity: the Rubber Elongation Factor (REF, 14kDa) and the Small Rubber Particle Protein (SRPP, 20kDa)¹⁷. Berthelot et al.¹⁸ reported that the nature and organization of the membrane depends on the size of the rubber particle. SRPP is usually present in SRPs membrane, while REF is found mostly on LRPs. Two different models of REF and SPRP were proposed. The difference in their hydrophobic nature is believed to play a role in their interaction with lipids in the biomembrane: REF has thus shown stronger binding insertion in comparison to SRPP (Figure 1.3a). On the other hand, lipids adsorbed on the surface of the globules have been classified into: neutral lipids, glycolipids and phospholipids. The neutral lipids comprised triglycerides. The glycolipids consisted mainly of free and esterified steryl glucosides, mono-galactosyl and digalactosyl diglycerides. Additionally, the main class of phospholipids present on the surface of the NR globules are phosphatidylcholines and

phosphatidylethanolamine lecithines. As in the case of proteins, the content of lipids in LRPs and SRPs also differs. The result of Chan et al¹⁹ indicate that there are more lipids in LRPs than in SRPs.

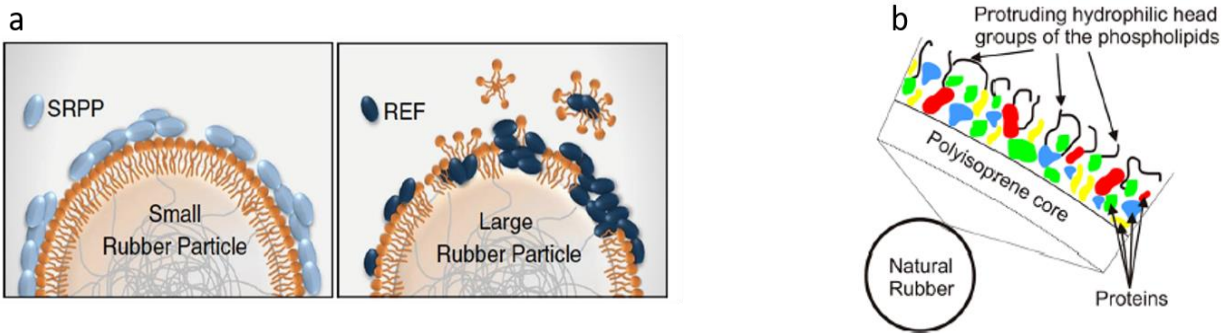


Figure 1.3. (a) Models illustrating the Small Rubber Particle Protein (SRPP) (light blue) and the Rubber Elongation Factor (REF) (dark blue) distribution in small rubber particles (left) and large rubber particles (right). (b) Latest proposed model of organizations of proteins and lipids in bio-membrane consisting of a protein-rich layer with a typical thickness of $\delta_1 = 3.5$ nm and a second layer containing hydrophilic heads of the lipids in contact with solution having very small thickness $\delta_1 = 0.6$ nm.

Although the nanoscale morphology of the shell still remains controversial, several possible scenarios have emerged on the proteins and lipids arrangement. First a double layer arrangement in which an inner layer of lipids resides beneath a protein layer was proposed²⁰. This derives from the fact that the principal phospholipids of the NR latex are of the lecithin type and they are strongly adsorbed on to the surfaces of the rubber particles. They are thought to be intermediaries by which the proteins are anchored on to the rubber particles. The adhesion between the proteins and the adsorbed lecithin has been accounted for the fact that the pH of fresh latex is neutral before addition of ammonia. The lipid layer carries a slight overall positive charge, whereas the proteins, being on the alkaline side of their iso-electric point are negatively charged, so that ionic interaction between the two layers is possible. Secondly a mixed monolayer composition was also proposed in the literature by Nawamawat et al²¹, arguing that such a layer is composed of 84% proteins and 16% lipids by using phase contrast images of AFM and confocal fluorescence microscopy.

In contrast, these biomembrane organizations were recently questioned by the work of Rochette et al²². coupling electrokinetics measurements and cryo-TEM experiments. This work proposed a new model suggesting the presence of a protein rich layer anchored to the polyisoprene core, of ~3.5 nm, and a very thin second layer containing the hydrophilic heads of lipids protruding towards the solvent, ~ 0.6 nm (Figure 1.3b).

The stability/flocculation behavior of NR globules is governed by the various attractive and repulsive forces involved in colloidal systems of all types. Those important forces which are operative between the rubber globules are:

- Electrostatic repulsive forces: it is common for colloids dispersed in water to have electric charges on their surfaces. The origin of the surface charge can be either ionization of chemical groups at the surface of the particles or the adsorption of charged species from the dispersion medium at the particle surface. In the case of NR globules, the lipo-protein layer confers a negative electric charge to the particle surfaces thereby making the latex electrostatically stabilized. Electrostatic stabilization of two NR globules can be represented schematically as given below (Figure 1.4);

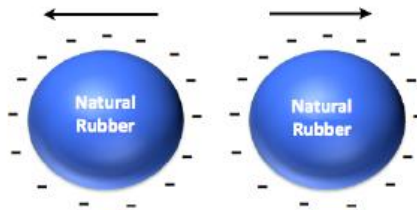


Figure 1.4. Electrostatic repulsion between NR globules in water or in ammoniated solution.

- Steric repulsive forces: this kind of stabilization is due to the presence of macromolecules or chains which are adsorbed or bonded on the particle surface and cause the repulsion. Therefore, if two globules get closer to each other, their hydrophilic layer will get overlapped, increasing the concentration of these molecules in a particular region as well as increasing the osmotic pressure. To maintain the equilibrium, the solvent will enter in the overlapping region separating the two particles.
- Solvation forces: when two colloidal particles come within nanometer distances in a liquid solvent, the solvent can mediate a force between them. This solvation force or hydration force, if the solvent is water is due to differences between the solvent ordering and/or density in the gap between the particles and in the bulk liquid region around them. The solvation layer arises from the presence of nonionic hydrophilic materials adsorbed on the particle surfaces and it is

formed by the solvent molecules surrounding either the hydrophilic heads of lipids or the hydrophilic part of a protein.

- Van der Waals attractive forces: the origin of these forces is the attraction between a temporary dipole and the corresponding induced dipoles (London theory). At molecular level, these interactions are quite weak with the attraction energy decreasing with the six power of the distance between the involved molecules.

Please note that, any reduction in the negative surface charge or increase in contact between the globules could force aggregation. In particular, the addition of divalent ions and mechanical agitation are possible ways to achieve aggregation between NR globules.

2.3. Natural rubber network and its mechanical properties

The structural arrangement and spatial organization of polyisoprene chains together with proteins and lipids of NR changes according to the physical state (solid or liquid). Once NR is solid, the colloidal structure of the globules is believed to be lost to give rise to the so called “natural rubber network” or “naturally occurring network”^{23,24}. The organization of such a network together with the overall NR mesostructured (term used to describe dry NR macromolecular structure and gel) have first been reported by Tanaka and Tarachwin et.al. in two successive reviews published in 2001²⁵ and 2009²⁶. Those publications summarize about 30 years of research presenting all the links established between the structure of the material and the known properties of NR. One of the main discoveries of Tanaka and co-workers reported that polyisoprene chains present in solid NR consist of two trans-isoprene units connected to a long chain of cis-isoprene units. Such polymeric chains are then substituted in α and ω positions linking with mono or di-phosphate groups associated with phospholipids by H-bonding at the α -terminal, whereas the ω -terminal is presumed to be modified with dimethylallyl groups linked to proteins by H-bonding (Figure 1.5a). In this structure the biomolecules could self-assemble creating domains of either lipids and/or proteins, forming a physical network where linear polyisoprene chains are connected with non-rubber components through functional terminals (Figure 1.5b).

Direct confirmation of the network structure encountered tremendous difficulties, so the researchers have tried to solve this problem by decomposing the naturally occurring network, i.e. removing proteins from NR to prepare DeProteinized Natural Rubber (DPNR), and removing phospholipids from DPNR to prepare TransEsterified DeProteinized Natural Rubber (TEDPNR)²⁷. Several analytical methods have been used to study such networking structure: the main ones refer to spectroscopy measurements (H,C,P-Nuclear Magnetic Resonance (NMR), Fourier Transformed InfraRed spectroscopy (FTIR), gel permeation chromatography, dielectric spectroscopy), scattering techniques

(Small-angle neutron scattering and small-angle x-ray scattering), and rheological studies. Due to the nanoscale size of non-rubber components, the use of highly resolved imaging techniques is necessary to explore the morphology of those compounds in such network. Only recently Wu et.al.²⁸ were able to describe the spatial organization of proteins and lipids in NR using a microscopy technique. More specifically, during their work they employed direct STochastic Optical Reconstruction Microscopy (d-STORM) in combination with measurements of solid state NMR and rheology. They confirmed the presence of proteins and lipids aggregates physically interacting with the terminal groups of rubber chains, which leads to the formation of a network.

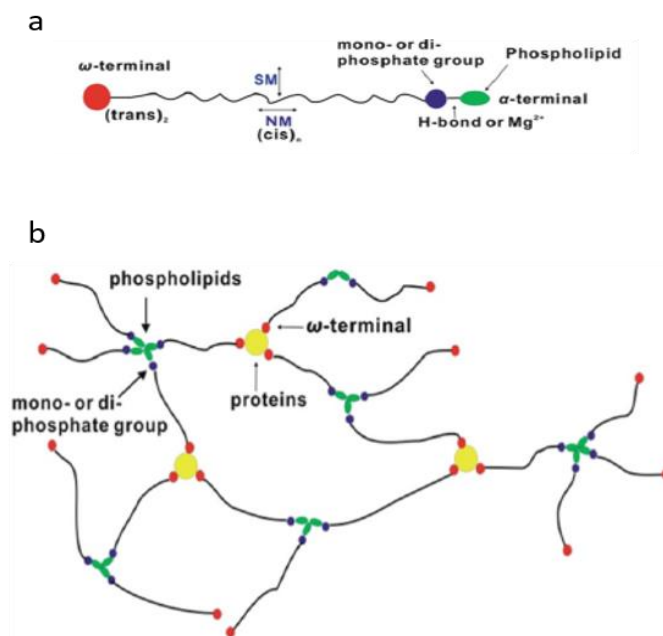


Figure 1.5. (a) Structure of polyisoprene chain in NR as proposed by Tanaka et al.²⁶. (b) Branching points formation giving rise to the natural rubber network²⁴.

The presence of proteins and lipids in the described network, which is believed to be responsible for the excellent properties of NR, unsurpassed by any synthetic counterpart²⁹. In fact, materials issued from NR extracted from *Hevea brasiliensis* exhibits excellent properties, such as high tensile and tear strength, good crack growth resistance and minimal heat buildup. The reason behind such outstanding properties is believed to be attributed to the strain-induced crystallization phenomenon that occurs in NR. This ability to crystallize under strain is often explained by the high regularity of the macromolecular structure, i.e its high percentage of chains being in cis-configuration, and by the presence of proteins and lipids in NR. Thus, the superior mechanical properties of NR over its synthetic counterpart can be partly attributed to the presence of proteins and lipids. The origin of exact role of proteins and lipids in terms of properties enchantment in unvulcanized NR has been studied by Amnuaypornsrri, Toki, Tanaka and Ichikawa^{30,31}. To investigate this role, they compared the stress-

strain curves of films prepared from different types of rubber latex: high ammoniated NR latex, DPNR latex, acetone extracted DPNR, TEDPNR, and synthetic cis-polyisoprene rubber (Figure 1.6). They showed that the mechanical properties of highly ammoniated NR are almost equivalent after removal of proteins. On the other hand, a significant loss was reported after transesterification, comparable to the one of synthetic rubber.

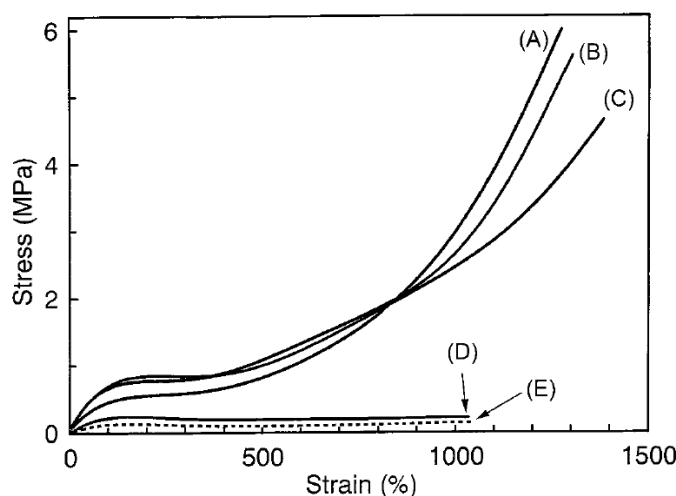


Figure 1.6. Strain-stress curves of (A) high ammoniated NR latex, (B) DPNR obtained from deprotenization of highly ammoniated NR latex, (C) acetone extracted DPNR, (D) transesterified DPNR giving rise to TEDPNR and (E) synthetic cis-polyisoprene³⁰.

Re-addition after removal of proteins and lipids was also explored. Lipase-treated DPNR (L-DPNR) was used as starting material. Proteins and phosphatidyl choline were separately added to L-DPNR, and stress-strain curve were measured. Results are shown in Figure 1.7 where it is interesting to note that the curves after re-addition of proteins or phosphatidyl choline to L-DPNR did not significantly improved the tensile properties. This finding suggested that the high tensile properties of NR are not directly caused by the presence of proteins and lipids alone in the matrix, but it is related to the networking structure which originates from the bonding of proteins and lipids with terminal units of the polyisoprene chain. It is clear that simple addition of such biomolecule is not sufficient to reconstruct the naturally occurring network.

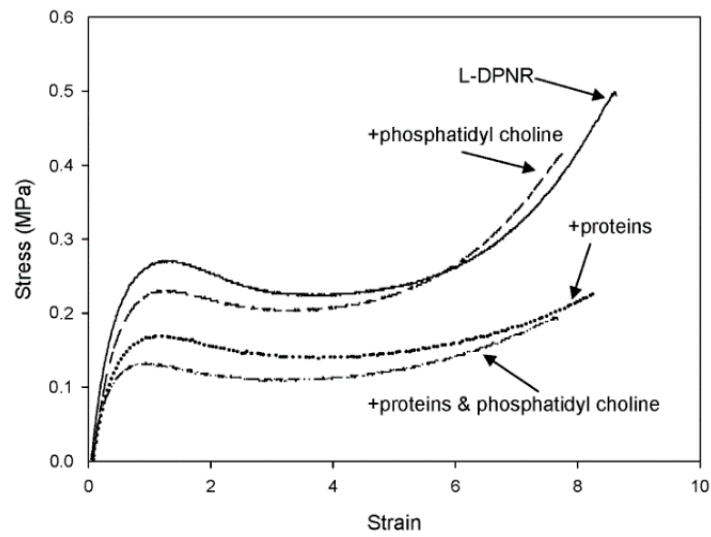


Figure 1.7. Stress-strain curves of *L*-DPNR loaded with extracted proteins and/or phosphatidyl choline³⁰.

3. Fillers for rubber reinforcement

Despite its natural intrinsic properties, NR is rarely used in its raw form, because “too weak” to fulfil practical requirements due to lack of hardness, strength properties and wear resistance. For this reason, fillers are used in order to improve the properties of rubber compounds reinforcing the material. As an example, a tire manufactured without the use of fillers will not be strong enough to withstand the stress encountered. However, it is difficult to give a precise definition of what is *reinforcement*, because this word is specifically related to a particular material and its applications. In general, reinforcement may be defined as the addition of species giving better mechanical properties to the composite over that of the pure polymer matrix, but what is expected as mechanical properties is very different considering the different matrices and applications.

Generally, when a stress-strain test is performed on rubber samples the three most important properties tested are the Young’s modulus, the tensile strength and the elongation at break. The tensile strength corresponds to the force needed to break the rubber specimen. The elongation at break is the maximum elongation the sample can undergo before breaking. The measurement of Young’s modulus in rubber materials is very difficult, because the stress needed to deform a rubber sample is small and usually special load cells are needed for a very precise measurement. Therefore, in most cases the ‘modulus’ is measured as the stress at a particular strain and it represents the stiffness of the material. Other mechanical properties used to characterize the rubber materials are hardness, compression set and abrasion resistance. A general effect of reinforcing filler on different compound properties (viscosity, hardness, tensile strength, compression, abrasion, elongation at break) is shown in Figure 1.8.

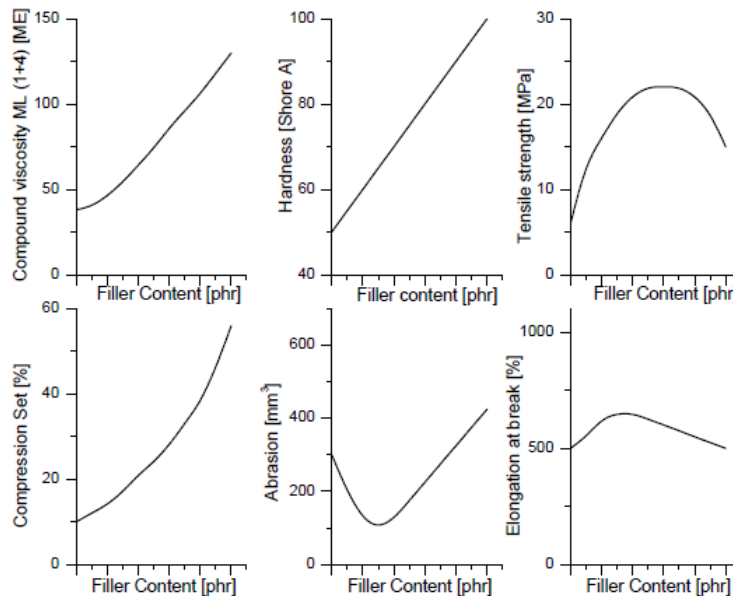


Figure 1.8. Influence of the amount of reinforcing fillers on several compound mechanical properties³².

Rubber goods derive many of their mechanical properties from the added mixture of these reinforcing fillers at quantities of 30% up to as much as 300% part per hundred rubber. The reinforcing mechanisms in rubber nanocomposite are very complicated and they are still not fully understood due to the complexity of the heterogeneous multicomponent systems and cross-linking structure of the rubber³³. Nowadays, the reinforcing mechanism of rubber composite attracts lots of interest especially with new filler applications giving rise to different rubber-filler combinations. What is actually needed to reinforce rubber materials? Why is rubber reinforced by fillers and what are the microscopic contributions that lead to a macroscopic reinforcement? Those are still today open questions. So the topic of reinforcement still remains very open but the comprehension of this mechanism goes beyond the main objectives of this thesis. However, years of work devoted to rubber reinforcement have yielded insights that allow the advancement of rubber products, highlighting some intrinsic characteristics which can be linked to a good reinforcement effect.

In general, the contribution of filler to rubber reinforcement is induced by a large difference in Young's modulus between rubber and filler. Rubber can be considered as a "soft" polymer while fillers are "hard" particles. In essence, fillers are harder than rubber and cannot be easily deformable³⁴.

The strong elements connected to the achievement of rubber reinforcement are directly linked to: hydrodynamic effect, polymer network, polymer-filler interaction, filler-fillers interaction, filler dispersion state in the rubber matrix, physico-chemical properties of the filler. The aim of the following subsection is to briefly introduce each one of the elements above mentioned.

3.1. Important parameters influencing rubber reinforcement

The reinforcing mechanism of filled-rubber systems was better understood after the pioneering study of Payne in the 60's. The scientist studied the relation between the three dimensional particulate filler aggregates and its dependence to two important parameters in dynamic mechanical properties: the storage modulus G' (corresponding to the elastic energy stored during experiments) and the loss modulus G'' (corresponding to the energy lost by viscous friction forces) on strain such as shear. Payne's works showed that, above some critical strain amplitude, the storage modulus G' decreases rapidly with increasing amplitude saturating at rather large deformations, while the loss modulus G'' shows a maximum in the region where the storage modulus decreases: this effect is called "Payne effect"; it depends on the filler content of the material and vanishes for unfilled elastomers. Payne concluded that in particulate filled rubber (e.g. rubber filled with carbon black and silica particles) the increase of storage modulus depends on four contributions, among which three of them are strain independent (polymer network, hydrodynamic effect and filler-rubber interaction), while the filler-filler contribution is strain dependent^{33,35,36}. Thereafter, the Payne concept has been widely used to describe the filler-filler interaction as well as filler-rubber interaction.

Concerning strain-independent contributions, the hydrodynamic effect arises from the inclusion of rigid particles and an increase in the cross-linking density created by polymer-filler bonding³⁷. It refers to the fact that the addition of the filler to an elastomer results in a composite material whose macroscopic mechanical properties are, by construction, some weighted average of the properties of the elastomer and the rigid filler³⁸.

With regards to the polymer network contribution, a networking structure already appears in small amount before vulcanization due to physical cross-linking of entangled chains. This contribution is particularly present before vulcanization in NR due to the presence of the naturally occurring network. After vulcanization, chemical cross-links dominantly contribute to the modulus in which the value is proportional to the cross-link density of the network.

Another important contribution to the increase of modulus is the filler-rubber contribution. On this topic, several models have been published concerning filler-rubber interactions in carbon black filled compound. The models are based on bound rubber, term used to define the non-extractable elastomeric part of rubber when the composite is immersed in a good solvent for the polymer for long time. Le Blanc et.al.³⁹ used proton nuclear magnetic resonance (H-NMR) to study the molecular flexibility of polymers when they are modified by filler particles. Their work demonstrated that bound rubber is composed of two bound layers with different level of molecular mobility (Figure 1.9). In fact, very close to filler particles, there is a thin layer of “tightly bound” rubber, which is likely to behave in a flow field exactly as the aggregate. Then there is a region of “loosely bound” rubber, i.e., chains attached to the particles, through the “tightly bound” rubber region, but able to undergo very large deformation during flow. This region eventually forms connective filaments between rubber-filler aggregates. The third portion is the unbound rubber, so-called because it can readily be extracted from uncured compound by a good solvent of the elastomer⁴⁰. In the layer of tightly bound rubber molecular motion is very constraint, the polymer chains are “anchored” onto the stiff filler particles forcing the chain into conformations that are different from the ones present in the bulk. The presence of such different conformation is thought to be responsible for macroscopic reinforcement. Besides “tightly bound” and “loosely bond” rubber, there is also rubber trapped inside the filler aggregates which fall under the name of “occluded rubber”. This trapped occluded rubber among the voids of the aggregates is shielded from deformation^{41,42}. Note that the model described above was specifically studied for carbon black filled synthetic rubber, but it can be a good base to understand the reinforcement mechanism in other type of nanocomposites. By way of conclusion, increasing rubber-fillers interaction and the strength of their bonds is a fundamental condition to achieve optimal rubber reinforcement.

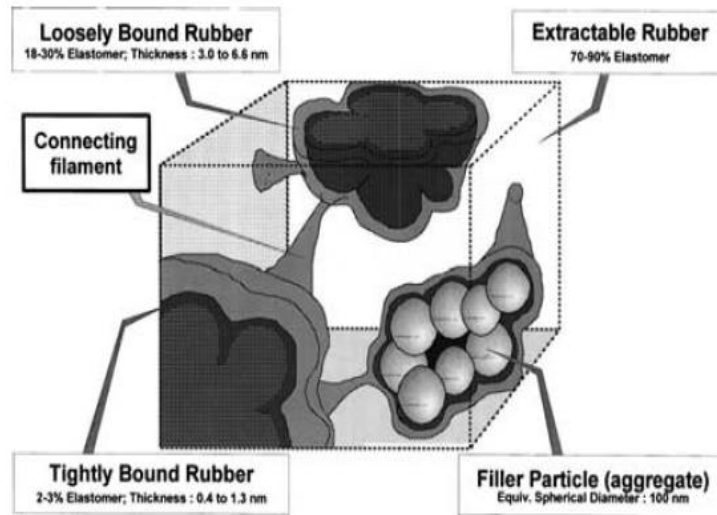


Figure 1.9. Schematic description of the bound rubber model introduced by Le Blanc et.al.³⁹ for carbon black filled synthetic rubber.

Another important parameter to consider concerns the structure of the filler in the polymer matrix and the related dispersion state of the filler^{43,44}. Different properties are obtained if the filler form a continuous percolating network or isolated hard regions. An objective of producing polymeric composites is to distribute and disperse the filler as homogeneously as possible so that the resulting mechanical properties of the polymer/filler composite will be uniform. Failure to meet this criterion causes locations for high stress concentration which act like “flaws” in the material. Thus, the uniform dispersion of the filler in the polymer matrix is essential for rubber compounding to achieve optimal properties. However, the formation of filler network, above a critical concentration, result in abrupt increase mechanical properties. This is known as percolation phenomena, which is strongly related to the loading level and dispersion state. In general, a more efficient mechanical reinforcement is obtained when a rigid percolating filler network is formed within the soft polymer matrix in which an increase of Young’s modulus is clearly observed. At small deformation, filler network play a major role on reinforcement⁴⁵. Thus, the morphology of the filler is of primary importance for the rheological properties of the composite⁴⁶⁻⁴⁸.

The physico-chemical properties of the filler also play a major contribution. One of the parameters capable to affect rubber-filler interaction is the average filler particle size. Particles larger than 10^3 nm do not have reinforcing capabilities, and generally increase viscosity by a mere hydrodynamic effect³⁹. The size of fillers is directly link to the surface area which plays a role in the interaction between the elastomer and filler surface. Reinforcing fillers with very small particle size in the range of 10-100 nm have a high surface area that provides more active contact sites with the rubber matrix. Due to the small size and increased surface area, nanofillers have emerged as promising fillers for improving the properties of polymer with lower filler loading.

Apart from specific surface area as discussed above, the structure and the surface activity of fillers are considered as crucial factors in controlling the reinforcement effect on rubbers. Surface activity can either be expressed in a chemical sense or physical sense. The former relates to the different functional groups present at the surface of the fillers such as lactone, quinone, carboxyl, hydroxyl, etc. In physical sense, the variations in surface energy of the filler, surface roughness, porosity, etc. are used to determine the ability and capacity for physisorption. Therefore, the interaction between filler and rubber depends significantly on the functionalities present on the filler's surface. Therefore, the physical state of filler (solid or liquid), as well as the one of the polymer matrix, can affect the rubber-filler interaction and the dispersion state. I would like to recall that the structure of NR in the latex state is not the same as in the solid or dried state. As shown earlier, in the liquid or latex phase, the rubber fraction is mainly contained in the form of core-shell NR particles, where the core is made of polyisoprene chains and the shell is mainly composed of phospholipids and proteins. On the other hand, in dried state, a NR network is formed. In such network, the polymer chains are more exposed in comparison to the liquid state where they are caged by a hydrophilic layer made of biomolecules. Based on this structural consideration, the chemical behaviors of NR changes between the liquid and the solid state. The overall structure can be considered hydrophilic in the liquid state and hydrophobic in the dried state. This change in behavior is most likely to influence the interaction between NR and the involved filler as it will be discussed in the next subchapter introducing the most common fillers usually coupled with NR.

3.2. Common fillers used in Natural Rubber Composites

The most commonly used fillers in the NR industry are CB and Si. However, other types of filler are also of relevant importance. The following section present the structure, the composition of CB and Si fillers used in this study as well as some generalities of their interaction with NR.

- **Carbon Black (CB)**

CB is the generic name for a family of small-size, mostly amorphous, or para-crystalline carbon particles grown together to form aggregates of different sizes and shapes⁴⁹. CB is produced by the incomplete combustion of hydrocarbons such as those found in petroleum oil or natural gas⁵⁰. During the reaction, carbon nodules are formed. The smallest units of CB are primary particles (~50nm)⁵¹ normally having a spherical shape. However, the lifespan of these particles is very short because they rather cluster together to form aggregates of approximately 200-500 nm. The aggregation between primary black particles involves the formation of covalent bonds between them. These bonds are very difficult to break down by physical methods. The size and shape of the aggregates can vary from individual spheroidal particles to clusters of a few or a multitude of primary particles with a more or less irregular three-dimensional, chain-like, fibrous, or grape-like morphology⁴⁹. Furthermore,

aggregates can form bond between themselves to form agglomerates. The bonds formed between aggregates are of electrostatic nature and they are weaker than those within aggregate, thus they can be broken by physical methods (sonication, agitation).

CB can be considered as a highly disordered form of graphitic carbon. Elementary analysis of CB yields not only carbon but also small quantities of oxygen, hydrogen, nitrogen and sulfur (Table 1.4). Most of these elements are concentrated on the surface of CB. Hydrogen and oxygen form surface-bound functional groups such as carbonyl, carboxyl, pyrone, phenol, quinone, lactol, ether, and anhydride. A schematic representation of the surface's composition of CB is displayed in Figure 1.10.

Table 1.4. Typical elemental carbon black composition⁴⁹.

Element	Content (% of wt)
Carbon	96-99.5
Hydrogen	0.2-1.3
Oxygen	0.2-0.5
Nitrogen	0- 0.7
Sulfur	0.1-1.0

Around 93% of CB usage is dedicated to rubber applications, and can be classified into two main categories: tires and mechanical rubber goods (e.g. automotive belts and hoses). The reinforcing properties of CB provide enhanced performance and durability to the rubber compounds in which they are used. CB used in rubber applications are typically categorized as N100±N900 series blacks, where increasing N number correlates with decreasing nitrogen surface area. The remaining 7% of carbon usage falls into a broad group of applications, of which the most predominant are plastics, inks, and coatings.

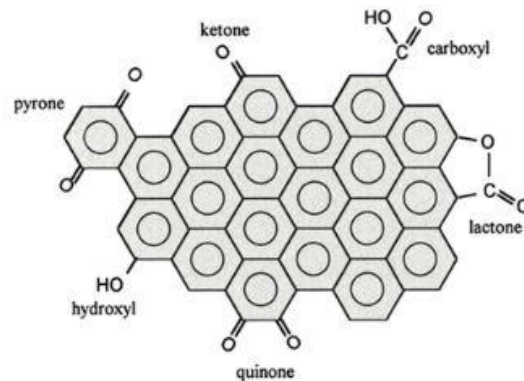


Figure 1.10. Surface chemistry of carbon black⁵².

When NR and CB are present in their *solid state*, the interaction between CB and NR is said to be regulated mainly by Van der Waals attraction forces⁵³. The origin of these attraction forces is related to the active sites originated from the cleavage of carbon-carbon bonds during the manufacturing process of CB.

One of the advantages of using CB in rubber materials is its ease in processing with either NR or SR. Once in the solid state, both rubber and CB are generally hydrophobic. This is perhaps, a reason of compatibility between CB and rubber. Additionally, the incorporation of CB into rubber creates an interface between a rigid solid phase and a soft solid phase. The interfaces area depends, on the volume fraction of the CB in the compound and on its specific surface area. For this reason, one of the most important properties of CB is its surface activity. All CBs possess a distribution of energy sites, which allow the chemisorption or physical adsorption of rubber at their surface.

On the other hand, the interaction between CB fillers in aqueous suspension and NR latex is not well understood. Martín-Pedrero *et al*⁵⁴ investigated a novel approach to form an elastomeric composite material starting from NR latex and CB in the *liquid state*. Their process was based on a bulk destabilization of a binary colloidal mixture composed of NR latex and CB filler, giving rise to a heterocoagulum. The two type of particles were either naturally destabilized or dispersed in water with the help of a surfactant. The researcher reported that heteroaggregation was achieved in both cases and that sol-gel transition was mainly governed by the amount of surfactant. This indicates an interaction between NR latex and CB in the liquid state. Indeed, the adsorption of surfactant molecules onto the CB surface tunes the interaction between the two types of particles and thus the homogeneity of the dispersion before its destabilization. Despite their important contribution, the fundamental understanding on the interaction between NR latex and CB filler in the liquid state is still at its infancy.

- **Silica (Si)**

Silica is an amorphous material, consisting of silicon and oxygen atoms connected in a non-regular 3D network of Si-O-Si bonds with silanol groups (Si-OH) present inside and on the surface (Figure 1.11). The chemical characteristics of the Si surface are mainly determined by the amount of silanol groups, the amount of adsorbed water and the pH. The silanol groups present on the Si surface can be divided into three different types, depending on the hydroxyl group⁵⁵, which are:

- Isolated silanol group: a single hydroxyl group on a silicon atom
- Vicinal silanol group: two hydroxyl groups on adjacent silicon atoms
- Geminal silanol group: two hydroxyl groups on the same silicon atom

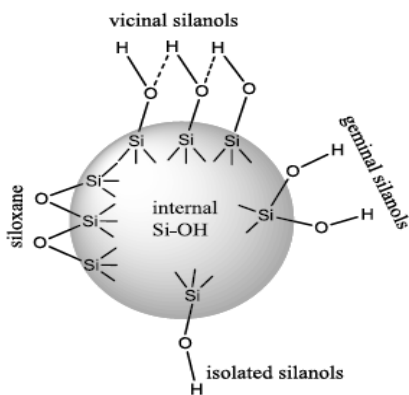


Figure 1.11. Structure of an amorphous colloidal silica particle, highlighting the presence of different silanol groups on the surface⁵⁶.

In addition to the silanol groups, a siloxane bridge is formed when one oxygen atom is shared by two silicon atoms. The silanol groups are directly responsible for the high polarity and hydrophilic character of Si. The characteristic structure of Si can be divided into agglomerates, aggregates and primary particles⁵⁷. The agglomerates of Si are typically ranged in the dimension of 1-40 μm . These agglomerates are formed by hydrogen bonding and Van der Waals forces between Si aggregates. The typical dimensions of Si aggregates are 100-1000 nm. Within the aggregates, the nano-size primary particles are linked together via siloxane bonds.

There are two types of commercially available Si, either precipitated or fumed. The precipitated Si is prepared by the reaction of sodium silicate and sulphuric acid under alkaline conditions and the fumed Si is prepared by oxidation of silicon tetrachloride vapor at high temperatures. In the rubber industry the precipitated Si is the preferred type of use because of the lower price and better mixing with the rubber material. The more expensive fumed Si has very low bulk density (very fluffy white powder) and it is mainly used in silicon rubber.

The introduction of Si fillers into **solid** rubber or NR presents the obstacle of incompatibility between the two components. Indeed, there is a large difference between the solubility and polarity of rubber polymers and Si, indicating difficult mixing of these two materials which usually results in large Si aggregates non-homogeneously dispersed throughout the rubber matrix. The challenge for rubber-silica nanocomposite is represented in achieving a good Si dispersion, and therefore homogeneous mechanical properties.

To compensate and overcome the incompatibility of Si with hydrophobic polymers the application of an organofunctional silane is often necessary to overcome the polarity differences in order to achieve a higher desirable Si dispersion level in the rubber compound⁵⁸. A bifunctional organosilane coupling agent, through the organo-functional and silicon-functional moiety, is able to chemically bond a polymer matrix to inorganic substrates such as Si. The bifunctional organosilane coupling agent serves two functions: one end is for coupling with the hydrophilic Si surface and the other end to couple with

the hydrophobic polymer or rubber. Hence, the coupling agent acts as a connecting bridge between Si and the rubber and improves the reinforcement of Si in rubber. In terms of surface chemistry, after the adsorption of the silane coupling agent onto the Si surface, hydroxyl groups on the Si surface start reacting with alkoxy groups of the silane coupling agent. This reaction is named “silanization” and it must undergo rapidly *in-situ* during the mixing process. Mainly, bi-functional-organosilanes based on the structure shown in Figure 1.12a are used. Among them, the bi-functional-organosilanes which have been most widely used in the tire industry so far are bis(triethoxysilylpropyl)tetrasulfide and bis(triethoxysilylpropyl)disulfide. The structures of them are shown in Figure 1.12b and c. Successful application of these molecules generally yield higher bound rubber content and a more successful reinforcement⁵⁹.

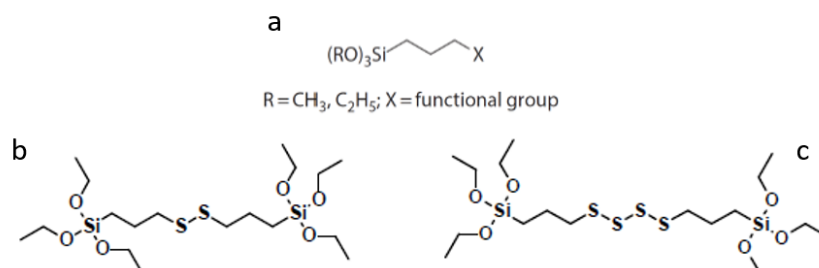


Figure 1.12. Basic structure of bi-functional organosilanes (a). The structure of Bis(triethoxysilylpropyl)tetrasulfide (b), triethoxysilylpropyl) disulfide (c).

On the other hand, when Si is mixed with NR in the *liquid state*, literature on the fundamental processes involved in the interaction between NR latex and Si filler in liquid is very limited. The only fundamental study focusing on interactions and heteroaggregation between NR globules and Si filler in aqueous conditions refers to the work of Chan et al.⁶⁰ It highlights some important physico-chemical parameters required to achieve NR–Si interaction under very diluted aqueous conditions.

Before describing the main results obtained by the work of Chan et.al., it is important to keep in mind that NR globules are generally hydrophilic because of the presence of their lipo-proteic membrane. In fact, in colloidal form, charged proteins and phospholipids are in control of the colloidal stability. Concerning the Si particles, their hydrophilic character is raised by the presence of silanol groups on their surface. Therefore, the interaction between Si particles and NR globules is hindered by the presence of negative charges on both particle’s surface. Thus, the interaction of these particles is electrolyte responsive.

Chan et.al.⁶⁰ demonstrated by fluorescence correlation spectroscopy (FCS) that the interaction between NR globules and Si fillers occurs only in the presence of an ionic medium. Figure 1.13 shows the normalized autocorrelation curves of the mixed solution of NR and Si filler, using different sizes of Si and different ionic medium.

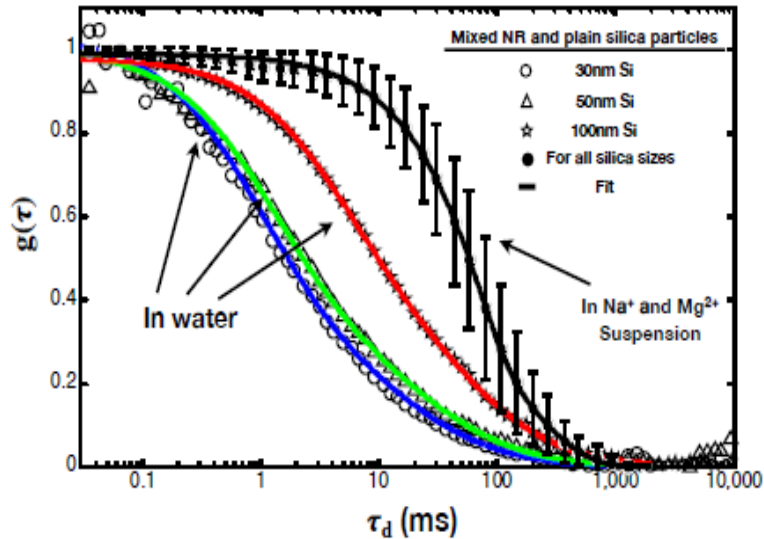


Figure 1.13. Normalized autocorrelation curves of the mixed solutions of NR and silica particles. In water the curves are similar to the ones obtained for free silica particles suggesting no interaction between NR and silica. In NaNO_3 and MgSO_4 at ionic strength of 100 Mm the curves are similar whatever the size of silica particles and a shift to longer diffusion times connotes interaction between NR and the filler⁶⁰.

The normalised autocorrelation curves and corresponding diffusion time in water are similar and very comparable to the diffusion times calculated for free Si particles in water (data not shown) suggesting a lack of interaction between NR globules and Si filler. However, in the presence of Na^+ and Mg^{2+} (ionic strength=100 mM) the two binary particles interact yielding a curve shifted to longer times. This result can be explained by the effect of salt addition on the Electrostatic Double Layer (EDL) thickness. As the salt concentration increases, more counter-ions are available to neutralize the colloidal surface charge resulting into a thinner double layer and decrease of energy barrier. In terms of the heteroaggregation kinetics, they also showed that the two binary particles interact immediately in Mg^{2+} solution. However, in Na^+ solution, when measured immediately they observed a curve similar to the one of free Si, and it took longer to observe the shift characteristic of the NR-plain silica particles interaction.

3.3. Other fillers for NR

Besides CB and Si, which are the most widely used filler in natural rubber materials, other fillers are also employed based on the industrial sector and the manufacturing process.

Clay has been an important NR filler for many years, but due to its large size and low surface activity, the reinforcing ability of clay is poor¹³. Layered silicates (LS) are the main active minerals in soils and clays. The layers are stacked by a weak dipole-dipole force and exhibit a net negative charge on the

surface. The interlayers between the galleries are normally occupied by cations such as Na^+ . As force that hold the stacks are relatively weak, the intercalation of small molecules between the layers can be done relatively easily. However, the exfoliated nanolayers of LS may not be easily dispersed in most polymers due to their preferred face-to-face stacking⁶¹.

Calcium carbonate is also widely used as non-reinforcing and reinforcing filler to impart desired color and reduce product cost in NR-based composites. There are two important types of CaCO_3 : ground limestone and precipitated CaCO_3 . The former is prepared by grinding mineral limestone, while the precipitated form is obtained by chemical precipitation of a salt solution⁶².

Recently, due to ecological concerns, bio-based fillers have been increasingly used as fillers in polymer composites. Such materials promise some advantages compared to traditional inorganic fillers, including their renewable nature, low density, nonabrasive properties, and reasonable strength and stiffness. This makes them competitive as reinforcing agents in certain composite applications⁶³. Commonly used bio-based fillers are cellulose whiskers, chitosan and starch nanocrystals.

Graphene is also gaining more and more interest as filler for natural rubber composites. In the last 10 years, graphene/thermo plastic polymer composites were extensively investigated. However, surprisingly, almost no studies involved the preparation and characterization of rubber/graphene composites until 2011, probably due to the dispersion and exfoliation problem of graphene in the cross-linked rubber matrix. Since 2013, the modification of rubber by using graphene nanofillers has become one of the hot topics in the area of graphene, aiming to the automobile or bicycle tire application. Graphene combines the conductivity of carbonaceous materials with the structural characteristics of clay sheets (widely used in the field of elastomeric materials), thus providing new strategies in the development of high-performance multifunctional rubber nanocomposites⁶⁴.

4. Mixing filler into rubber compounds – strategies for filler dispersion

Mixing is central to rubber technology. The mixing step between rubber and filler is a very important task because it will define how fillers are distributed and dispersed as well as their degree of interactions with the host polymer matrix. If the base compound is inadequately mixed, problems cascade down through the subsequent processes of shaping and curing into the end product. It is therefore of value to understand not only the practical procedures of mixing, but also the physical processes involved at smaller scale.

Usually, there are five main types of ingredient in a normal rubber mix: the rubber itself, fillers, plasticizers, minor chemical ingredients and curatives. In most mixing operations, curatives are added at a second, lower temperature stage, either on a mill (sometimes directly after the drop mill), in a

repass through the high shear mixer, or in a relatively low shear mixer⁶⁵.

Several strategies have been proposed for the mixing of rubber with filler and other ingredients (solid mix, melt compounding etc.)⁵³. The most conventional way consists in inserting fine particulate filler powder into a solid mixing machine (two roll mill, internal mixer) together with solid rubber sheets. The most common machine used to manufacture large quantities of composite is the Banbury internal mixer. The Banbury mixer is a tangential type internal mixing machine, in which two slightly spiraled rotors revolve side by side towards each other within a chamber shaped like two short cylinders lying together with adjacent sides open. The chamber has a top opening called hopper, which can be closed by pneumatic means for inserting the material and a bottom gate, which can be hydraulically opened, to drop out the contents after mixing. Research on detailed designs of mixer rotors for mixing and plastics in an internal mixer has continued to the present time. Later patents have generally involved new rotor designs where the number, shape and angles of the vanes on the rotor are designed in particular manners but the detailed description is beyond the scope of this manuscript.

Although its wide employment, conventional solid mixing method is not the most efficient way to disperse the filler in the polymer matrix. Accordingly, there is a need to improve the methods that mix filler with rubber. Different procedures have been developed to achieve better filler dispersion: sol-gel techniques, *in situ* generation of filler²³, liquid phase mixing. Among those, liquid phase mixing looks very promising. This type of mixing involves the elastomer in the form of latex, and an aqueous dispersion of filler, commonly called “slurry”. Once the slurry is mixed with the elastomer latex, more options are available: the mixture can simply be dried to form a continuous polymer film with embedded filler³⁴, or it can be coagulated.

During the last few decades, a great effort has been made to produce CB-elastomers compounds by combining polymer-latex with a CB and then coagulating the mixture chemically⁶⁶. However, other solutions have been proposed to obtain this coagulation reducing the mixing time and increase productivity. In the early 2000s, a senior Chinese scientist called Wang Meng-Jiao was working for Cabot Corporation (Boston, US). With his team, he developed and patented a novel technology which continuously disperses CB in clean NR latex giving rise to the first NR-filler-batch made with a continuous liquid mixing process. The composite material manufactured with this novel method achieves excellence performance and a superior mechanical properties in comparison with their solid-mixed counterparts⁶⁷, so that Cabot marketed the product under the name of Cabot Elastomer Composites (CEC). In the production process of CEC, a CB-slurry is first prepared by finely disperse the filler in water without any surfactant (Figure 1.14). Subsequently, the slurry is injected into the mixer at very high speed and continuously mixed with the NR latex stream. Under highly energetic and turbulent conditions, the mixing and coagulation of polymer with filler is completed mechanically at room temperature in less than 0.1 second, without the aid of chemicals. The obtained coagulated material is a mixture of NR and fillers which follows a process of dewatering and drying.

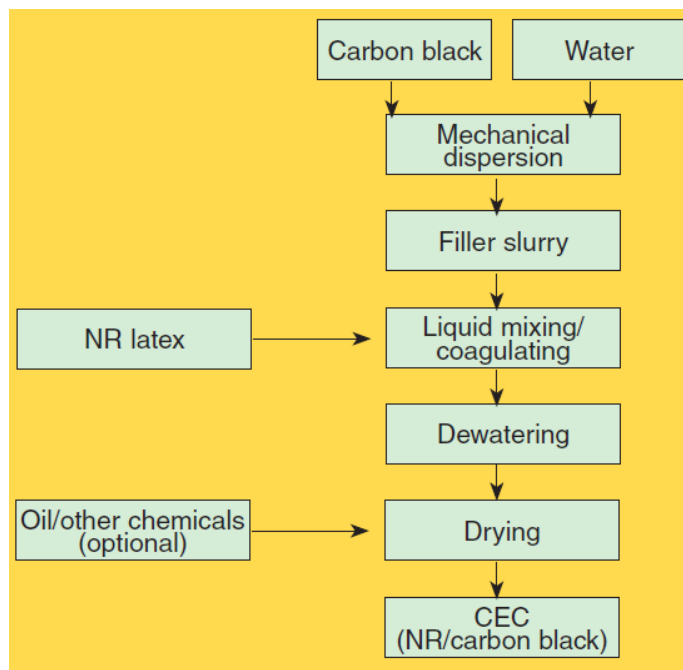


Figure 1.14. Schematic representation of the CEC process⁶⁷.

Wang claimed that one of the reason behind the superior mechanical properties of CEC stands in its superior filler dispersion in comparison to the obtained conventional dry mixed compound. This was demonstrated by investigating the dispersion using transmission electron microscopy and further analysis of the properties (Figure 1.15). For N234-filled CEC, the composite shows good dispersion and distribution throughout the NR matrix, whereas in case of dry-mixed compound, although an extensive mixing has been applied, the dispersion and distribution are poorer than in CEC. Due to highly dispersed filler, the obtained mechanical properties also improved. For example, it is reported that in CEC compounds, the hysteresis, stress-strain properties and abrasion resistance of the vulcanized materials are significantly improved over their dry-mixed counterparts. Therefore, crucial benefits can be related to the appropriate use of such technology for the production of filled-rubber composites. For this reason, Michelin bought a license from Cabot to use the liquid-phase mixing technology.

As previously mentioned, the CEC product has been developed for specific use of CB filler. However, the extension of this technology for other type of fillers, such as amorphous Si is also very interesting and promising. At the moment, the use of liquid phase mixing in case of Si does not exclude an independent silanization process. In fact, the industrial workflow consists in the addition of a silane coupling agent after coagulation and drying by a thermomechanical step.

Overall, liquid phase mixing is a novel technology which did not replaced the production of composites by internal mixers as yet, but over a long term, this is surely a possible way forward.

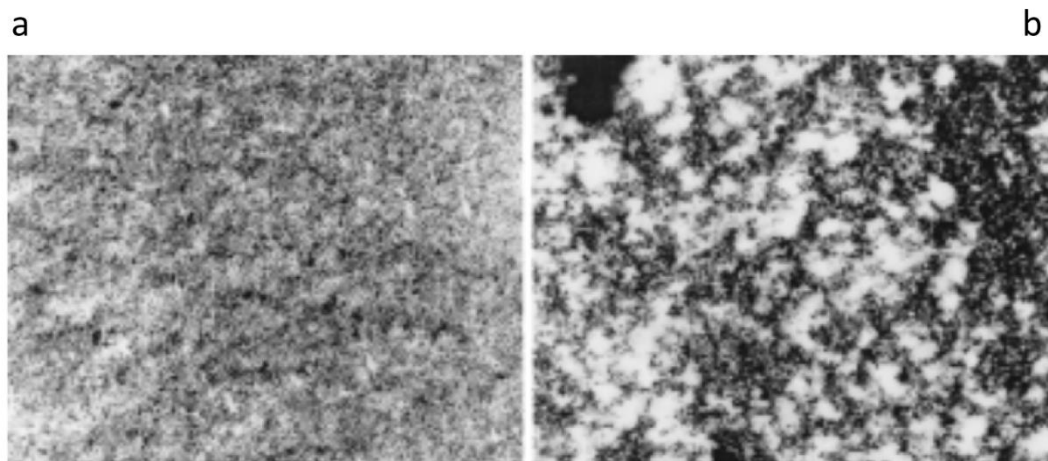


Figure 1.15. TEM images of (a) dewatered CEC and (b) dry mixed NR-CB composite⁶⁷. Images have the same size and were taken with a magnification power of 1000x.

5. Knowledge gap and novelty of the study

Several years after the invention of the liquid phase mixing technology, the technological process parameters are under control at the engineering level, but studies are required to enrich the fundamental knowledge of the heteroaggregation mechanism. In particular, the structural characterization of the obtained coagulum and its evolution toward a composite along drying remains unknown. The structural and physico-chemical characterization of a material along the several steps of an industrial process is essential in order for continued progress to be made. Therefore, understanding what is happening at the nano-microscopic scale during the liquid mixing process is a pioneer work of fundamental interest. In other words, filling the gap between the nano-world and the macroscopic scale is very challenging, but better understanding of the structure along the process and of the undergoing interaction occurring during coagulation could help future development of materials made by this novel mixing method. This is the reason behind our work, which started from a collaboration between MICHELIN and the Institut des Sciences Moléculaires d'Orsay (ISMO).

At the moment, available literature on this subject is very limited and mostly focuses on the mechanical properties of the obtained composite rather than structural characterization studies. It is in this context that, we report on the structural characterization and evolution of a coagulum obtained by mixing NR latex with either CB or Si filler. For the first time, we followed the nanoscale structural evolution dynamics of the coagulum, until the formation of a dried composite. The role of external physical stresses, such as shear and sonication applied in the binary colloidal suspension of NR latex and filler was also tested, reporting a structural effect on the formed coagulum. Additionally, only in case of NR-Si coagulation, the spatial distribution of proteins and lipids of NR, and their organization in respect to the filler was also unraveled. To do so, we employed a set of highly resolved microscopy techniques composed of Field Emission Scanning Electron Microscopy (FESEM), optical super-resolution microscopy (d-STORM), and Atomic Force Microscopy coupled InfraRed spectroscopy (AFMIR). This set of techniques gave specific and complementary insights to reach answers and conclusions that can be found in chapter 3 and chapter 4, while the detailed description of each experimental technique can be found in chapter 2.

REFERENCES

1. Goyal, R. K. *Nanomaterials and nanocomposites: synthesis, properties, characterization techniques, and applications*. (Taylor & Francis, CRC Press, 2018).
2. B. Pereira, A. & A.O. Fernandes, F. Introductory Chapter: The Importance of Composites in the World. in *Renewable and Sustainable Composites* (eds. B. Pereira, A. & A. O. Fernandes, F.) (IntechOpen, 2019). doi:10.5772/intechopen.89427.
3. Honarvar, Z., Hadian, Z. & Mashayekh, M. Nanocomposites in food packaging applications and their risk assessment for health. *Electron. Physician* **8**, 2531–2538 (2016).
4. Jones, W. E., Chiguma, J., Johnson, E., Pachamuthu, A. & Santos, D. Electrically and Thermally Conducting Nanocomposites for Electronic Applications. *Materials* **3**, 1478–1496 (2010).
5. Dishovsky, N. & Mihaylov, M. *Elastomer-based composite materials: mechanical, dynamic and microwave properties and engineering applications*. (Apple Academic Press, 2017).
6. McKeen, L. Elastomers. in *The Effect of Sterilization Methods on Plastics and Elastomers* 305–351 (Elsevier, 2018). doi:10.1016/B978-0-12-814511-1.00010-X.
7. *Advances in elastomers. 2: Composites and nanocomposites*. (Springer, 2013).
8. Peace, M. H. K. & Mitchell, G. R. Conductive elastomeric composites. *J. Phys. Conf. Ser.* **183**, 012011 (2009).
9. Cornish, K., Siler, D. J., Grosjean, O.-K. & Goodman, N. Fundamental Similarities in Rubber Particle Architecture and Function in Three Evolutionarily Divergent Plant Species. 11.
10. Samanani, N. & Facchini, P. J. Compartmentalization of Plant Secondary Metabolism. in *Recent Advances in Phytochemistry* vol. 40 53–83 (Elsevier, 2006).
11. Bottier, C. Biochemical composition of *Hevea brasiliensis* latex: A focus on the protein, lipid, carbohydrate and mineral contents. in *Advances in Botanical Research* vol. 93 201–237 (Elsevier, 2020).

12. Santipanusopon, S. & Riyajan, S.-A. Effect of field natural rubber latex with different ammonia contents and storage period on physical properties of latex concentrate, stability of skim latex and dipped film. *Phys. Procedia* **2**, 127–134 (2009).
13. Front Matter. in *Polymer Chemistry Series* (eds. Thomas, S., Han Chan, C., Pothen, L., Joy, J. & Maria, H.) vol. 2 P001–P004 (Royal Society of Chemistry, 2013).
14. Sando, T. *et al.* Histochemical study of detailed laticifer structure and rubber biosynthesis-related protein localization in *Hevea brasiliensis* using spectral confocal laser scanning microscopy. *Planta* **230**, 215–225 (2009).
15. Bristow, G. M. & Westall, B. The molecular weight distribution of natural rubber. *Polymer* **8**, 609–617 (1967).
16. Habib, M. A. H. *et al.* Proteomics analysis of latex from *Hevea brasiliensis* (clone RRIM 600). *Biochem. Cell Biol.* **95**, 232–242 (2017).
17. Berthelot, K. *et al.* Rubber Elongation Factor (REF), a Major Allergen Component in *Hevea brasiliensis* Latex Has Amyloid Properties. *PLoS ONE* **7**, e48065 (2012).
18. Berthelot, K. *et al.* Rubber particle proteins, HbREF and HbSRPP, show different interactions with model membranes. *Biochim. Biophys. Acta BBA - Biomembr.* **1838**, 287–299 (2014).
19. Chan, A. J. *et al.* LIPID CONTENT IN SMALL AND LARGE NATURAL RUBBER PARTICLES. *Rubber Chem. Technol.* **88**, 248–257 (2015).
20. Cornish, K., Wood, D. F. & Windle, J. J. Rubber particles from four different species, examined by transmission electron microscopy and electron-paramagnetic-resonance spin labeling, are found to consist of a homogeneous rubber core enclosed by a contiguous, monolayer biomembrane. 12.
21. Nawamawat, K. *et al.* Surface nanostructure of *Hevea brasiliensis* natural rubber latex particles. *Colloids Surf. Physicochem. Eng. Asp.* **390**, 157–166 (2011).

22. Rochette, C. N. *et al.* Shell Structure of Natural Rubber Particles: Evidence of Chemical Stratification by Electrokinetics and Cryo-TEM. *Langmuir* **29**, 14655–14665 (2013).
23. *Chemistry, Manufacture and Applications of Natural Rubber*. (Elsevier, 2014).
doi:10.1016/C2013-0-16344-1.
24. Liu, J. *et al.* New evidence disclosed for networking in natural rubber by dielectric relaxation spectroscopy. *Soft Matter* **11**, 2290–2299 (2015).
25. Tanaka, Y. Structural Characterization of Natural Polyisoprenes: Solve the Mystery of Natural Rubber Based on Structural Study. *Rubber Chem. Technol.* **74**, 355–375 (2001).
26. Tanaka, Y. & Tarachiwin, L. Recent Advances in Structural Characterization of Natural Rubber. *Rubber Chem. Technol.* **82**, 283–314 (2009).
27. Huang, C. *et al.* Research on architecture and composition of natural network in natural rubber. *Polymer* **154**, 90–100 (2018).
28. Wu, J. *et al.* Super-Resolution Fluorescence Imaging of Spatial Organization of Proteins and Lipids in Natural Rubber. *Biomacromolecules* **18**, 1705–1712 (2017).
29. Xu, L. *et al.* A rheological study on non-rubber component networks in natural rubber. *RSC Adv.* **5**, 91742–91750 (2015).
30. Amnuaypornsi, S. *et al.* Strain-Induced Crystallization of Natural Rubber: Effect of Proteins and Phospholipids. *Rubber Chem. Technol.* **81**, 753–766 (2008).
31. Amnuaypornsi, S., Sakdapipanich, J. & Tanaka, Y. Green strength of natural rubber: The origin of the stress-strain behavior of natural rubber. *J. Appl. Polym. Sci.* **111**, 2127–2133 (2009).
32. Edwards, D. C. Polymer-filler interactions in rubber reinforcement. *J. Mater. Sci.* **25**, 4175–4185 (1990).
33. Sahakaro, K. Mechanism of reinforcement using nanofillers in rubber nanocomposites. in *Progress in Rubber Nanocomposites* 81–113 (Elsevier, 2017). doi:10.1016/B978-0-08-100409-8.00003-6.

34. Oberdisse, J. Aggregation of colloidal nanoparticles in polymer matrices. *Soft Matter* **2**, 29–36 (2006).
35. Payne, A. R. A note on the conductivity and modulus of carbon black-loaded rubbers. *J. Appl. Polym. Sci.* **9**, 1073–1082 (1965).
36. Warasitthinon, N., Genix, A.-C., Sztucki, M., Oberdisse, J. & Robertson, C. G. THE PAYNE EFFECT: PRIMARILY POLYMER-RELATED OR FILLER-RELATED PHENOMENON? *Rubber Chem. Technol.* **92**, 599–611 (2019).
37. Bokobza, L. The Reinforcement of Elastomeric Networks by Fillers. *Macromol. Mater. Eng.* **289**, 607–621 (2004).
38. Goudarzi, T., Spring, D. W., Paulino, G. H. & Lopez-Pamies, O. Filled elastomers: A theory of filler reinforcement based on hydrodynamic and interphasial effects. *J. Mech. Phys. Solids* **80**, 37–67 (2015).
39. Leblanc, J. L. Rubber±@ller interactions and rheological properties in @lled compounds. *Prog Polym Sci* **61** (2002).
40. Mitchell, M. R. *et al.* Rubber-Filler Interactions and Its Effect in Rheological and Mechanical Properties of Filled Compounds. *J. Test. Eval.* **38**, 101942 (2010).
41. Kraus, G. A Carbon Black Structure-Concentration Equivalence Principle. Application to Stress-Strain Relationships of Filled Rubbers. *Rubber Chem. Technol.* **44**, 199–213 (1971).
42. Medalia, A. I. Morphology of aggregates. *J. Colloid Interface Sci.* **32**, 115–131 (1970).
43. Witten, T. A., Rubinstein, M. & Colby, R. H. Reinforcement of rubber by fractal aggregates. *J. Phys. II* **3**, 367–383 (1993).
44. Oberdisse, J., Straube, E. & Pyckhout-Hintzen, W. Structure Determination Of Polymer Nanocomposites By Small-Angle Scattering. in *Recent Advances in Polymer Nanocomposites* 397–438 (Brill Academic Publishers, 2009). doi:10.1163/ej.9789004167261.i-528.112.

45. Chabert, E. *et al.* Filler–filler interactions and viscoelastic behavior of polymer nanocomposites. *Mater. Sci. Eng. A* **381**, 320–330 (2004).
46. Heinrich, G. & Klüppel, M. Recent Advances in the Theory of Filler Networking in Elastomers. in *Filled Elastomers Drug Delivery Systems* vol. 160 1–44 (Springer Berlin Heidelberg, 2002).
47. Oberdisse, J., El Harrak, A., Carrot, G., Jestin, J. & Boué, F. Structure and rheological properties of soft–hard nanocomposites: influence of aggregation and interfacial modification. *Polymer* **46**, 6695–6705 (2005).
48. Tatou, M. *et al.* Reinforcement and Polymer Mobility in Silica–Latex Nanocomposites with Controlled Aggregation. *Macromolecules* **44**, 9029–9039 (2011).
49. Spahr, M. E. & Rathon, R. Carbon Black as a Polymer Filler. in *Fillers for Polymer Applications* (ed. Rathon, R.) 261–291 (Springer International Publishing, 2017). doi:10.1007/978-3-319-28117-9_36.
50. Jebur, S. K. Carbon black production, analyzing and characterization. 86.
51. *Encyclopedia of materials: science and technology*. (Elsevier, 2001).
52. Gazal, U., Khan, I., Usmani, M. A., Bhat, A. H. & Mohamad, M. K. H. Rubber-Based Nanocomposites and Significance of Ionic Liquids in Packaging Applications. in *Bionanocomposites for Packaging Applications* (eds. Jawaid, M. & Swain, S. K.) 227–242 (Springer International Publishing, 2018). doi:10.1007/978-3-319-67319-6_12.
53. Thomas, S., Chan, C. H., Pothen, L. A., Joy, J. P. & Maria, H. J. *Natural Rubber Materials: Volume 2: Composites and Nanocomposites*. (Royal Society of Chemistry, 2013).
54. Martínez-Pedrero, F. *et al.* Making an elastomeric composite material via the heteroaggregation of a binary colloidal dispersion. *Soft Matter* **8**, 8752 (2012).
55. Sato, M. Reinforcing mechanisms of silica / sulfide-silane vs. mercapto-silane filled tire tread compounds. (2018).

56. Miloskovska, E. E. Structure-property relationships of rubber/silica nanocomposites via sol-gel reaction. (2013) doi:10.6100/ir739216.
57. Boehm, H.-P. The Chemistry of Silica. Solubility, Polymerization, Colloid and Surface Properties, and Biochemistry. VonR. K. Iler. John Wiley and Sons, Chichester 1979. XXIV, 886 S., geb. £ 39.50. *Angew. Chem.* **92**, 328–328 (1980).
58. Kaewsakul, W., Sahakaro, K., Dierkes, W. K. & Noordermeer, J. W. M. OPTIMIZATION OF RUBBER FORMULATION FOR SILICA-REINFORCED NATURAL RUBBER COMPOUNDS. *Rubber Chem. Technol.* **86**, 313–329 (2013).
59. Sae-oui, P., Sirisinha, C., Thepsuwan, U. & Hatthapanit, K. Roles of silane coupling agents on properties of silica-filled polychloroprene. *Eur. Polym. J.* **42**, 479–486 (2006).
60. Chan, A. J. *et al.* Natural Rubber–Filler Interactions: What Are the Parameters? *Langmuir* **31**, 12437–12446 (2015).
61. Joly, S., Garnaud, G., Ollitrault, R., Bokobza, L. & Mark, J. E. Organically Modified Layered Silicates as Reinforcing Fillers for Natural Rubber. *Chem. Mater.* **14**, 4202–4208 (2002).
62. Suki, F. M. M. & Rashid, A. A. Effect of dispersion preparation technique of calcium carbonate (CaCO₃) fillers on mechanical properties of natural rubber (NR) latex films. in 040015 (2017). doi:10.1063/1.4993357.
63. Mousa, A., Heinrich, G. & Wagenknecht, U. Bio-Based Fillers. in *Encyclopedia of Polymeric Nanomaterials* (eds. Kobayashi, S. & Müllen, K.) 1–4 (Springer Berlin Heidelberg, 2014). doi:10.1007/978-3-642-36199-9_285-1.
64. Wang, J., Zhang, K., Bu, Q., Lavorgna, M. & Xia, H. Graphene-Rubber Nanocomposites: Preparation, Structure, and Properties. in *Carbon-related Materials in Recognition of Nobel Lectures by Prof. Akira Suzuki in ICCE* (eds. Kaneko, S. *et al.*) 175–209 (Springer International Publishing, 2017). doi:10.1007/978-3-319-61651-3_9.

65. Bhowmick, A. K., Hall, M. M. & Benarey, H. A. Rubber Products Manufacturing Technology. 915.
66. Krishnan, S., Alex, R. & Kurian, T. HAF/SILICA/NANOCLAY “TERNARY” MASTERBATCH AND HAF/SILICA BINARY MASTERBATCH FROM FRESH NATURAL RUBBER LATEX. *Rubber Chem. Technol.* **87**, 250–263 (2014).
67. Wang, T. *et al.* CEC and its application in off-the-road tires. *Rubber world*, 6 (2003).

CHAPTER 2: Imaging methods for structural
characterization of polymer composites: focus on
FESEM, d-STORM and AFMIR

- 1-Characterization techniques for composite materials: a brief overview**
- 2-Electron Microscopy (EM)**
- 3-EM approach in this study**
- 4-Optical microscopy- a focus on d-STORM**
- 5- d-STORM set-up in this study**
- 6- Atomic Force Microscopy combined with Infrared spectroscopy: AFM-IR method**

Recent advances in imaging technology have had a huge impact on materials characterization, including composites. The aim of this chapter is first to give a brief and not exhaustive overview of composite characterization techniques, and subsequently present the multimodal microscopy approach employed during this study.

1. Characterization techniques for composite materials: a brief overview

From the characterization perspective, there are many techniques that can be used to characterize composite materials. An exhaustive review of all of them is beyond the scope of this subsection, which only aims to a brief introduction to the most used techniques. These methods can be categorized into: space scattering techniques, microscopy techniques, spectroscopy techniques and methods related to mechanical properties as shown in Figure 2.1.¹

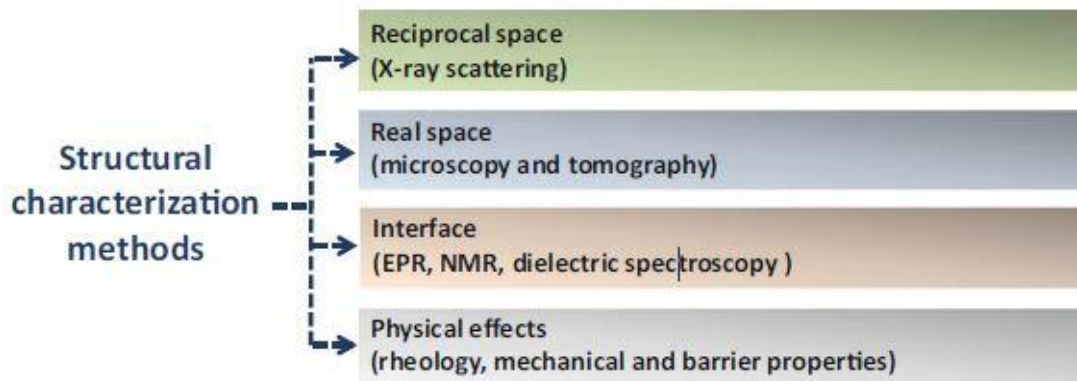


Figure 2.1. Categorization of methods used to analyze composite materials¹.

Scattering techniques such as small angle neutron or X-ray scattering are very powerful methods capable of probing the whole bulk of the sample. Neutron scattering is sensitive to fluctuations in the density of nuclei in the sample, while X-ray scattering is sensitive to inhomogeneities in the electron density. Such methods can be used to characterize the structure of both the polymer matrix and the fillers, either at rest or in a deformed state. In particular, neutron scattering techniques have been used to gain information on both polymer chain configurations and fillers distribution. Remarkable work in this domain has been done by Oberdisse et al².

In terms of microscopy, techniques such as optical microscopy (OM), electron microscopy (EM) and scanning probe microscopy (SPM) play a vital role in the characterization of polymer nanocomposite morphology on different length scale³ (Figure 2.2). Historically, both scanning probe microscopy (comprising scanning tunneling microscopy (STM) and Scanning Force Microscopy (SFM)) and electron microscopy (including Scanning Electron Microscopy (SEM) and Transmission Electron

Microscopy (TEM)) have been privileged due to their intrinsic nanoscale resolution. However, the recent development of novel fluorescence microscopy methods, such as direct Stochastic Optical Reconstruction Microscopy (d-STORM) and Photo-Activated Localization Microscopy (PALM) that allow details below the diffraction limit of light opens new perspective to the use of photonic microscopy in the field of composite and polymer science⁴. All these microscopy techniques have the advantage that data are acquired in direct and real space, whereas scattering methods are measured in reciprocal space.

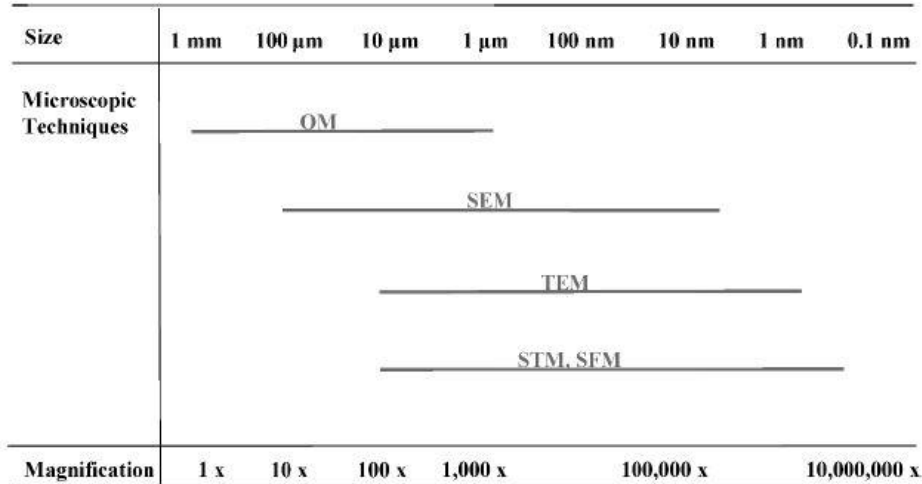


Figure 2.2. Scheme showing the resolution power of different microscopic techniques³.

Elsewhere, Nuclear Magnetic Resonance (NMR), dielectric spectroscopy, electron paramagnetic resonance, Fourier Transform InfraRed spectroscopy (FTIR) are widely used techniques to study interfacial areas and polymer dynamics. Latest developments in NMR have enabled interpretation of the effect of fillers on the chain dynamics of polymers under external stress and high temperature⁵.

Moreover, rheology and physical testing methods are used to determine the mechanical properties of the composite. Typical test used to measure the mechanical properties include tensile, flexural, compression and shear tests⁶.

In this work, we used a set of multimodal highly resolved imaging methods comprising mainly: Field Emission Scanning Electron Microscopy (FESEM), d-STORM and Atomic Force Microscopy coupled with InfraRed spectroscopy (AFM-IR). In addition to these techniques other imaging approaches such as Transmission Electron Microscopy (TEM) and Cryo-Scanning Electron Microscopy (cryo-SEM) were also attempted. The working principles of each of these methods as well as their original approach undertaken in our study are reviewed in the next subsections.

2. Electron Microscopy (EM)

Electron microscopy (EM), as it is understood today, is not just a single technique but a diversity of different ones that offer unique possibilities to gain insights into structure, topology, morphology, and composition of a material. The wealth of very different information collected by various methods is caused by the multitude of signals that arise when electrons interact with a specimen. Gaining a basic understanding of these interactions is an essential prerequisite to interpret the wide variety of information related to an EM study.

Electrons are a type of ionizing radiation that is capable of removing other electrons from the attractive field of the nucleus while transferring some of their incident energy to the individual atoms in the specimen^{7,8}. When an electron hits onto a material, a wide range of secondary signals is usually generated, as summarized in Figure 2.3.

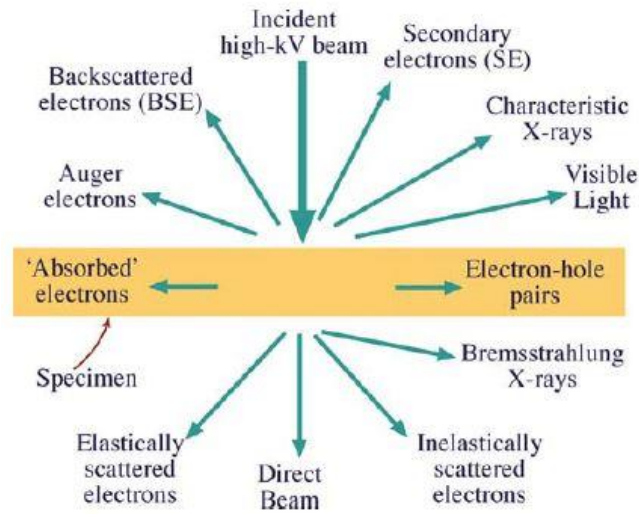


Figure 2.3. Scheme of electron-matter interactions arising from the impact of an electron beam onto a specimen⁷.

Usually, the reactions noted on the top side of the diagram are utilized when examining thick or bulk specimens, while the reactions on the bottom side are those examined in thin or foil specimens. Thick or bulky sample are usually better suited for Scanning Electron Microscopy (SEM) imaging while thin or foil specimen are mostly analyzed by TEM. In this study, SEM constitutes the main characterization technique, but also TEM and Cryo-SEM were approached. All these techniques offer nanoscale resolution mostly due to the wavelength of electrons which is much smaller than that of photons.

Transmission Electron Microscopy (TEM)

TEM produces a high-resolution, black and white image from the interaction that takes place between prepared samples and energetic electrons in a vacuum chamber. Thus, dehydration of the sample is a requirement when using conventional TEM with observation at room temperature. To minimize the effect of drying on samples, several chemical protective agents are often added. Upon contact with the sample, electrons are diffracted and transmitted/scattered⁹. The use of diffracted electrons is usually reserved to solve crystallographic problems and their analysis was not involved in our study. On the other hand, transmitted electrons are used to form a highly resolved image. During their passage through the sample, these electrons can be deflected with different angles based on their interaction with the sample. This interaction is what provides the image contrast as some electrons pass through the sample and others are bounced away. The transmitted electrons are then focused onto a CCD camera to produce an image. Today, TEM constitutes arguably one of the most efficient and versatile tools for the characterization of materials over spatial ranges from the atomic scale, through the ever-growing nanoscale⁷. The main drawback of TEM lies in the need of extremely thin specimen sections (around 100 nm when using operating voltage of 100 kV) to achieve electron transparency as well as the use of staining with heavy atoms to achieve sufficient contrast.

Scanning Electron Microscopy (SEM)

The basic SEM is probably the most versatile instrument in materials science. In SEM, an electron beam is scanned in the X-Y plane of the specimen and the top side interactions shown in Figure 2.3 are generated. These interactions can be divided into two major categories: elastic interactions and inelastic interactions. The first kind is characterized by a negligible energy loss during the collision and a wide-angle direction change of the scattered electron. In SEM, elastic scattering includes BackScattered Electrons (BSE), often used to gain compositional information. On the other hand, inelastic interactions refer to an energy loss of the primary electron beam upon interaction with the sample. The amount of energy loss depends on whether the specimen electrons are excited singly or collectively and on the binding energy of the electron to the atom. As a result, the excitation of the specimen electrons during the ionization of specimen atoms leads to the generation of Secondary Electrons (SE), which are conventionally defined as possessing energies of less than 50 eV and can be used to image or analyze the sample. In addition to SE, a number of other signals are generated by inelastic interactions, including the emission of X-rays and Auger electrons. Like TEM, the use of SEM requires vacuum conditions, and the addition of chemical fixating or contrasting agents is most often a requirement. For this study we employed an original SEM approach, combining a specific chemical fixation method as well as multi-detection mode of electrons: BSE and SE imaging. These particular signals are discussed in more details in the following sections.

Backscattered electrons (BSE)

BSE are high-energy electrons that are produced by the elastic scattering of the primary beam electrons with the atom nuclei (Figure 2.4.) BSE lose a significant amount of energy from the incident beam. Roughly 10–50% of the beam electrons are backscattered toward their source, and on an average these electrons retain 60–80% of their initial energy¹⁰.

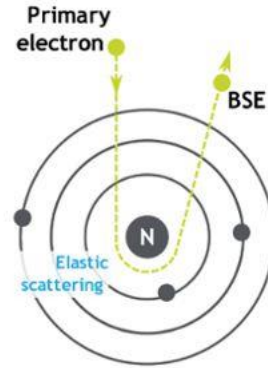


Figure 2.4. Schematic illustration of the formation of backscattered electrons (BSE), source: *Azo materials*.

Backscattering is quantified by the backscattered coefficient η , defined as:

$$\eta = \frac{nBSE}{nB} = \frac{iBSE}{iB} \quad (1)$$

where, nB is the number of incident beam electrons on the specimen, and $nBSE$ is the number of BSE. The same coefficient can be express using currents, where iB is the incident beam current and $iBSE$ is the BSE current. Such coefficient is influenced by several parameters, notably by: the atomic number of the sample, the incident beam angle or tilt angle. Monte Carlo simulations have been a great tool helping to predict the behavior of BSE coefficient in function of the aforementioned parameters. Figure 2.5a shows the backscattering coefficient in function of the atomic number, using different monoatomic samples. The plot shows a general, monotonic increase in the backscatterig coefficient as a function of the atomic number. Typically, heavier elements, because of their bigger nuclei, can deflect incident electrons more strongly than lighter elements. This dependence give rise to an atomic number contrast used in our study after fixation of the sample with vapor of osmium, a heavy element. Due to the osmium affinity for NR, BSE contrast is generated between rubber-like phase and the filler. A second important parameter influencing the BSE coefficient is the incident beam angle or tilt angle. Their relationship has also been investigated by Monte Carlo simulation as it is shown in Figure 2.5b. At very high tilt angles, the BSE coefficient highly increases.

This is due to the fact that at high angles, electrons tend to travel in proximity to the samples surface, limiting the penetration. Thus, they can exit the sample to form BSE electrons. Whereas, at low angles the electrons have more tendency to penetrate the target.

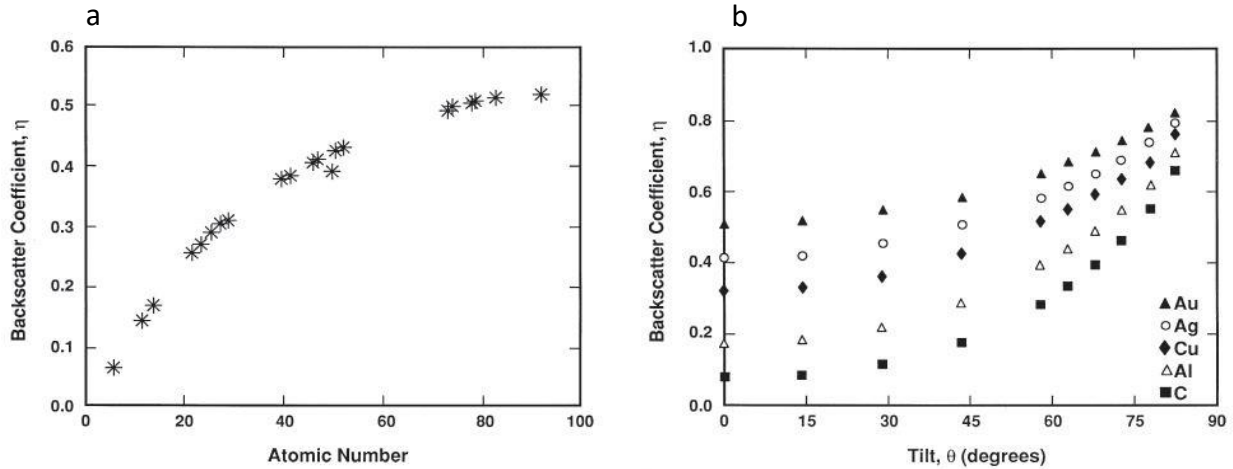


Figure 2.5. Backscattered electron coefficient as function of (a) atomic number and (b) tilt angle¹¹.

Another important consideration when working with BSE refers to the sampling depth. From which max depth arises the information carried by BSE?

First of all, the penetration depth is influenced by the beam energy. As the beam energy increases, the electron beam can penetrate greater depths, generating more BSE, because the electrons enter the specimen with more energy and lose it at a lower rate. The interaction volume in iron is shown as a function of beam energy for the range 10–30 keV in Figure 2.6.

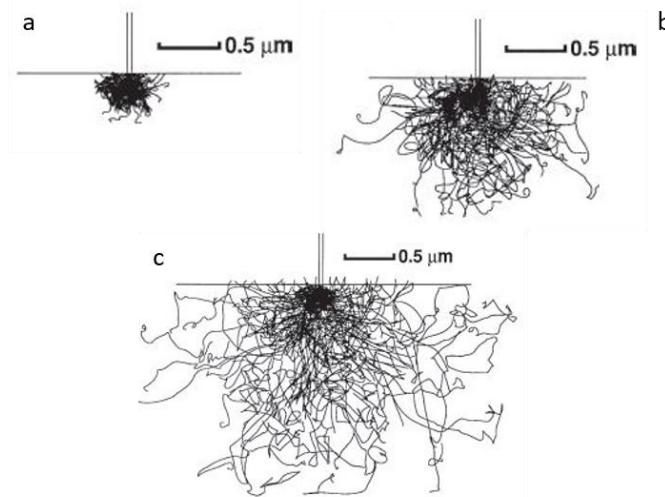


Figure 2.6. Monte Carlo electron trajectory simulations of the interaction volume in iron as a function of beam energy: (a) 10 keV, (b) 20 keV, (c) 30 keV¹¹.

Considering 5 keV, a tension very similar to the ones used in our study, a recent investigation reported the Z-axis backscattered depth distribution function for BSE emissions (Figure 2.7)¹².

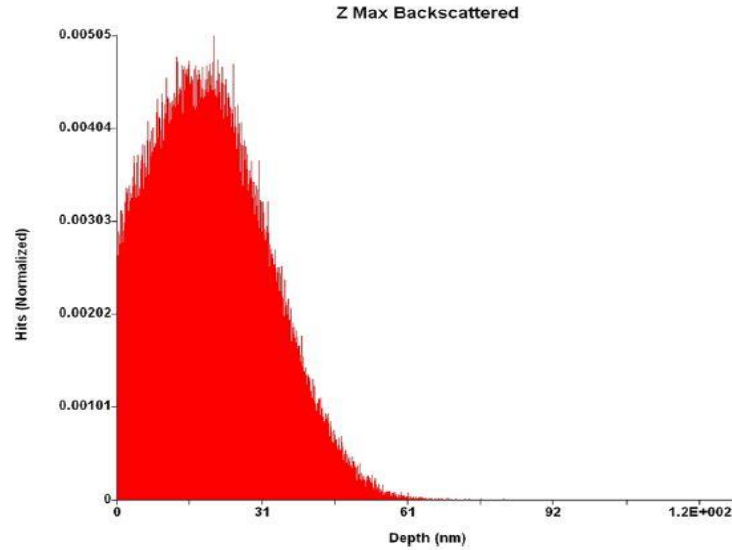


Figure 2.7. Depth distribution function generated from a steel sample, using a tension of 5 keV¹².

Secondary Electrons (SE)

SE are loosely bound outer shell electrons from the specimen atoms which receive sufficient kinetic energy from the incident beam electrons during inelastic scattering of the incident beam to be ejected from the atom and set into motion (Figure 2.8).

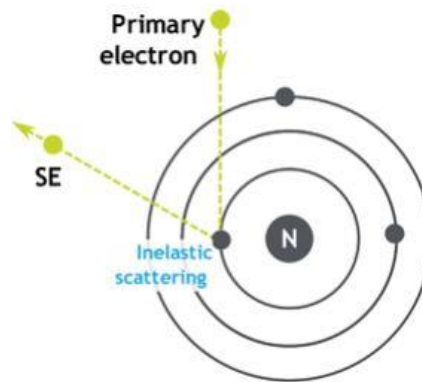


Figure 2.8. Schematic illustration of the formation of secondary electrons (SE), source: Azo materials.

These electrons have typically low energy, with an average of around 3-5 eV. For this reason, they can only escape from a region within a few nanometers from the material surface¹⁰. As in the case of BSE, a secondary electron coefficient is given by:

$$\delta = \frac{nSE}{nB} = \frac{iSE}{iB} \quad (2)$$

where nSE (iSE) is the number (current) of SE emitted from the incident nB (iB), the number (current) of incident beam electrons.

Contrarily to η , δ does not increase while increasing the beam energy, but it decreases instead. The sum of SE and BSE coefficients as a function of the beam energy is shown in Figure 2.9. At high beam energy, typically above 10 keV, the value of δ is very low, but it begins to increase significantly as the beam energy decreases¹¹. This is due to the shallow escape depth of SE. Below 10 keV, the interaction volume decreases, so that increasing fraction of SE are produced near the surface, leading to increasing δ . E_2 represent a cross-over point, where $\eta + \delta$ reaches a value of unity. As the energy continues to decrease, the sum of the emission coefficient reaches a peak. After the peak, the emission decreases for lower beam energies, reaching a second cross-over point, called E_1 . Below E_1 , $\eta + \delta$ decreases with decreasing beam energy. By way of conclusion, SE signal arises from a very low penetration depth, typically in the range of few nanometers. So SE accurately mark the position of the beam and give topographic information.

In contrast to BSE, SE are also very poorly influenced by the atomic number of the specimen, except for carbon which leads to lower SE emission, and gold, leading to a high value of δ .

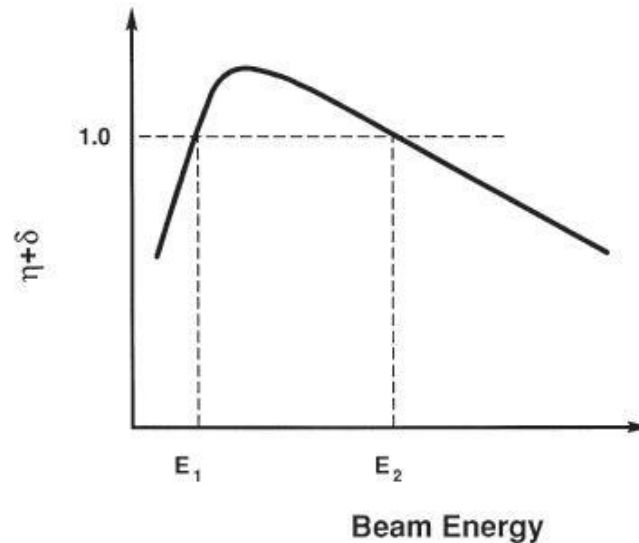


Figure 2.9. Plot of the total emission coefficient as a function of beam energy¹¹.

Cryo-EM

The fast development of EM has enabled unprecedented achievements in the field of life science and materials science. In particular, the 2017 Nobel Prize of chemistry was awarded to three scientists who contributed significantly to develop cryo-electron microscopy (cryo-EM)¹³. Essentially, cryo-EM is a type of EM that allows for the specimen of interest to be viewed at cryogenic temperatures. Such method is very effective in imaging of samples containing moisture. In general, biological molecules form an intact structure in fully hydrated or in partly hydrated form (e.g. when embedded in a lipid membrane) and generally perform their function with large areas of their surface exposed to aqueous environment. The primary advantage of cryo-EM techniques is that it allows to observe such structure in their near-native environment, without the use of chemical fixating or contrasting agents. In the cryo-EM procedure, specimens are created by rapid freezing of biomolecules in solution and loaded into the column of an electron microscope operating at high-vacuum and at low temperature to keep the ice in amorphous state. This procedure has three distinct advantages over chemical fixation: (i) it is achieved within milliseconds and it ensures simultaneous immobilization of all macromolecular components; (ii) it can facilitate the study of dynamic processes while sublimation of the sample occurs inside the microscope chamber; (iii) it lowers samples induce radiation damage without the use of coating agents. Cryo-EM can be used for structure determination of isolated biomolecular complexes across a wide molecular mass range from proteins with several tens kilo-Daltons to virus particles with many mega-Daltons and to whole cells^{14,15}. Additionally, once the sample is frozen it is usually fractured before analysis on the microscope. Such fracture, especially in Cryo-SEM, exposes surfaces that might otherwise remain obscure or not accessible.

3. EM approach in this study

The aim of this subchapter is to report the EM approaches used during our work. Not only the specific technique that led to the main conclusions or hypothesis, but rather a complete set of imaging methods used to attempt nanoscale understanding of our system. Therefore, a brief outcome of the micrographs obtained with each imaging technique as well as pros and cons for imaging our system are discussed along the sections.

EM- sample preparation

Samples were prepared by mixing an aqueous suspension of fillers (Si or CB) with NR latex. In terms of concentration of components, two main approaches were investigated:

□ (a) **CONCENTRATED PROTOCOL**: High ammoniated NR latex with 60wt% in rubber was mixed with a slurry of fillers (silica/CB) (silica: Kisker Biotech, 100nm) (CB: N234) at 5wt%. In case of silica, the slurry was prepared in ionic suspension composed of magnesium sulfate (MgSO₄) (Sigma-Aldrich) with ionic strength of 0,1 M. In both cases, the mixing gives rise to instant coagulation, and further formation of a composite after evaporation of the solvent (Figure 2.10).

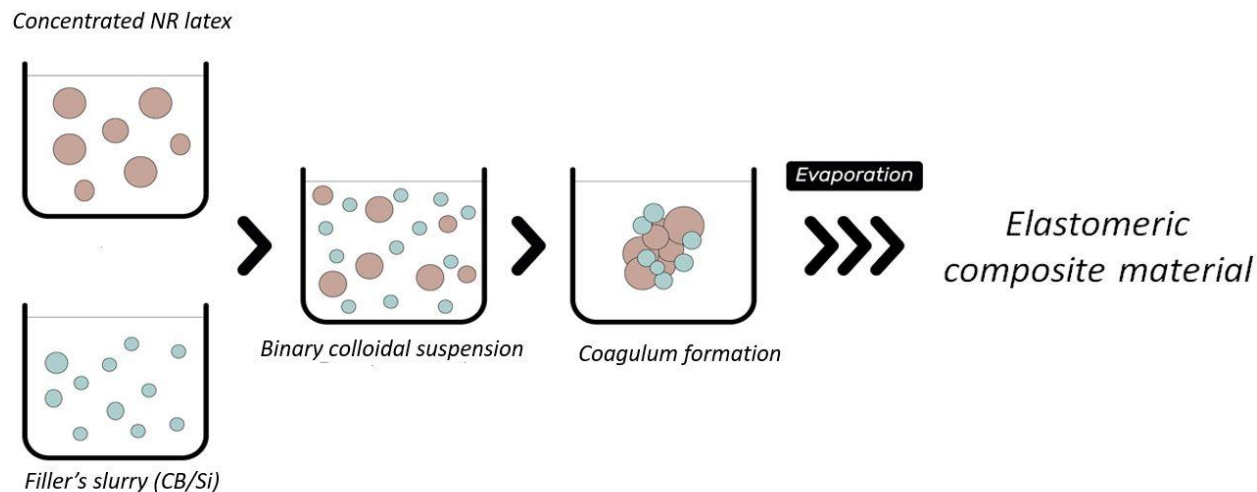


Figure 2.10. Schematic illustration of coagulum and composite formation using the concentrated protocol.

□ (b) DILUTED PROTOCOL: High ammoniated NR latex was diluted to 0.075 wt% (to visualize individual rubber particles) and then combined with an aqueous suspension of fillers, to obtain a binary colloidal suspension. Immediately after mixing, 100 μL of this suspension were deposited on the microscope support (grid/coverslip/cupule), resulting in a casted drop with a spherical cap shape. In these conditions, flocculation occurs on the deposited drop inducing a phase-separation, giving rise to a coagulum, macroscopically visible after 1h from deposition ($t=1\text{h}$). At $t=24\text{h}$, after complete solvent evaporation, a composite is then obtained (Figure 2.11).

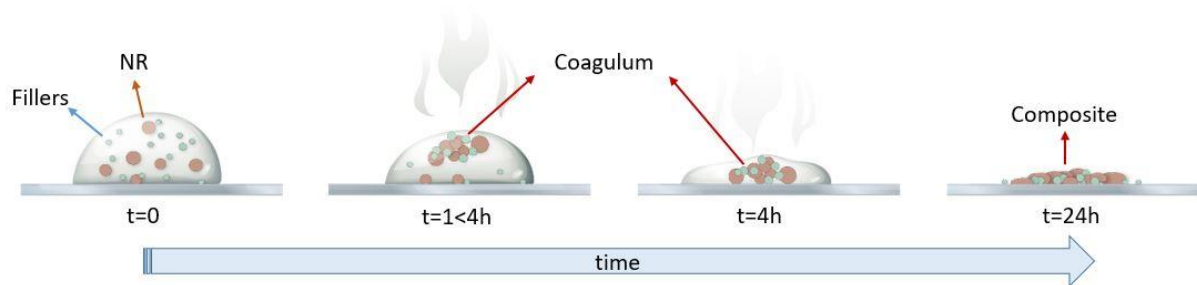


Figure 2.11. Schematic illustration of coagulum and composite formation after the deposition of the binary colloidal suspension on the glass coverslip.

Cryo-SEM: an attempted approach to structurally characterize the system

To approach the industrial protocol, we first attempted to structurally characterize the coagulum produced with the concentrated protocol. Cryo-SEM was chosen as technique to investigate the nanostructure of the formed material. The specimen preparation involved insertion of a small portion of the formed coagulum in cupule carriers, and subsequent high-pressure freezing. Such type of freezing method is currently the only method available to vitrify “thick” sample (up to $200\mu\text{m}$)¹⁶. The

high-pressure freezing machine (EM HMP100, Leica) consisted of a largely automated system with an integrated workstation. The optimum pressure of 2100 bar needs to be applied to the sample which solidifies within 8-10 ms, followed by immediate rapid cooling to at least -140 °C to prevent the introduction of artifacts caused by high pressure. Freezing at this pressure theoretically prevents ice crystal formation (Figure 2.12). The centerpiece is a versatile cartridge, consisting of highly durable polymer pieces. The assembled cartridge holds the specimen carrier sandwich (or other container) and guides it automatically through the freezing process, finally releasing cartridge, carriers, and sample in liquid nitrogen. This guarantees that the whole freezing sequence from pickup of the specimen to liquid nitrogen is consistent and reproducible.

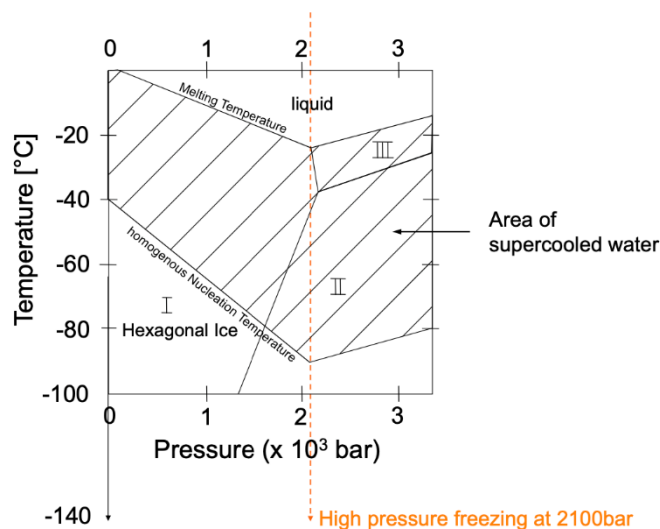


Figure 2.12. Diagram showing the stable states of water depending on pressure and temperature. At 2100 bar water can be rapidly cooled to -140 °C changing to a very viscous liquid. I, II and III show ranges in which water is present as hexagonally oriented ice, or ice crystals. Source: EM HMP100 Leica manual.

Typical cryo-SEM micrographs of the fracture sample showing the structure of the coagulum obtained mixing a slurry of Si with NR latex using the concentrated protocol are shown in Figure 2.13. The images coagulum shows a fiber-like organized matrix in which few NR particles are deposited up-on. In Figure 2.10c, the colloidal form of few LRPs and Si fillers can be noticed. However, the very few amount of NR particles led to a difficult interpretation of the image. With the aim to visualize more individual NR particles, cryo-SEM was also employed to structurally characterized the binary colloidal suspension obtained with the diluted protocol. This time, high-pressure freezing was applied on the binary colloidal suspension, but unfortunately results did not lead to the visualization of NR globules and fillers. The high amount of frozen solvent hindered the visualization of the particles. Overall, although the advantages previously reported using cryo-EM techniques, the constraint encountered while employing such methods led us towards the employment of both FESEM and TEM with a prior chemical fixation method.

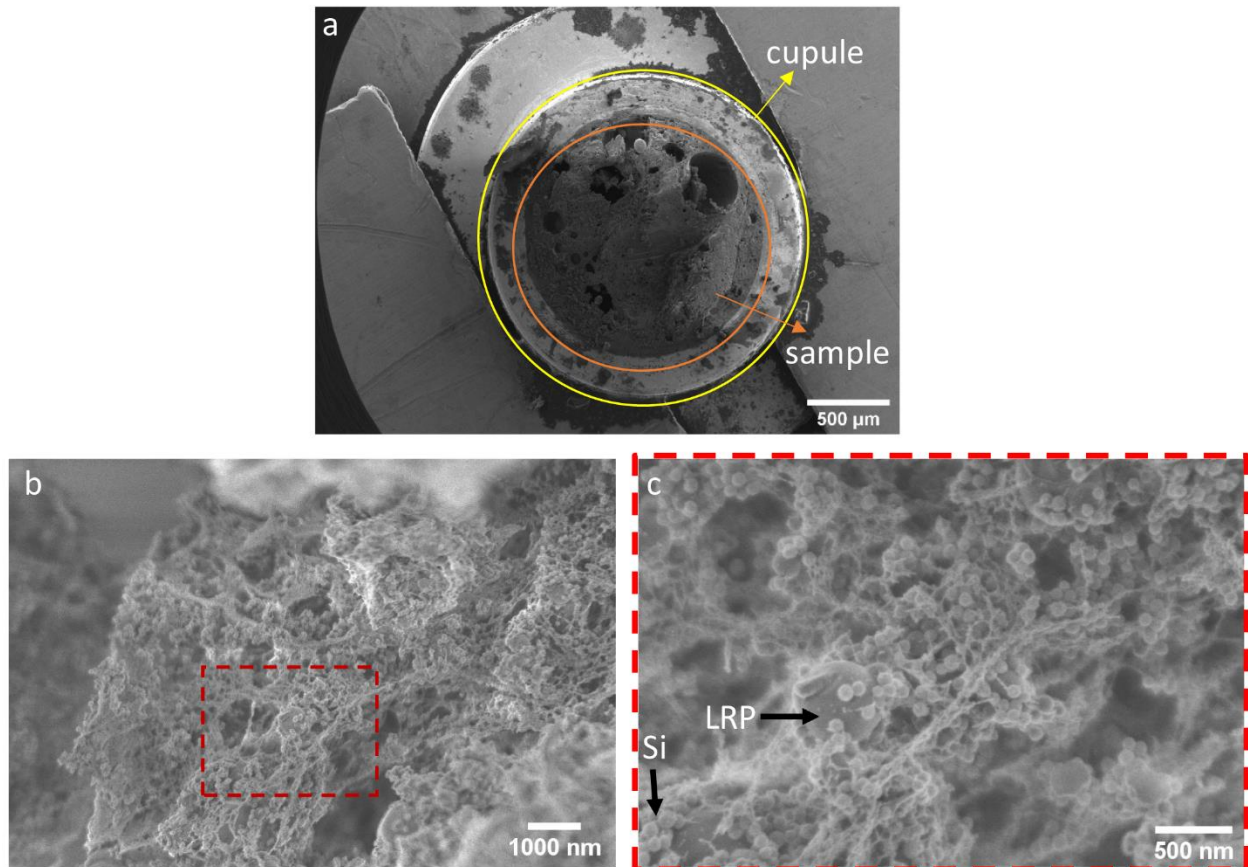


Figure 2.13. Cryo-SEM micrographs of coagulum prepared with concentrated protocol. (a) Large view. (b) Typical view of an inner fractured plane of the sample. (c) Magnified view of the boxed region in b.

Chemical fixation: preparation for TEM and SEM

As previously mentioned, the employment of SEM and TEM requires dehydration of the sample during preparation and observation condition. For this reason, the use of fixating and contrasting agents is most often required when using these techniques. One of the originalities of our EM approach lies on the chemical sample's fixation using vapor of osmium tetroxide. This agent acts not only as fixative, but also as an electron dense stain, and this is one of its major advantages over most known fixatives.

Osmium tetroxide is a powerful oxidizing agent and is extremely volatile; it melts at 41°C to give a pale yellow liquid which boils at 131°C¹⁷. It is generally believed that fixation of cell membranes by osmium tetroxide involves unsaturated lipids¹⁸. The presence of a double bonds in the lipid molecule appears to be a prerequisite to any reaction between lipids and osmium. One molecule of osmium reacts with one double bond, leading to the formation of a cyclic osmic acid monoester. This monoester is not very stable and it is easily hydrolyzed reacting with diols, giving rise to a stable diester, as shown in Figure 2.14.

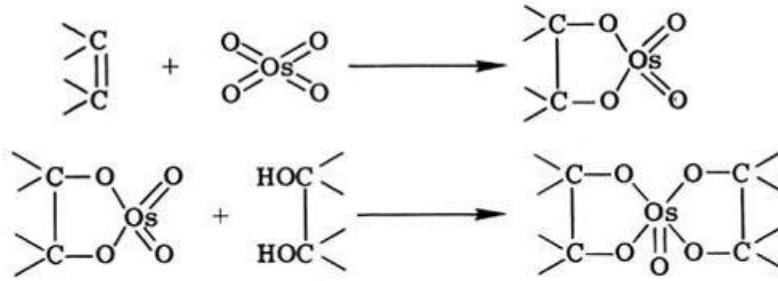


Figure 2.14. Reactions occurring during fixation of lipids with osmium tetroxide.

Very little is known about the interaction between osmium tetroxide and proteins. However, there is evidence that osmium tetroxide has a fixative cross-linking function on tissue protein and that protein-lipid crosslinking may occur in systems where these components are intimately mixed¹⁸.

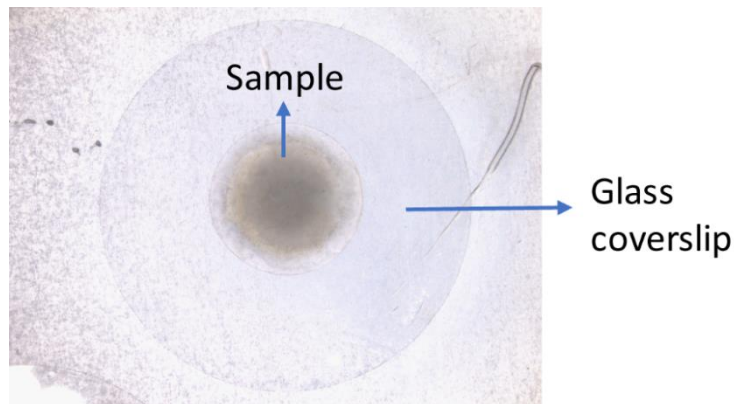


Figure 2.15. Complete chemical fixation with osmium tetroxide shown on sample deposited on glass coverslip.

To avoid immersion and direct contact of the specimen with the osmium tetroxide solution, vapor fixation has been employed. To do so, a 1% solution of osmium tetroxide was prepared extemporaneously. Subsequently, drops of osmium tetroxide were deposited around the sample's support placed in a hermetic box protected from light. After 30 minutes, the specimen showed a black color indicating the presence of reduced osmium, and fixation was considered complete (Figure 2.15).

This type of fixation can be applied at any stage, independently to the degree of solvent evaporation, allowing to preserve the structure of either NR particles, fillers, or the resulted coagulum and composite. A typical SEM micrograph showing the structure of NR globules obtained after fixation with osmium tetroxide is shown in Figure 2.16a. In comparison, when no fixation is applied, the colloidal structure is shown as collapsed (Figure 2.16b).

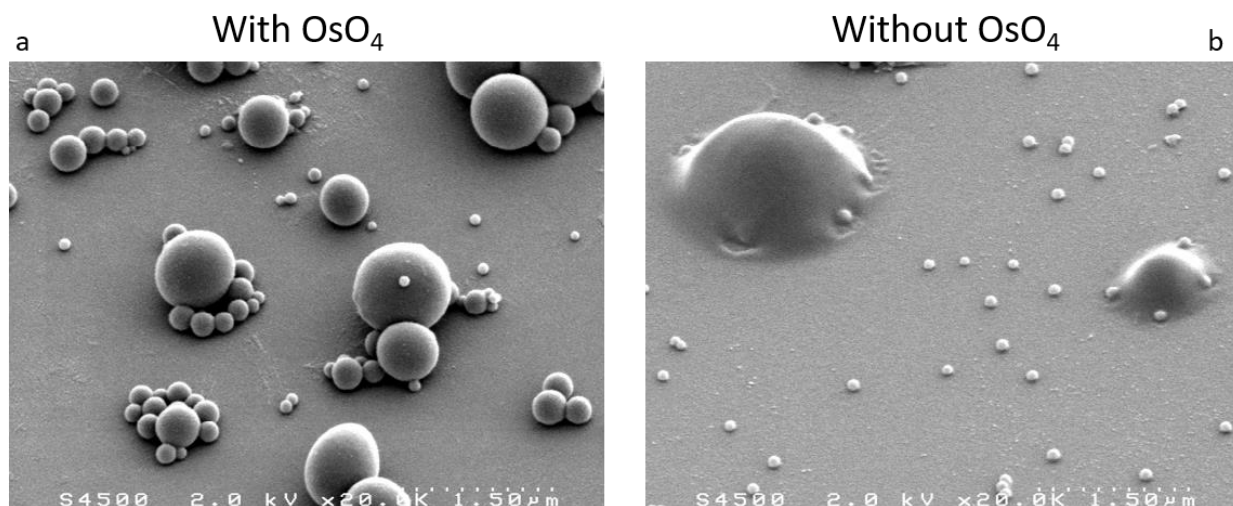


Figure 2.16. SEM micrograph showing the structure of NR globules obtained (a) post osmium tetroxide fixation and (b) without the use of any fixating agents.

Additionally, in the case of SEM, because of the high affinity of osmium tetroxide for NR, this type of fixation allowed us to exploit BSE imaging based on chemical contrast. This is one of the advantages in the use of SEM imaging over TEM as presented in the next subsection.

TEM vs SEM

After chemical fixation, both TEM and SEM imaging were employed to study our system. The aim of the subsection is to present both approaches, showing typical images, and to discuss advantages and disadvantages of the corresponding techniques for imaging our system.

Our TEM approach consisted in the deposition of the NR-filler binary colloidal suspension on formvar/carbon grids and consequent fixating with osmium tetroxide at different evaporation stages. Typical TEM micrographs showing the structure of the fixed NR-Si binary colloidal and the obtained composite material after complete solvent evaporation are shown in Figure 2.17a and Figure 2.17b, respectively. Please note that, the structural transition between the two stages is one of the main point of our work and it will be discussed in chapter 3 and chapter 4. Herein, the discussion is limited on the advantages and drawbacks of the techniques. During imaging of the binary colloidal suspension with TEM, LRPs can easily be distinguished, while SRPs and Si fillers show similar opacities. On the other hand, the composite material showed the major presence of tiny filaments, probably relating to polyisoprene chains. Although the high resolution allowed imaging of the polymer chains, it is not easy to distinguish Si fillers. Additionally, because of the accumulation of the information along the z-axis, it is not possible to understand the topography of the sample.

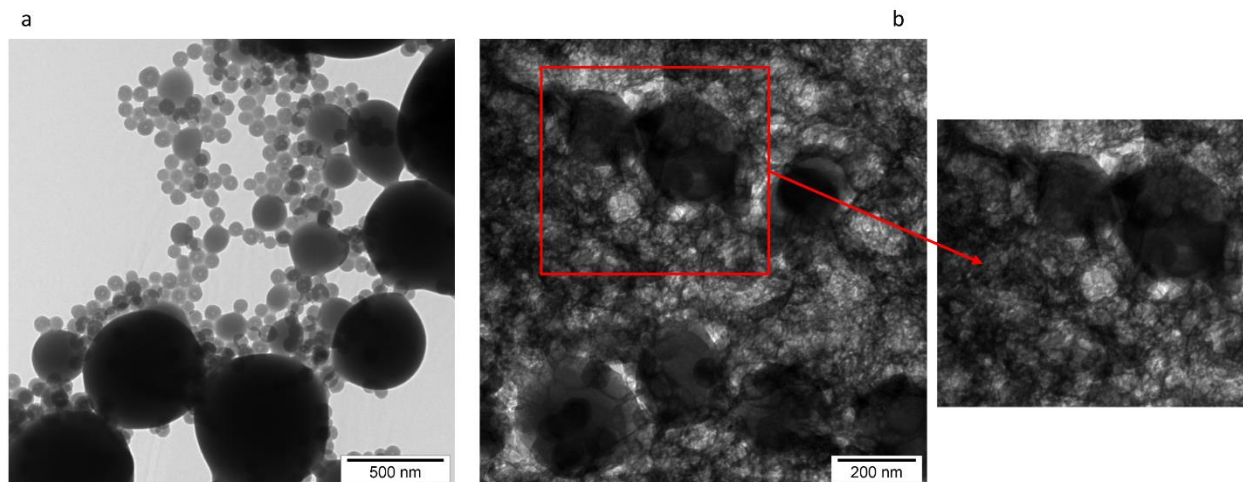


Figure 2.17. TEM micrographs of NR-Si obtained after fixation of (a) binary colloidal suspension and (b) the resulting composite after complete solvent evaporation.

One of the main differences between SEM and TEM relies on the choice of the support for the deposition of the sample. When using TEM, it is very often necessary to deposit the sample on grids, whereas the employment of SEM allows a more flexible choice for supports. Glass coverslip can be used when working with SEM, while they cannot be used for TEM. Another difference concerns coating often applied when using SEM, to avoid overcharging effects while imaging. In this work, 10 nm carbon layer were deposited on the sample by double thread evaporation in high vacuum (10⁻⁵ mbar) with an ACE600 device (Leica, Germany). Typical SEM micrographs, exploiting both SE and BSE signals, obtained by post fixation and coating of the NR-Si binary colloidal suspension deposited on glass coverslips and corresponding composite are shown in Figure 2.18. Please note that, the reported example involves Si fillers, but similar conclusion can be made when working with CB. In both cases, SE allows to understand the topography of the sample by analysis of the SE signal, while the BSE signal exploits chemical contrast. By combining the information given from both signals, we can now more easily distinguish osmium-labelled NR globules from Si fillers, as well as LRPs from SRPs (Figure 2.18a and Figure 2.18b). Moreover, the use of SEM gives access to information on the distribution of fillers in the resulting composite (Figure 2.18c and Figure 2.18d). Additionally, the less cumulative z information allowed to better understand the structural transition from the binary colloidal suspension to the resulting composite, one of the major aims of our study.

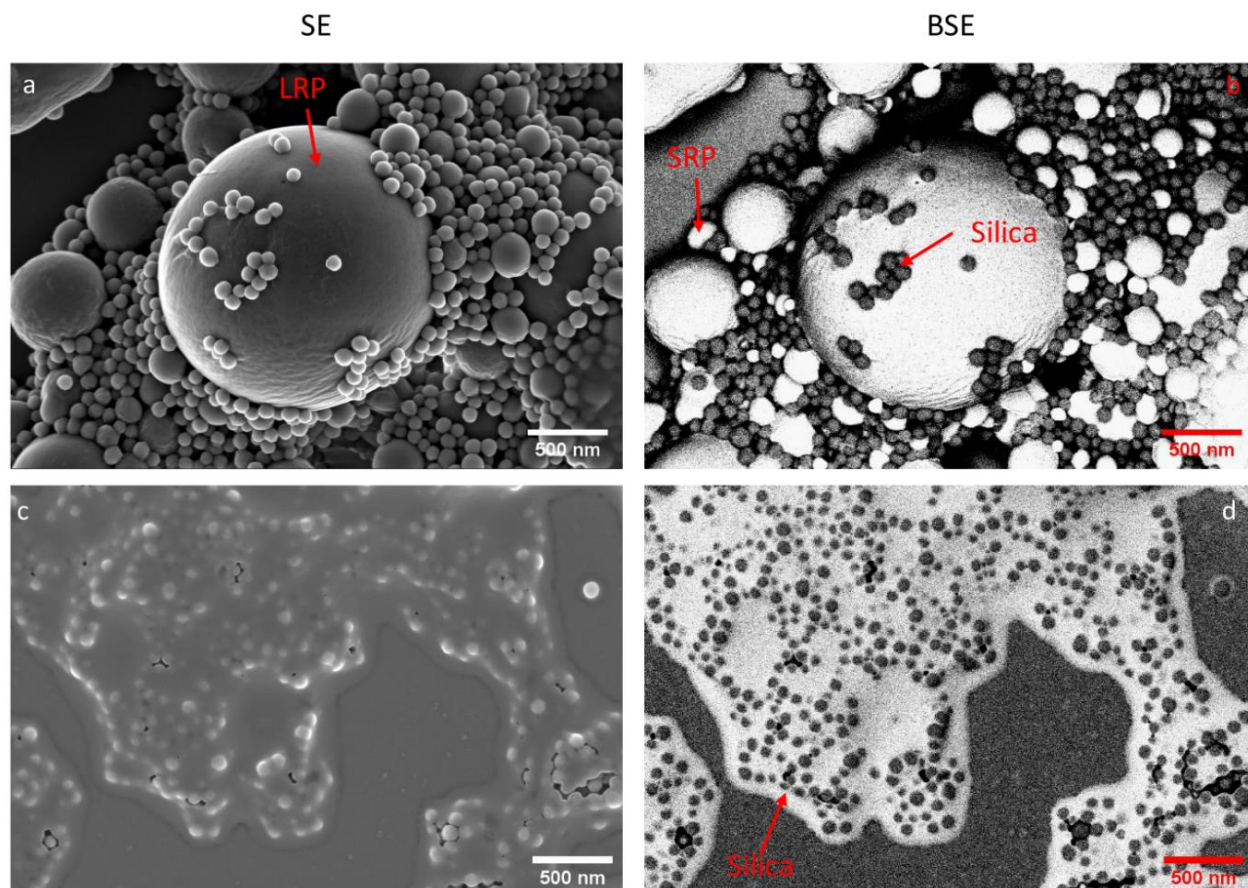


Figure 2.18. SEM micrographs of NR-Si obtained after fixation and coating of binary colloidal suspension and its resulting composite. (a) SE and (b) BSE image of the binary colloidal suspension. (c) SE and (d) BSE image of the resulting composite obtained after complete solvent evaporation. Si fillers appear dark in BSE images.

By way of conclusion, advantages and drawbacks of TEM and SEM employment in our study are summarized in Table 2.1. TEM offers high magnification and the best resolution. However, the z cumulative information prevents to access the topography. On the other hand, SEM has several advantages over TEM. These main advantages refer to (i) the possibility to access the topography, (ii) the combination with BSE imaging, (iii) access to distribution of fillers in the composite and (iv) a flexibility in the use of several supports.

For these reasons, the original SEM approach described was chosen as main EM technique employed in the study.

Table 2.1. Advantages and drawbacks of TEM and SEM as imaging techniques of our system.

TEM	SEM
<p style="text-align: center;"><u>Advantages</u></p> <ul style="list-style-type: none"> -Best resolution -Visualization of polyisoprene chains 	<p style="text-align: center;"><u>Advantages</u></p> <ul style="list-style-type: none"> -Topography - Possibility of BSE imaging - Distribution of fillers in composite - Flexible adaptation to supports (grids, glass)
<p style="text-align: center;"><u>Drawbacks</u></p> <ul style="list-style-type: none"> -Not easy to distinguish between Si fillers and SRPs - z cumulative information - Necessarily to work with thin samples -Not flexibility in the use of several supports (not possible with glass coverslip) 	<p style="text-align: center;"><u>Drawbacks</u></p> <ul style="list-style-type: none"> -Necessity of coating - Very surface related information - Slow imaging (slow scan + line average)

FESEM workstation

Since the first commercial product development by Cambridge Instruments in 1965, the SEM has been improving in terms of resolution, image contrast and operability, etc., to show remarkable progress in today's instruments. A high brightness electron source is essential for attaining high resolution SEM. In 1968, Prof. A.V. Crewe of the University of Chicago developed the field emission (FE) electron source. Using FE source, electrons are extracted by the intense electric field which provides 1000 times higher brightness than a conventional thermionic electron source with tungsten filament¹⁹. The FE electron gun source was then commercialized giving rise to the FESEM era.

In this work, FESEM was performed using a Gemini500 (Zeiss, Germany) driven by SmartSEM (version 6.3), operating in high vacuum (10^{-6} mbar in the observation chamber). In the set-up, electrons are extracted by the electric field and they are accelerated at a voltage ranging from 0.02 V and 30 kV to be focused on the sample by the use of a condenser and objective lenses (nano-twin objective lens system). The image area is irradiated by the electrons in a sequential pattern, controlled using scanning coils (Figure 2.19a). SE signal was collected with the corresponding in-lens detector located beyond the objective lens. BSE signal were collected with the Energy Selective BSE in lens detector using filtering grid > 400 V to filter out SE signal. The detection efficiency of this type of detector results from its geometric position in the beam path and from the combination with the electrostatic/electromagnetic lens (Figure 2.19b).

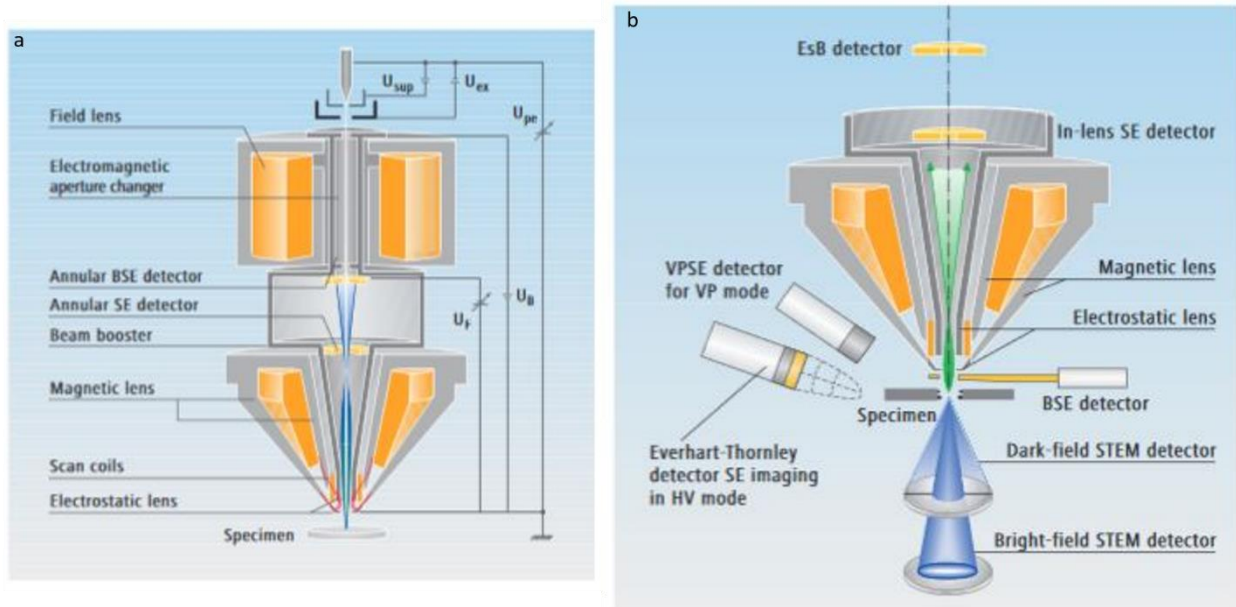


Figure 2.19. Simplified schematic illustration of the FESEM setup. (a) Main elements of the set-up. (b) Magnified view of the detection system²⁰.

4. Optical microscopy- a focus on d-STORM

Recent advances in fluorescence microscopy, together with a large panel of fluorescent probe have undoubtedly transform life sciences investigations. However, adoption of these techniques by materials science has been at a slower pace. Nanoscale imaging of materials has been mostly performed with EM or SPM. With the advent of super-resolution microscopy (or nanoscopy), which typically offers a spatial resolution of tens of nanometers, the resolution gap between fluorescence imaging and EM/SPM is closing⁴. This improvement opens new opportunities, to unravel new insights in structures of materials. In this work, commonly employed fluorescence protocol and techniques applied in biological studies (confocal and d-STORM microscopy) were transposed to the field of polymer composites. This subsection reports the fundamentals fluorescence microscopy, followed with a description of the employed fluorescence imaging methods.

Fundamentals of fluorescence spectroscopy and microscopy

When light interacts with matter, several processes may occur at molecular level depending on the physical and chemical properties of the sample (Figure 2.20a). The processes involved in an absorption and emission of light are usually well described using the Perrin-Jablonski diagram (Figure 2.20b): first molecules undergo transition from ground (S_0) to an excited state (S_1, S_2, \dots, S_n) by absorbing photons of appropriate wavelengths corresponding to the energy gap between the ground and the excited states. Once the molecule is in its excited state, there are several possible de-excitation pathways are available. In particular, the return to the ground state can occur non radiatively (wavy arrows in Figure 2.20b) or radiatively from either the first singlet excited state (fluorescence) or the singlet triplet state (phosphorescence). Thus, when a molecule returns from S_1 to its ground state S_0 while emitting photons, it fluoresces. The photon emission for these states occurs from the lowest vibrational sate, thus the energy of the emitted photon will always be less than the one of the incident photon. This results in a fluorescence emission spectrum shifted to higher wavelengths than that of the absorption spectrum. The shift between the maximum of the first absorption band and the maximum of fluorescence is called Stokes shift²¹. This is a very important parameter in the selection of fluorescent probes for fluorescence microscopy. As described below, experimentally it is necessary to separate the fluorescence emission form the absorption and thus the use of fluorophores with large Stokes shift is preferred.

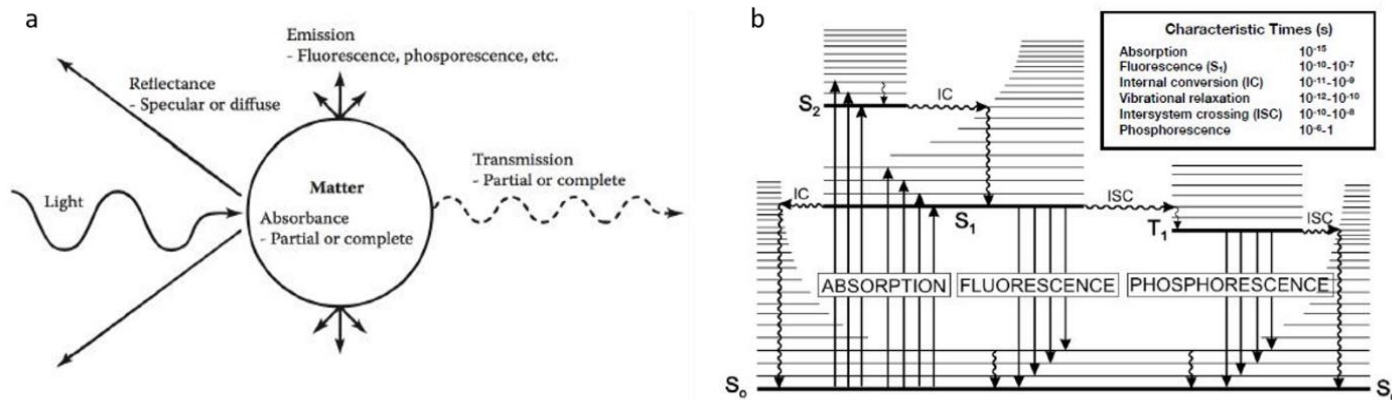


Figure 2.20. (a) Possible interaction between light and matter. (b) Perrin-Jablonski diagram and the characteristic times of the different processes. Straight arrows denote radiative process and wavy arrows denote non-radiative processes²¹.

Confocal laser scanning fluorescence microscopy

The golden age of fluorescence microscopy came with the development of laser scanning microscopy in the 1980s, and further use of Confocal Laser Scanning Microscopy (CLSM). *Confocal* means that the image is obtained from one focal plane only, while any noise resulting from any other planes is removed. On the other hand, *laser scanning* means the images are acquired point by point under localized laser excitation rather than wide field illumination, as in conventional fluorescence microscopy. To eliminate the noise resulting from the planes other than the focal one, two optically conjugated pinholes are integrated on the excitation and detection pathways (Figure 2.21)²². In this way, confocal microscopy is able to minimize “pollution” of the fluorescence signal by adjusting the size of the pinhole: the smaller the pinhole, the narrower the depth of the in-focus field.

Even though resolution is somewhat enhanced with confocal microscopy over conventional wide field techniques, the fluorescence emitted by a point is not imaged to a point in the detection, but it is spread by diffraction. This pattern refers to as Point Spread Function (PSF). The result of this phenomena is an image of the point source that is much larger than the actual size of the object. The size of the PSF determines the lateral and axial resolution. It depends on the numerical aperture of the objective, on the light excitation wavelength and on the fluorescence wavelength of the fluorescent particle. Typically, in the visible domain, the lateral resolution is of few hundreds of nanometers (200-400 nm) and the axial resolution of some micrometers (3-5 μm).

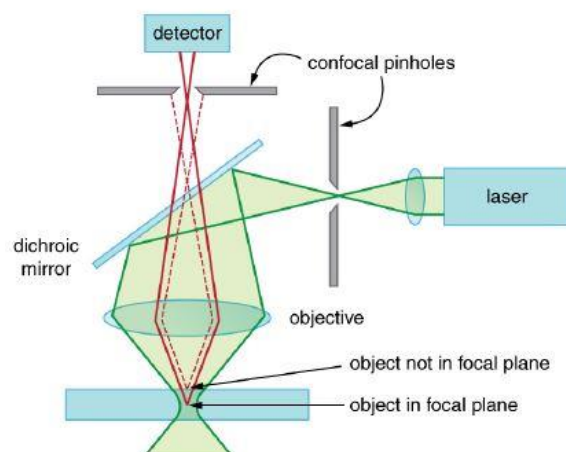


Figure 2.21. Schematic illustration of the main elements of confocal laser scanning microscopy (CLSM).

Although very few studies have employed CLSM to investigate the structure of NR²³, our group has successfully employed CLSM to identify some important parameters for NR- Si fillers aggregation during the liquid route²⁴: importance of ionic medium, size of the filler particles, filler/rubber volume percent ratio. To do so, fluorescent Si particles were used, while NR can be seen by transmission images. However, the method fails to distinguish the spatial distribution of proteins from the one of the lipids and their localization in respect to Si fillers as illustrated in the Figure 2.22, where proteins and lipids appeared as co-localized in an aggregate.

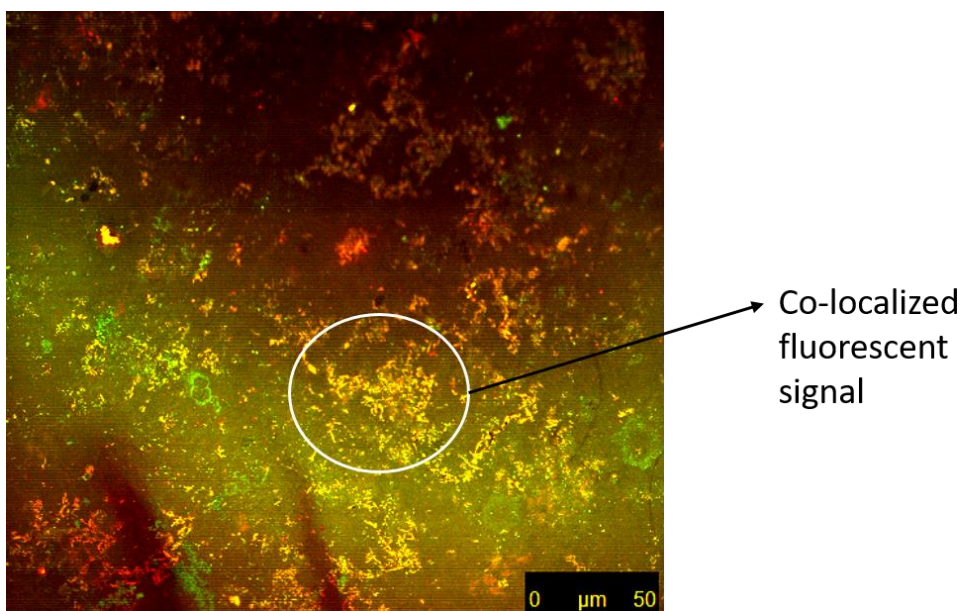


Figure 2.22. Fluorescence intensity image (acquired on a Confocal microscope) on adhered NR – 100nm plain Silica heteroaggregate, with fluorescent labelling of proteins (red) and lipids (green) of NR. The image shows a co-localized signal for proteins and lipids (yellow part).

Super-resolution fluorescence microscopy

Super-resolution fluorescence microscopy is the term commonly given to fluorescence techniques with resolution that are not limited by the diffraction of light. The super-resolution microscope, development of which won the 2014 Nobel Prize in Chemistry, has been widely employed for biomedical applications but nowadays an increasing number of laboratories are starting it to study materials⁴. However, adoption of super-resolution fluorescence microscopy by materials science has been at a slow pace. Nanoscale imaging of materials is typically performed by electron microscopy or scanning probe techniques. While these techniques offer an unrivalled resolution, they have limitations concerning the labeling and distinction of biological and chemical elements. To date, super-resolution methods can be separated into two categories. The first one concerns deterministic methods based on patterned excitation (or depletion), including STimulated Emission Depletion (STED) microscopy, Ground State Depletion (GSD) microscopy²⁵ and (saturated) structured illumination microscopy ((S)SIM)²⁶. The second one concerns stochastic methods based on single molecule localization, such as (fluorescence) Photo Activated Localization Microscopy ((f)PALM), (direct) STochastic Optical Reconstruction Microscopy ((d)STORM) and Points Accumulation for Imaging in Nanoscale Topography (PAINT). The group of these techniques fall under the common name of Single Molecule Localization Microscopy (SMLM).

In this study we employed d-STORM imaging method.

d-STORM imaging

In this subsection we will introduce the principle of d-STORM and briefly discuss the protocol designed for the experiments.

d-STORM imaging relies on three key points: (i) the use of photo-switchable fluorescence probes, called fluorophores, (ii) stochastic activation and temporal separation of the fluorescence signal to separate single molecules in space and time, and (iii) single molecule localization²⁷. To achieve stochastic photo-switching, the probes are modulated between an “ON” and “OFF” state (Figure 2.23). When most of the fluorophores are forced to reside in a long-lasting dark off-state, only a small subset in the on state emits fluorescence at a given time²⁸. In each single image, the PSF of single molecules is approximated with a Gaussian function, and it provides information on the localization of the probe. By sequentially imaging typically several thousand subsets of spatially distinguishable fluorophores, all of the emitters are detected over time, and an artificial image can be reconstructed. As a result, d-STORM and similar methods provide a list of single-molecule coordinates, which is in contrast to conventional microscopy techniques which provide intensity information directly.

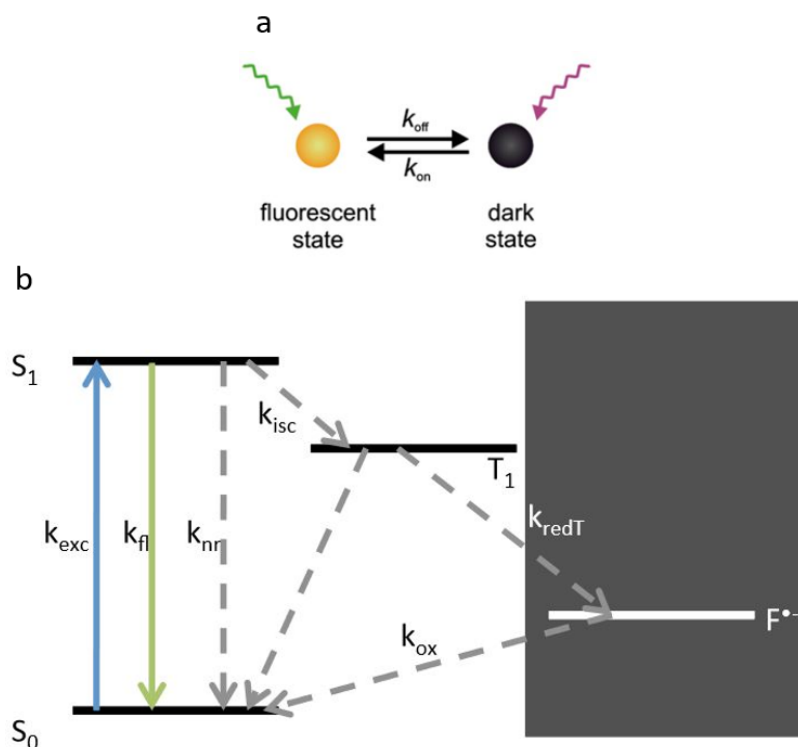


Figure 2.23. Schematic illustration of *d*-STORM principle. (a) Photoswitchable fluorophores are transferred from a fluorescent bright state into a non-fluorescent dark state. (b) Perrin-Jablonski diagram associated with photo-switching occurring during (*d*)STORM. The left white part is the normal Jablonski diagram with the associated ground state S_0 , excited state S_1 and triplet state T_1 . Corresponding rates are the excitation rate k_{exc} , emission rate (k_{fl}), non-radiative decay rate k_{nr} and inter-system-crossing rate k_{isc} . The $F^{\bullet-}$ denotes the radical anion dark-state.

As briefly mentioned in subsection 3.1, when a fluorophore accesses its excited state, besides relaxing directly to the ground state through either photon emission or non-radiative internal conversion, it can release its excess energy by undergoing several other intramolecular and intermolecular processes. Through the intramolecular transition process known as intersystem crossing, fluorophores can reach an intermediate energy state called the triplet state (T_1). Such state has a much longer lifetime than the fluorescence state, typically several microseconds. Once in this state, and in the presence of a reducing agent which match the redox potential of the fluorophore, an electron transfer reaction can occur. The result of such a reaction can be a non-fluorescent radical state ($F^{\bullet-}$) in which it can remain for several seconds or minutes²⁹. This radical state represents the non-fluorescent OFF state of the probe. Upon reaction with molecular oxygen or irradiation with UV light, the molecule returns to the ground state, and fluorescence is recovered.

The rate for the transition from the fluorescent ON-state into the non-fluorescent OFF-state is controlled by the concentration of the reducing agent as well as the intensity of the excitation source. The reducing agent is contained in the imaging buffer. Commonly used reducing agents are: mercaptoethylamine³⁰, dithiothreitol³¹, and glutathione³¹. In addition to the reducing agents, other

chemicals are also added. In particular, the imaging buffers rely on an enzymatic oxygen scavenging system³². In fact, molecular oxygen plays an important role in many of the fluorophore's electronic state transition. Since the ground state of molecular oxygen is also a triplet it easily reacts with a triplet-state fluorophore in an electron transfer reaction. This can return the fluorophore to its ground state, but it also produces singlet oxygen and reactive oxygen species. To avoid so, oxygen must be removed from the imaging solution by adding enzymatic systems such as combination of glucose oxidase, glucose, and catalase.

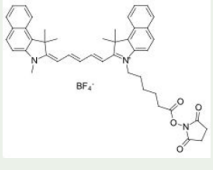
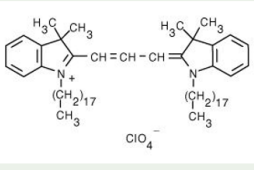
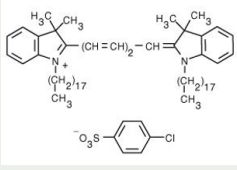
Another important point to consider when performing d-STORM refers to the choice of the fluorophore. The chosen fluorophore should be as bright as possible to ensure that sufficient signal is detected and distinguished from the background noise. Additionally, the non-fluorescent dark times of fluorophores must be long enough to guarantee the separation of single-molecules signals. The dye Alexa Fluor 647 is a typical fluorophore of choice for SMLM studies, due to its robust photoswitching and good photons yield. The latter parameter has a direct influence on the accuracy of SMLM measurements. Several formulas have been introduced to estimate the resolution of SMLM measurements^{33,34}. For high signal to noise ratio, the resolution limit of SMLM can be simplified to

$$d_{SMLM} = \frac{d}{\sqrt{N}} \quad (3)$$

Where d is the conventional resolution limit and N is the number of photons detected in a single fluorescence spot²⁸.

In our study, we were interested with fluorescent probes capable to independently target proteins and lipids of NR and silica fillers. The latter were purchased fluorescently stained from Kisker-biotech. Although the company did not reveal the specific type of fluorophore used they disclosed that its position is located in the inner part of the silica particle rather than on its surface. For the labelling of proteins, click chemistry was exploited. Specifically, we used a cyanine 5 (Cy5) fluorophore carrying a NHS ester group capable to react with primary amines groups of proteins under aqueous condition forming a stable amide bond. On the other hand, affinity based-labelling was used to target lipids. In particular, indocarbocyanine fluorophores (Dil or DID) were used as probes to stain lipids of NR. The fluorescence of these molecules is strongly increased when they merge into membranes or bound to lipophilic biomolecules. In terms of structure, Dil and DID are amphiphilic probes comprising a charged group and a lipophilic aliphatic tail that insert into hydrophobic membranes. The good performance of these probes for d-STORM experiments on cell membranes has been previously tested showing good blinking capabilities³⁵, without affecting any physiological feature and cell mobility. Additionally, both proteins and lipids probes were previously reported for their specific labelling in NR during the work of Wu et al³⁶. The molecular formula together with spectroscopic properties of the fluorophores involved in this study are summarized in Table 2.2.

Table 2.2. Structure and spectroscopic properties of the fluorophores used in this study.

Fluorophore	Cy5-NHS	DiI	DiD	Fluorophore for silica particles
Structure				Undisclosed
Molecular formula	$C_{36}H_{42}N_3BF_4O_4$	$C_{59}H_{97}ClN_2O_4$	$C_{67}H_{103}ClN_2O_3S$	Undisclosed
Molecular weight (g* mol^{-1})	667.54	933.88	1052.08	Undisclosed
λ_{exc} max (nm)	646	548	644	540
λ_{em} max (nm)	662	570	670	582
Target	Proteins	Lipids	Lipids	Silica

5. d-STORM set-up in this study

The key technical requirements for a d-STORM optical set-up are (i) a powerful laser to photo-bleach most fluorophores and activate only a small portion of sparsely distributed single fluorophores, (ii) a high numerical aperture (NA) objective to efficiently collect the limited number of photons emitted by single molecule, and (iii) a powerful camera with high quantum efficiency and low noise to record the image from individual fluorescent emitters at a high signal to noise ratio³⁷.

A schematic of the optical set-up used in this study is presented in Figure 2.24. It is equipped with a Nikon Eclipse Ti inverted microscope with a Nikon perfect focus system. The excitation was performed thanks to two different laser lines: 532 nm (Verdi G5, 5W, Coherent) and 637 nm (Obis 637LX, 140mW, Coherent) (the excitation light is represented by a green light in Figure 2.24). Both laser beams are focused onto a rotating diffuser to homogenize the spatial distribution of the beams illumination. They are further projected onto the sample through a high numerical aperture and magnification objective (APO TIRF x100 1.49NA, Nikon).

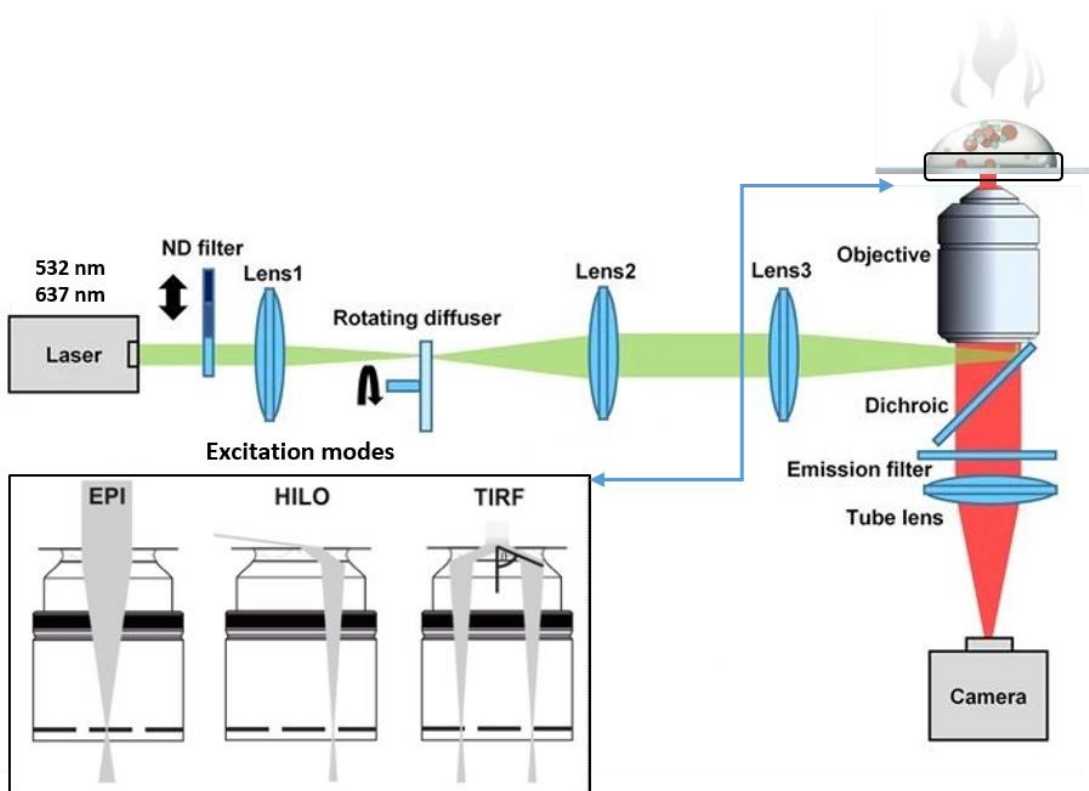


Figure 2.24. Schematic diagram of the experimental set-up for d-STORM imaging. A 532 nm and 637 nm were used as excitation source, but for simplicity only a green light representing the 532 nm laser source is represented. Through series of lenses and passing through a rotational diffuser the excitation beam is focused on the objective (APO TIRF x100 1.49NA, Nikon). Three types of excitation modes are available comprising wide field (EPI), Total Internal Reflection Fluorescence (TIRF) and Highly inclined laminated optical sheet (Hilo). The collected fluorescence path is represented by a red light, and it passes through a dichroic mirror before being projected on a sensible complementary metal oxide semiconductor camera (iXon 3, Andor).

A movable mirror enables to switch among wide-field illumination, total internal reflection fluorescence (TIRF)³⁸ and highly inclines laminated optical sheet (Hilo) illumination³⁹ (Figure 2.25). TIRF is very effective in reducing the background noise, but only fluorophores in a very thin layer close to the coverslip are excited. The penetration depth achieved using TIRF illuminations is limited to 300-400 nm from the glass surface. Thus, in case of NR globules adhered on the surface only a section of LRP can be illuminated (Figure 2.25a and a₁). An alternative to TIRF excitation is to illuminate the sample using Hilo illumination. In this mode, the excitation laser light leaves the objective at a very narrow angle, which results in an inclined beam passing through the sample. In this way, deeper penetration depth can be achieved (few micrometers) (Figure 2.25b). This illumination in the form of an optical light sheet is then almost perpendicular to the detection path of the microscope. In this study, both modes have been tested as it will be discussed in more details in chapter 4. Briefly, due to the thickness of the sample, most of the experiments have been performed using Hilo

illumination, which allows the excitation of the whole sample volume of the sample.

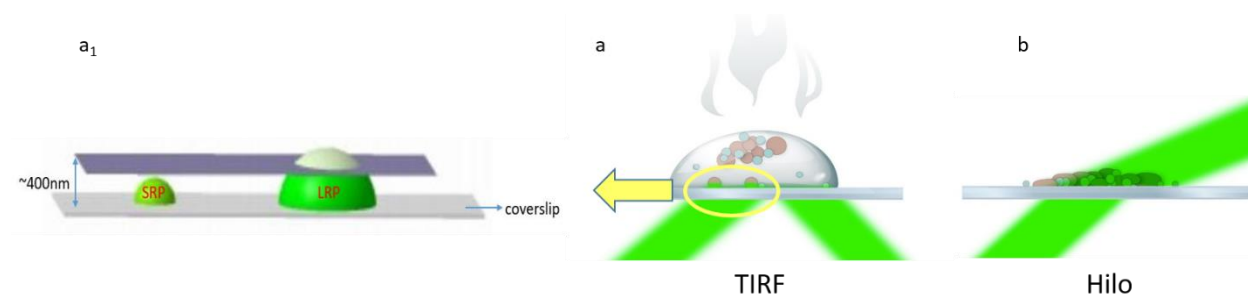


Figure 2.25. Schematic illustration of (a) TIRF and (b) Hilo excitation applied to our system. The penetration depth when using TIRF is limited to 300-400 nm so that only a section of LRPs adhered on the coverslip can be excited. Using Hilo excitation, the penetration depth is of several micrometers.

Regardless of the type of excitation mode, the fluorescence emitted from the sample (represented by a red light in Figure 2.24) is collected by the objective and further passes through a dichroic mirror containing multiband filter to eliminate residual laser light. Finally, the fluorescence light is then focused on a complementary metal oxide semiconductor camera with 50 ms exposure time (iXon 3, Andor).

For certain experiment, in particular to control how NR globules adhere on the coverslip, direct optical nanoscopy with axially localized detection (DONALD) was employed. To do so, the detection part of the set-up was modified combining the d-STORM information with Supercritical-Angle Fluorescence analysis⁴⁰. The complete description of the DONALD system is detailed elsewhere⁴¹ and it goes beyond the scope of this manuscript. However, the advantage of this technique relies on the possibility to achieve 3D nanometer resolution gaining information on the axial position of fluorophores within ~400 nm from the coverslip interface. A typical 3D view of NR globules adhered on the coverslip is shown in Figure 2.26a revealing that NR particles adhere on the coverslip forming a cap shaped 3D semi-sphere which can be recognized on the magnified view of a single LRP (Figure 2.26b).

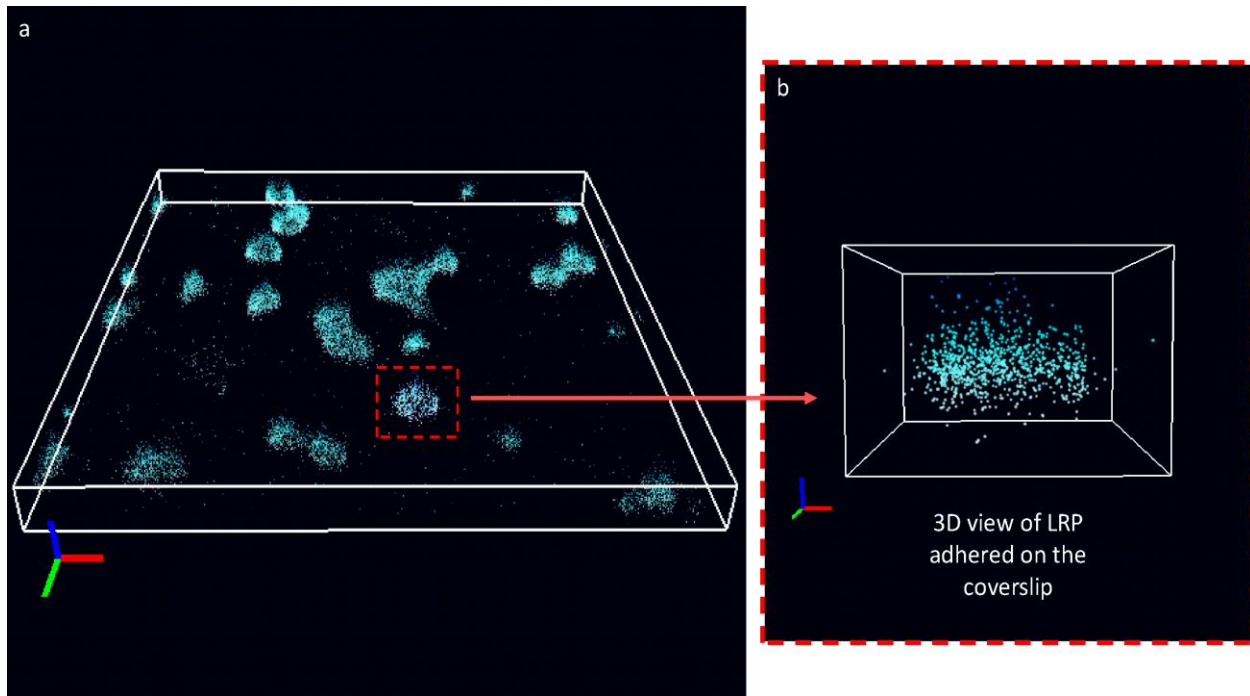


Figure 2.26. Typical 3D image of NR globules adhered on the coverslip using DONALD detection. Large view of several NR globules (a). Magnified 3D view on a single LRP showing the axial position of the detected fluorophores revealing that NR globules adhered on the coverslip forming a cap shaped semi-sphere.

6. Atomic Force Microscopy combined with Infrared spectroscopy: AFM-IR method

We have used for the first time a highly performant and resolute technique combining atomic force microscopy (AFM) and infrared spectroscopy (IR), named AFM-IR. The technique allows to image and identify the chemical composition of a sample with tens of nanometers spatial resolution. Prior to directly describe the technique, we will first recall basic elements of AFM and IR spectroscopy.

Atomic Force Microscopy (AFM)

AFM belong to the family of SPM techniques. Since its invention by binning and coworkers in 1986, it has become an essential tool for material research. It allows visualization and investigation of the surface properties of samples with nanometer resolution without the use of chemical agents. In AFM, a sharp tip attached to the end of a cantilever is approached to the surface⁴². As a consequence, a force appears between the tip and the surface causing the cantilever to bend. To measure these movements, a laser is reflected on the backside of the cantilever. The change in the laser reflection is then detected using a plane photodetector (usually a photodiode). By linking the voltage to a function of the spatial position of the laser on the photodiode (top-bottom and left-right), it is possible to have direct access to the movement of the cantilever (Figure 2.27). In this way it possible to obtain a topographic map of the sample surface. In such set-up, the lateral x-y resolution mainly depends on the radius of the apex of the AFM tip⁴³, while the vertical one strongly depends on the noise of the photodiode⁴⁴.

There are several available modes of imaging allowing AFM to characterize all varieties of materials hard or soft, synthetic or natural. The sample is usually image in air, but it can be in liquid environment and in some cases under vacuum⁴². The most common imaging modes can be classified into: contact mode, and tapping mode. In contact mode the tip scans the sample surface by remaining in close contact to it. The sample surface profile is generated by operating in constant force mode, adjusting the pixel-by-pixel height of the tip. The contact force causes the cantilever to bend and therefore accommodate changes in topography. Although contact mode is widely used, its application for soft material or biological systems poses difficulties because of friction and the force applied between the tip and the sample. For this reason, tapping mode was invented. In such mode, the cantilever tip oscillates at or near its natural resonance frequency while allowing the tip to impact the sample surface for a minimal amount of time. The cantilever's oscillation amplitude changes with sample surface topography, and the topography image is obtained by monitoring these changes⁴⁵. However, the topographic contrast relies on complex interaction mechanisms between the AFM tip and the sample. Stiffness, roughness, surface charge and chemistry can change the oscillation of the tip⁴⁶.

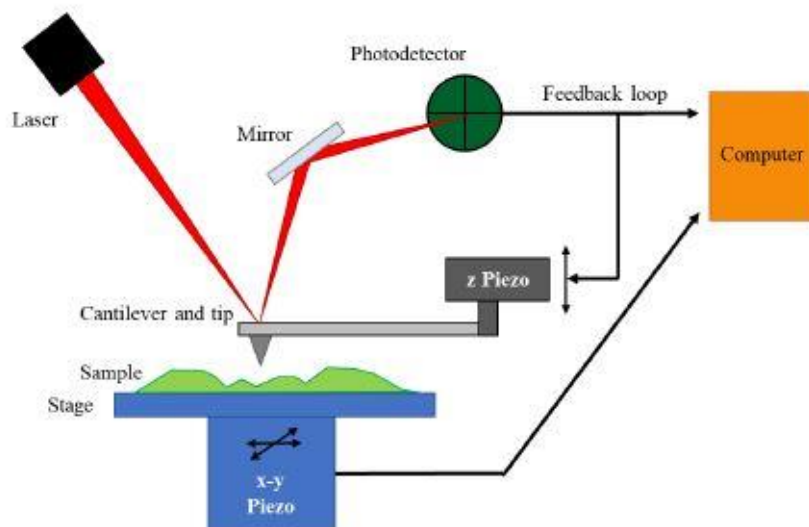


Figure 2.25. Schematic illustration of the AFM set-up⁴⁷.

The AFM method is a very versatile technique, that besides topography characterization of a surface also offers the possibility to measure the surface forces, mechanical properties and adhesion forces of a sample. Such utilization of AFM is outside the scope of this thesis but was still used by our group to discriminate the mechanical properties of small (SRP) and large (LRP) rubber particles in aqueous environment⁴⁸.

IR spectroscopy

IR spectroscopy deals with the measurement of the interaction of IR radiation with matter. In particular, absorption of an IR photon occurs when the frequency of the absorbed radiation matches a characteristic vibrational frequency of the molecule involved in the interaction⁴⁹. Thus, in the IR domain, it is the vibrational levels of the chemical bonds that are called upon. The absorption of IR radiation by a molecule can be likened to two atoms attached to each other by a massless spring. Taking the simple case of diatomic molecules, such molecules have three degrees of translational freedom and two degrees of rotational freedom. The atoms in the molecules can also move relative to one other, that is, bond lengths can vary or one atom can move out of its present plane. This is a description of stretching and bending movements that are collectively referred to as vibrations⁵⁰ (Figure 2.26). More energy is needed to stretch a bond, than that to bend it. For this reason, stretching occurs at higher frequencies than bending. Additionally, some bond can stretch in-phase or symmetrically, while others can stretch out of phase or asymmetrically. Similarly, bending radiation can also be in plane or out of plane.

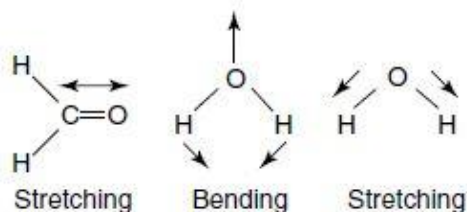


Figure 2.26. Example of stretching and bending modes.

The interesting aspect about IR spectroscopy is that functional groups of molecules adsorb radiation in specific ranges of frequencies, giving rise to a “signature” of that group. This feature allows the identification of unknown compound. In terms of ranges of frequencies, the IR region is mainly divided into: the near-IR, the mid-IR, and the far-IR⁴⁹. Near-IR region goes from 14000 cm^{-1} to 4000 cm^{-1} , the mid-IR goes from 4000 cm^{-1} to 400 cm^{-1} , and the far-IR from 400 cm^{-1} to 10 cm^{-1} . The mid-IR region is particularly interesting for the analysis of the vibration of chemical bonds in organic compounds as most of the fundamental transitions of organic functional groups are found between 4000 to 600 cm^{-1} . Whereas, the region below 1200 cm^{-1} is known as “fingerprint” region, because it is composed of a series of sharp peaks which correspond to a particular compound rather than functional groups. It is in this last region, at 1100 cm^{-1} , that the Si fillers used in this study present a very sharp and characteristic peak, corresponding to the Si-O-Si asymmetric stretching. This signature has been used to localized Si fillers in the NR matrix, using a combination of both AFM and IR spectroscopy; a novel approach of AFM-IR.

AFM-IR

AFM-IR is a hybrid technique that combines the spatial resolution of AFM with the chemical analysis capability of IR spectroscopy⁵¹. This coupling benefits from the advantages of the two individual techniques, overcoming their respective limitations, and achieving chemical mapping at nanometer scale. In terms of working principle, the sample is here placed on an IR transparent support (e.g. ZnSe, CaF_2), and irradiated with a tunable infrared laser focused in the proximity of a probe tip from an atomic force microscope. If the tunable IR laser is set to a wavelength that corresponds to an absorbing wavelength of the sample, the absorbed light induces a photo-thermal response in the sample, resulting in thermal expansion in the absorbing region. The AFM tip can then be used to detect such thermal expansion¹². The detected signal is then proportional to the absorption coefficient⁵³, and two type of acquisition are possible. The position of the AFM tip can be fixed, while the laser wavenumber changes, in order to create IR adsorption spectra with nanoscale resolution. Alternatively, the tip can scan the sample surface, while the IR laser wavenumber is fixed. In this case, a chemical map of the scanned sample is obtained together with the sample topography. In this configuration, a classic AFM

topographic image can now discriminate components based on their IR absorption. Thus, information on chemical composition can be acquired with the same resolution as for AFM images. The conventional set-up for AFM-IR is shown in Figure 2.27. The set-up has been developed by Dazzi et al.⁵⁴ in 2005, and further patented in 2007 in partnership with Anasys Instruments. The assembly consists of a standard AFM system which can operate in contact mode in the open air. The sample is placed on a IR transparent prism of ZnSe and illuminated by the IR beam from below the sample in a total reflection configuration. The angle of illumination at the prism-object interface is chosen so that an evanescent wave is produced at this interface. This allows a relatively homogeneous illumination of a thin object, whatever its optical index, while limiting as much as possible the illumination of the tip and the lever which could greatly disturb the measurement.

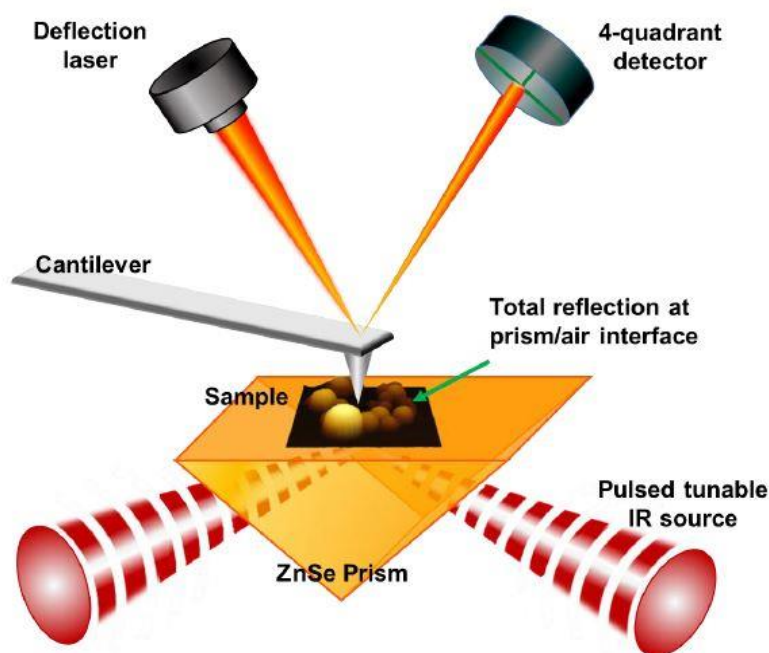


Figure 2.27. Schematic representation of the conventional AFM-IR set-up⁴⁷.

Recently, a new configuration set-up has been developed (Figure 2.28). The major innovation consists in the illumination of the sample and the elimination of the prism. Therefore, in this configuration, the sample can be deposited on a wide range of substrates, as long as they are IR transparent. Moreover, this recent set-up allows the acquisition of chemical maps choosing between the AFM tapping or contact mode. While contact mode is suitable for a large number of samples, objects that are soft (like NR) or not very adherent to the surface are better imaged using tapping mode. From the AFM-IR point of view, the major challenge in using this mode is to be able to synchronize the AFM-IR measurement with the intermittent contact with the surface. This coupling has recently been developed⁵⁵, and it was chosen as imaging mode during our study.

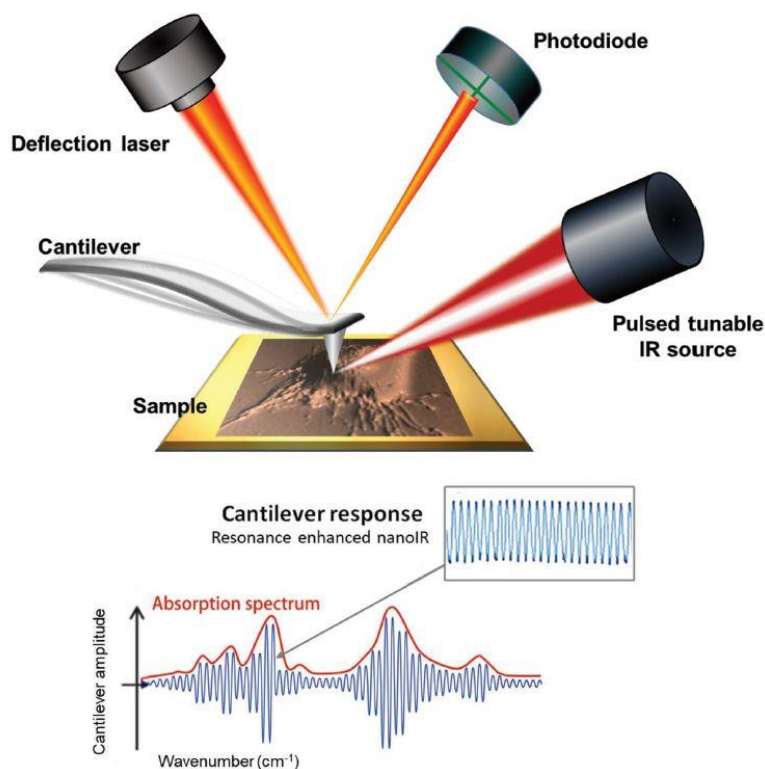


Figure 2.28. Recent configuration of AFMIR set-up⁵⁵.

AFM-IR is finding numerous applications in the field of polymers, polymer blend and composites. Tang et al.⁵⁶ used for the first time this method to study the composition of high-impact polypropylene. Additionally, Brown and Bhushan⁵⁷ investigated nanocomposite films of polycarbonate containing nanoparticles for superoleophobic surfaces.

To our knowledge, our study represents the first application of the techniques to study a composite material composed of a NR matrix. Additionally, during the aforementioned studies, contact imaging mode was coupled with IR spectroscopy. Whereas, the novelty of our work is also related to the use of the tapping AFM-IR mode to study the distribution of Si fillers in the obtained composite.

REFERENCES

1. Bandyopadhyay, J. & Sinha Ray, S. Structural Characterization of Polymer Nanocomposites. in *Processing of Polymer-based Nanocomposites* (ed. Sinha Ray, S.) vol. 277 87–126 (Springer International Publishing, 2018).
2. Oberdisse, J., Straube, E. & Pyckhout-Hintzen, W. Structure Determination Of Polymer Nanocomposites By Small-Angle Scattering. in *Recent Advances in Polymer Nanocomposites* 397–438 (Brill Academic Publishers, 2009). doi:10.1163/ej.9789004167261.i-528.112.
3. Adhikari, R. & Michler, G. H. Polymer Nanocomposites Characterization by Microscopy. *Polymer Reviews* **49**, 141–180 (2009).
4. Wöll, D. & Flors, C. Super-resolution Fluorescence Imaging for Materials Science. *Small Methods* **1**, 1700191 (2017).
5. Böhme, U. & Scheler, U. Interfaces in polymer nanocomposites – An NMR study. in 090009 (2016). doi:10.1063/1.4942305.
6. Lila, M. K., Komal, U. K. & Singh, I. Characterization Techniques of Reinforced Polymer Composites. in *Reinforced Polymer Composites* (eds. K. Bajpai, P. & Singh, I.) 119–145 (Wiley-VCH Verlag GmbH & Co. KGaA, 2019). doi:10.1002/9783527820979.ch7.
7. Williams, D. B. & Carter, C. B. *Transmission electron microscopy: a textbook for materials science*. (Springer, 2008).
8. Watt, I. M. *The principles and practice of electron microscopy*. (Cambridge University Press, 1997).
9. *Transmission Electron Microscopy Characterization of Nanomaterials*. (Springer Berlin Heidelberg, 2014). doi:10.1007/978-3-642-38934-4.
10. Zhou, W., Apkarian, R. P., Wang, Z. L. & Joy, D. Fundamentals of Scanning Electron Microscopy. 40.

11. Goldstein, J. I. *et al. Scanning Electron Microscopy and X-ray Microanalysis*. (Springer US, 2003). doi:10.1007/978-1-4615-0215-9.
12. Piños, J., Mikmeková, Š. & Frank, L. About the information depth of backscattered electron imaging: ABOUT THE INFORMATION DEPTH. *Journal of Microscopy* **266**, 335–342 (2017).
13. Wang, Y. Cryo-electron microscopy finds place in materials science. *Sci. China Mater.* **61**, 129–130 (2018).
14. McDonald, K. L. A review of high-pressure freezing preparation techniques for correlative light and electron microscopy of the same cells and tissues: HPF TECHNIQUES FOR CORRELATIVE LM AND EM OF SAME CELLS AND TISSUES. *Journal of Microscopy* **235**, 273–281 (2009).
15. Murata, K. & Wolf, M. Cryo-electron microscopy for structural analysis of dynamic biological macromolecules. *Biochimica et Biophysica Acta (BBA) - General Subjects* **1862**, 324–334 (2018).
16. Kaech, A. & Ziegler, U. High-Pressure Freezing: Current State and Future Prospects. in *Electron Microscopy* (ed. Kuo, J.) vol. 1117 151–171 (Humana Press, 2014).
17. Jenkins, R. A. Osmium tetroxide vapor fixation of dividing and regenerating *Blepharisma*. 162.
18. Nielson, A. J. & Griffith, W. P. Tissue fixation by osmium tetroxide. A possible role for proteins. *Journal of Histochemistry & Cytochemistry* **27**, 997–999 (1979).
19. *Biological field emission scanning electron microscopy*. (Wiley, 2019).
20. Steigerwald, D. M. EsB Detection Low Voltage – BSE Imaging. 2.
21. Valeur, B. Molecular Fluorescence Principles and Applications. *Molecular Fluorescence* 399 (2001).
22. *Confocal Laser Microscopy - Principles and Applications in Medicine, Biology, and the Food Sciences*. (InTech, 2013). doi:10.5772/50821.

23. Liao, S. A Review on Characterization of Molecular Structure of Natural Rubber. *MOJ Polymer Science* **1**, (2017).
24. Chan, A. J. *et al.* Natural Rubber–Filler Interactions: What Are the Parameters? *Langmuir* **31**, 12437–12446 (2015).
25. Hell, S. W. & Kroug, M. Ground-state-depletion fluorescence microscopy: A concept for breaking the diffraction resolution limit. *Applied Physics B Lasers and Optics* **60**, 495–497 (1995).
26. Gustafsson, M. G. L. & Webb, W. W. Nonlinear Structured-Illumination Microscopy: Wide-Field Fluorescence Imaging with Theoretically Unlimited Resolution. *Proceedings of the National Academy of Sciences of the United States of America* **102**, 13081–13086 (2005).
27. Endesfelder, U. & Heilemann, M. Direct Stochastic Optical Reconstruction Microscopy (dSTORM). in *Advanced Fluorescence Microscopy* (ed. Verveer, P. J.) vol. 1251 263–276 (Springer New York, 2015).
28. Turkowyd, B., Virant, D. & Endesfelder, U. From single molecules to life: microscopy at the nanoscale. *Analytical and Bioanalytical Chemistry* **408**, 6885–6911 (2016).
29. van de Linde, S. *et al.* Direct stochastic optical reconstruction microscopy with standard fluorescent probes. *Nature Protocols* **6**, 991–1009 (2011).
30. Widengren, J., Chmyrov, A., Eggeling, C., Löfdahl, P.-Å. & Seidel, C. A. M. Strategies to Improve Photostabilities in Ultrasensitive Fluorescence Spectroscopy. *The Journal of Physical Chemistry A* **111**, 429–440 (2007).
31. Heilemann, M., van de Linde, S., Mukherjee, A. & Sauer, M. Super-Resolution Imaging with Small Organic Fluorophores. *Angewandte Chemie International Edition* **48**, 6903–6908 (2009).
32. Olivier, N., Keller, D., Rajan, V. S., Gönczy, P. & Manley, S. Simple buffers for 3D STORM microscopy. *Biomedical Optics Express* **4**, 885 (2013).

33. Mortensen, K. I., Churchman, L. S., Spudich, J. A. & Flyvbjerg, H. Optimized localization analysis for single-molecule tracking and super-resolution microscopy. *Nature Methods* **7**, 377–381 (2010).
34. Smith, C. S., Joseph, N., Rieger, B. & Lidke, K. A. Fast, single-molecule localization that achieves theoretically minimum uncertainty. *Nature Methods* **7**, 373–375 (2010).
35. Shim, S.-H. *et al.* Super-resolution fluorescence imaging of organelles in live cells with photoswitchable membrane probes. *Proceedings of the National Academy of Sciences* **109**, 13978–13983 (2012).
36. Wu, J. *et al.* Super-Resolution Fluorescence Imaging of Spatial Organization of Proteins and Lipids in Natural Rubber. *Biomacromolecules* **18**, 1705–1712 (2017).
37. Ma, H., Fu, R., Xu, J. & Liu, Y. A simple and cost-effective setup for super-resolution localization microscopy. *Sci Rep* **7**, 1542 (2017).
38. Total Internal Reflection Fluorescence (TIRF) Microscopy. *Nikon's MicroscopyU*
<https://www.microscopyu.com/techniques/fluorescence/total-internal-reflection-fluorescence-tirf-microscopy>.
39. Tokunaga, M., Imamoto, N. & Sakata-Sogawa, K. Highly inclined thin illumination enables clear single-molecule imaging in cells. *Nature Methods* **5**, 159–161 (2008).
40. Ruckstuhl, T., Enderlein, J., Jung, S. & Seeger, S. Forbidden Light Detection from Single Molecules. *Anal. Chem.* **72**, 2117–2123 (2000).
41. Bourg, N. *et al.* Direct optical nanoscopy with axially localized detection. *Nature Photon* **9**, 587–593 (2015).
42. Haugstad, G. *Atomic force microscopy: understanding basic modes and advanced applications*. (John Wiley & Sons, 2012).
43. Binnig, G., Quate, C. F. & Gerber, Ch. Atomic Force Microscope. *Phys. Rev. Lett.* **56**, 930–933 (1986).

44. Mr Sameer & S Gajghate. Introduction to Atomic Force Microscopy (AFM). (2017)
doi:10.13140/RG.2.2.11394.38089.
45. Jalili, N. & Laxminarayana, K. A review of atomic force microscopy imaging systems: application to molecular metrology and biological sciences. *Mechatronics* **14**, 907–945 (2004).
46. Dufrière, Y. F. *et al.* Imaging modes of atomic force microscopy for application in molecular and cell biology. *Nature Nanotechnology* **12**, 295–307 (2017).
47. Dazzi, M. *et al.* Thèse présentée et soutenue à Orsay, le 15 Décembre 2017 : 258.
48. Chan, A. J., Sarkar, P., Gaboriaud, F., Fontaine-Aupart, M.-P. & Marlière, C. Control of interface interactions between natural rubber and solid surfaces through charge effects: an AFM study in force spectroscopic mode. *RSC Adv.* **7**, 43574–43589 (2017).
49. Theophanides, T. Introduction to Infrared Spectroscopy. in *Infrared Spectroscopy - Materials Science, Engineering and Technology* (ed. Theophanides, T.) (InTech, 2012).
doi:10.5772/49106.
50. Stuart, B. H. Infrared Spectroscopy: Fundamentals and Applications. 208.
51. Dazzi, A. & Prater, C. B. AFM-IR: Technology and Applications in Nanoscale Infrared Spectroscopy and Chemical Imaging. *Chemical Reviews* **117**, 5146–5173 (2017).
52. Dazzi, A., Prazeres, R., Glotin, F. & Ortega, J. M. Subwavelength infrared spectromicroscopy using an AFM as a local absorption sensor. *Infrared Physics & Technology* **49**, 113–121 (2006).
53. Dazzi, A., Glotin, F. & Carminati, R. Theory of infrared nanospectroscopy by photothermal induced resonance. *Journal of Applied Physics* **107**, 124519 (2010).
54. Dazzi, A., Prazeres, R., Glotin, F. & Ortega, J. M. Local infrared microspectroscopy with sub-wavelength spatial resolution with an atomic force microscope tip used as a photothermal sensor. *Optics Letters* **30**, 2388 (2005).
55. Pancani, E. *et al.* High-Resolution Label-Free Detection of Biocompatible Polymeric Nanoparticles in Cells. *Particle & Particle Systems Characterization* **35**, 1700457 (2018).

56. Tang, F., Bao, P. & Su, Z. Analysis of Nanodomain Composition in High-Impact Polypropylene by Atomic Force Microscopy-Infrared. *Analytical Chemistry* **88**, 4926–4930 (2016).
57. Brown, P. S. & Bhushan, B. Durable, superoleophobic polymer–nanoparticle composite surfaces with re-entrant geometry via solvent-induced phase transformation. *Scientific Reports* **6**, (2016).

CHAPTER 3: Natural rubber – carbon black: following the nanostructure evolution from a colloidal suspension to an elastomeric composite

Introduction

The production of a rubber latex–carbon black (CB) masterbatch by liquid phase mixing is a procedure of interest in rubber technology. One of the first approaches consisted in mixing natural rubber (NR) latex and a CB slurry and then coagulating the mixture chemically, by addition of acid. The use of dispersing agents, such as surfactants, to the CB slurry was also recognized as a possibility to increase filler's dispersion in the obtained masterbatch. However, the long mixing and coagulation times of such processes reduces productivity. Recently, Cabot Corporation commercially launched its continuous coagulation/liquid phase mixing technology. Here, a CB slurry prepared without the use of any surfactant is injected into a mixer at very high speed and mixed continuously with NR latex stream. Under high shearing condition, the mixing and coagulation is completed very rapidly, without the aid of chemicals. The formed coagulum is subsequently extracted and dried. In 2013, Michelin bought a license from Cabot to use this liquid-phase mixing process for its tire application. If the technological process parameters are under control at engineering level the fundamental knowledge of the underlying hetero-aggregation mechanism and of the processes triggering coagulation are still at its infancy. The understanding of these processes is essential to improve the preparation of a NR-CB masterbatch.

It is in this context that the first part of the thesis is focused. Our investigation is focused on the nanoscale structural characterization and evolution of a coagulum obtained from a binary colloidal suspension of NR latex and a CB slurry. We investigated the dependence of NR-NR and CB-CB homo-aggregation vs NR-CB hetero-aggregation, the structural evolution dynamics of the formed coagulum, and the impacts of external stresses, such as shear and sonication. For this investigation, we selected an original Field Emission Scanning Electron Microscopy (FESEM) approach as main technique. The results are presented and discussed in the form of an article entitled “*Natural Rubber- Carbon Black coagulation: following the nanostructure evolution from a colloidal suspension to an elastomeric composite*”, submitted to the *journal of Applied Polymer Science*.

Article 1: Natural rubber – carbon black: following the nanostructure evolution from a colloidal suspension to an elastomeric composite

Gianluca Cattinari^{*1}, Karine Steenkeste¹, Catherine le Bris¹, Alexis Canette², Matthieu Gallopin³,
Marc Couty³, Marie-Pierre Fontaine-Aupart¹

¹ Université Paris-Saclay, CNRS, Institut des Sciences Moléculaires d'Orsay, 91405, Orsay, France

² Sorbonne Université, CNRS, Institut de Biologie Paris-Seine, 75005, Paris, France

³ Manufacture Française de Pneumatiques Michelin, Clermont Ferrand Cedex, France

Submitted to journal of Applied Polymer Science

Natural rubber-carbon black coagulation: following the nanostructure evolution from a colloidal suspension to an elastomeric composite

Gianluca Cattinari^{*1}, Karine Steenkeste¹, Catherine le Bris¹, Alexis Canette², Matthieu Gallopin³, Marc Couty³, Marie-Pierre Fontaine-Aupart¹

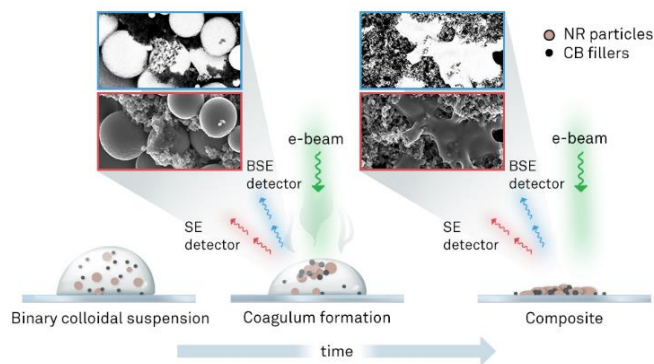
¹ Université Paris-Saclay, CNRS, Institut des Sciences Moléculaires d'Orsay, 91405, Orsay, France

² Sorbonne Université, CNRS, Institut de Biologie Paris-Seine, 75005, Paris, France

³ Manufacture Française des Pneumatiques Michelin, Clermont Ferrand, France

ABSTRACT

Making elastomeric composite materials via heteroaggregation of a binary colloidal suspension of Natural Rubber (NR) latex and Carbon Black (CB) filler is an interesting production method to obtain an efficient dispersion in the polymer matrix. This study successfully employs an original approach of field emission scanning electron microscopy (FESEM), combining a specific chemical fixation method with the backscattered electron (BSE) and secondary electron (SE) imaging modes to investigate for the first time the nanostructure evolution of a coagulum originated from the aggregation of NR globules with CB filler in suspension. Additionally, the role of external physical stresses, like mechanical shear and sonication was also investigated in terms of structural effect induced on the formed coagulum at the nanoscopic scale. Our results highlight destabilization of NR globules, either induced by direct interaction with small CB aggregates or governed by solvent evaporation. Reduction in the size of CB agglomerates, obtained using sonication, highly improved filler distribution and confirmed that the size of CB aggregates is an important parameter responsible for the destabilization of NR globules.



1. INTRODUCTION

Field natural rubber (NR) latex extracted from *Hevea brasiliensis* is a colloidal dispersion of first importance for many applications¹, especially in the tire industry. In its raw state, it is composed of ~35% rubber, 5% nonrubber components (proteins, lipids, sugars) and ~60% water². The rubber fraction is contained in the form of colloidal NR particles, corresponding to a bimodal distribution of small rubber particles (SRPs) and large rubber particles (LRPs), with diameters ranging from 100-500 nm and 500-1000 nm, respectively. Both types are characterized by a polyisoprene core surrounded by a thin biomembrane primarily made of lipids and proteins^{3,4} (thickness ~3.5 nm). Despite its unique properties, NR is seldom used in its raw state. For example, particulate fillers such as carbon black (CB) have been widely used to improve the mechanical properties (modulus, durability, etc.) of NR⁵⁻⁷. However, mixing NR and fillers is a critical step that determines the performance characteristics of rubber compounds. It has long been thought that if a CB dispersion could take place in a liquid phase process,

many of the shortcomings in the dry mixing method could be eliminated⁸. Over the past decades, efforts have been made to produce master batches by mixing NR latex with a slurry of CB under mechanical stress^{9–11}, giving rise to a coagulated material that is further subjected to dehydration and drying. This type of mixing is called the “liquid route” or “colloidal dispersion pathway”. Industrially, the technological process parameters are controlled at the engineering level, but studies are required to understand the fundamental mechanism regulating the heteroaggregation between the NR particles and CB fillers as well as the structural evolution of the formed coagulum. Such investigations are essential to improve the preparation of elastomeric composite materials and cannot be undertaken without the availability of highly resolved imaging methods. In this context, we employed an original field emission scanning electron microscopy (FESEM) approach to study the nanoscale structural evolution of an NR-CB coagulum along with solvent evaporation. The originality of the approach relies on (i) the fixation of the specific chemical sample, thus preserving the colloidal structure of the NR particles as well as enhancing contrast, (ii) and the backscattered electron (BSE) and secondary electron (SE) FESEM imaging modes. We successfully visualized the structural evolution dynamics of the coagulum from the early stage of particle contact to the formation of a composite material. In particular, the role of mechanical shear stress and sonication was investigated at the nanoscopic level in terms of the structural effects induced on the formed coagulum.

2. EXPERIMENTAL

A slurry of CB (N234; density=1.8 g cm⁻³; surface area=120 m²/g, Cabot Corporation, Boston, US) at 5 wt% was obtained by mixing the black powder with distilled water while using an Ultra-Turrax for 5 min to prevent the formation of large CB agglomerates. Highly ammoniated NR latex (Michelin, Clermont Ferrand, France) was used for most of the experiments, which was obtained by centrifugation of field NR latex containing 0.7 wt% ammonia to eliminate free components and nonrubber particles as well as to preserve the structure of NR globules¹². Some experiments were also realized with deproteinized natural rubber (DPNR) latex obtained from a proteinase enzyme treatment of the highly ammoniated latex. Regardless of the type, latex was diluted to 0.075 wt% rubber content and combined with the CB slurry with a CB/rubber mass percent ratio fixed at ~40% in the binary colloidal suspension to approach to the industrial process. Immediately after mixing, 100 μL of this suspension was deposited on a rounded glass cover slip (coverslip thickness: 170 μm, MENZEL-GLASER), resulting in a casted drop with a spherical cap shape, as illustrated in Figure 1. Under these conditions, flocculation occurred on the deposited drop, inducing phase separation, which was macroscopically visible at t=1 h. At t=4 h, when most of the solvent was evaporated, the floating objects adhered on the glass surface. A schematic representation showing the formation of such a phase-separated material is illustrated in Figure 1. Herein, the term “coagulum” refers to the phase-separated material floating on the top of the

deposited drop, while the term “composite” refers to the material obtained after the complete evaporation of the solvent 24 h after the deposition of the sample on the coverslip ($t=24$ h). In case of samples composed of only NR latex, and absence of CB filler, the deposition follows the same protocol.

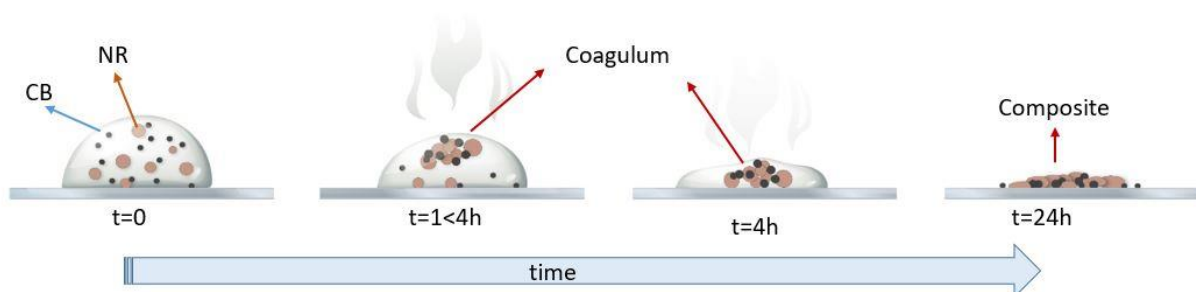


Figure 1. Schematic illustration showing the coagulum and composite formation after the deposition of the NR-CB binary colloidal suspension on the glass coverslip.

2.1 Application of controlled mechanical shear in the liquid suspension

For these experiments, the preparation of the sample followed the detailed description given above; this glass coverslip constituted both the sample support and one of the shearing plates. A second microscopy coverslip was placed above the deposited drop and corresponded to the second shearing plate. The perfect planarity and parallelism of these two microscopy coverslips were suitable for the application of controlled shear. This was obtained using a commercial device called RheOptiCAD^{13,14} (CAD instrument). It provided the ability (i) to move the top plate down at a constant and low speed to prevent excessive compression of the sample until a gap width of 500 μm was reached between the plates and (ii) to connect each plate to a motor controlled by software that allowed straight translation. In these experiments, only the upper plate was displaced. The applied shear consisted of 10 oscillation cycles for a total of 10 min. Each oscillation cycle corresponded to a total displacement in the upper plate of 1 mm (500 μm on either side from the central position) at a frequency of 10 Hz for 60 s, thereby keeping a constant gap between the plates. The shear stress was applied immediately after the deposition of the NR-CB binary suspension ($t=0$) (Figure 2a) or once the floating coagulum was formed ($t=1$ h) (Figure 2b). Additionally, the shearing device was designed to fit on an inverted microscope, allowing shearing and simultaneously transmission imaging of the sample. Herein, it was installed onto an inverted microscope (Axiovert, ZEISS) equipped with a 60x high numerical aperture (1.1) water immersion objective (Olympus) and a charge-coupled device (CCD) camera (UCBO, Olympus).



Figure 2. Schematic illustration showing the application of mechanical shear on the binary NR-CB suspension (a) and the formed coagulum (b).

2.2 NR-CB mix under sonication

NR-CB mixing under sonication was performed using an ultrasonic homogeniser probe (Sonopuls homogeniser HD 2070, Sound frequency: 20kHz, BANDELIN, electronic GmbH, Berlin, Germany). The NR latex particles suspension was placed in a glass vial and sonicated for 1 min at 35 W power with a 13 mm sonication probe (SH 70 G). The CB slurry was then inserted from the top using a pipette, and the 15 mL binary NR-CB suspension was kept under sonication for 2 min. After the total sonication time (3 min), 100 μ L were extracted and deposited on a glass coverslip as illustrated in Figure 1.

2.3 FESEM

One of the originalities of our approach relies on the chemical sample's fixation which can be applied both in the presence or absence of solvent. Fixation was performed by depositing 50 μ L drops of osmium tetroxide (EMS, USA) solution (1% in water, prepared extemporaneously) around the sample's coverslip in a hermetic box protected from light. After 30 minutes the fixation was considered complete. This type of vapour fixation allowed us to (i) avoid immersion of the deposited specimen, (ii) to preserve the colloidal structure of NR (iii) to exploit both SE and BSE imaging based on topographic and chemical contrast, respectively. Indeed, the high affinity of osmium tetroxide for NR particles results in an important differentiation between NR and CB in BSE images: CB fillers appear dark while NR globules are bright (Figure 3). This chemical fixation was applied on samples at times: $t=1h$, $t=4h$, $t=5h$ and $t=24h$. The fixed sample's coverslips were mounted on 25.4 mm aluminium pin stubs (Micro to Nano, the Netherlands) with double-sided sticky and conductive tabs (EMS, USA). Samples were then coated with a 10 nm carbon layer by double thread evaporation in high vacuum (10^{-5} mbar) with an ACE600 device (Leica, Germany). FESEM was performed using a Gemini 500 (Zeiss, Germany) driven by SmartSEM (version 6.3), operating in high vacuum (10^{-6} mbar in the observation chamber), at 3 kV, with high current mode, a 20 μ m aperture (beam current on the specimen experimentally measured in those conditions: 43.2 pA), and around 2 mm working distance. SE signal was collected with the corresponding in-lens detector. BSE signal was collected with the Energy Selective BSE in lens detector using filtering grid > 400 V to filter out SE signal. Images were acquired with a 1024 x 768 pixel definition, with a dwell time of 6,4 μ s and a line averaging of 25. Please note that both SE and BSE signals are surface selective, but while SE images are generated at the extreme surface (depth of few nanometres), BSE images are capable of providing information arising from a depth of few tens of nanometres¹⁵. For each sample, at least two different zones were recorded using a range of magnification power spanning from x5000 to x80000.

2.4 Determination of the NR particle Feret diameter

The quantification of rubber globule elongation was derived from the BSE images recorded at 5000x at two different zones for each sample. A nonlocal means filter was first applied to subtract the noise from the image. Subsequently, the MorphoLibJ Plugin (ImageJ) was employed on the binary image with the application of watershed segmentation to detect only NR particles. Their size was reported in terms of the maximum Feret diameter¹⁶, which meant the longest direction of the globule (Figure 4c). This parameter is used in microscopy measurements for the size analysis of nonspherical particles. The obtained Feret diameter was the result calculated by the average of approximately 1000 NR particles regardless of their size. Thus, the elongation of NR particles was calculated from the difference between the average Feret diameter at $t=4$ h and its corresponding measurement at $t=1$ h.

3. RESULTS AND DISCUSSION

3.1 NR-CB coagulum: its structural evolution during drying

The nanoscale structure of the coagulum was imaged using FESEM with both BSE and SE detection, at different aging times, so that its structural evolution dynamic during drying was reported.

Figure 3 illustrates the typical structure of the NR-CB coagulum early after its formation ($t=1$ h) when the solvent is still present. One major observation is that the NR particles and CB fillers are not homogeneously distributed; this can be specifically highlighted by the BSE images (Figure 3b and f).

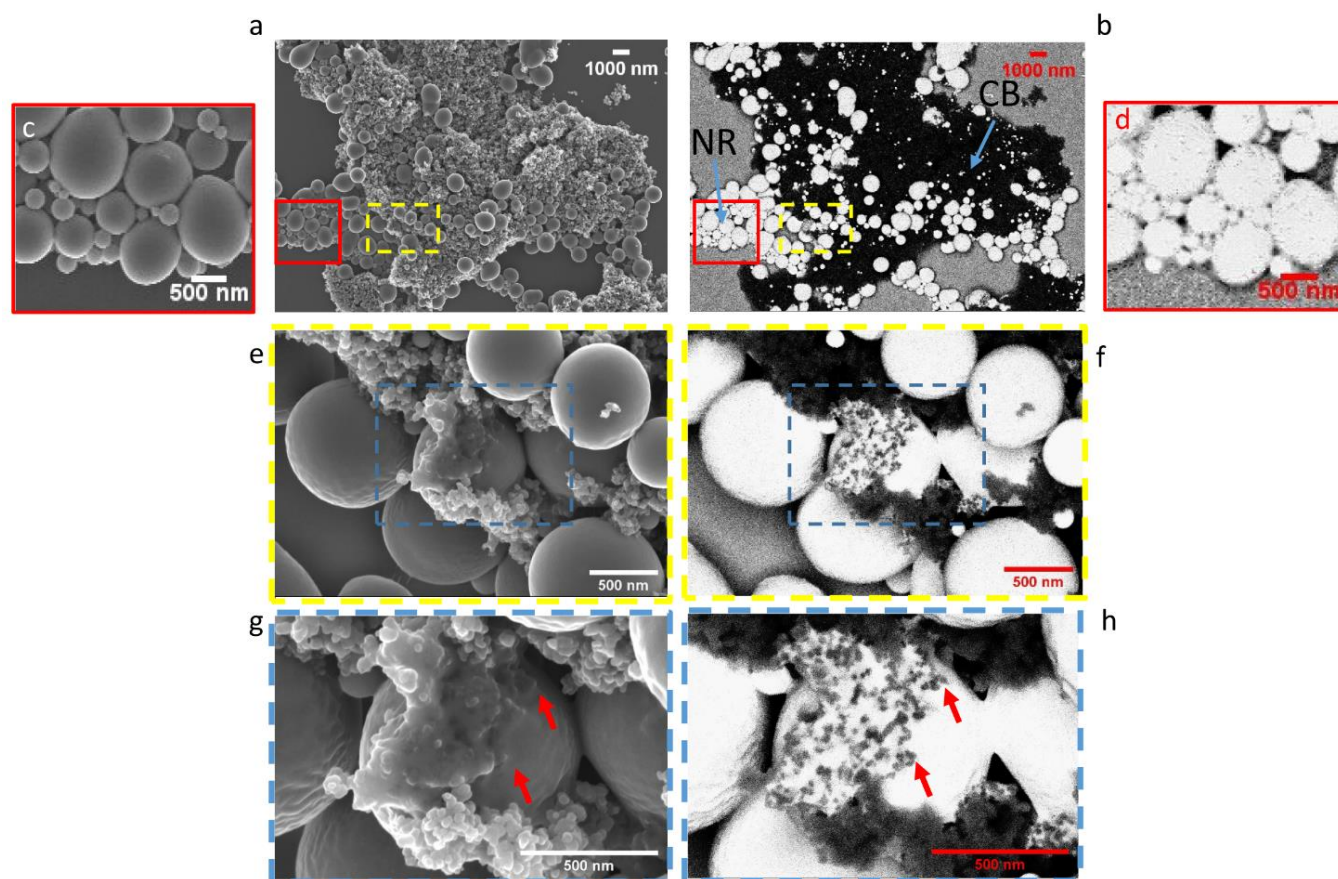


Figure 3. Typical FESEM micrographs of the NR-CB coagulum fixed at $t=1$ h. The mass ratio in liquid suspension is 40% CB/rubber. (a) SE and (b) BSE images where CB appears completely dark while NR particles are bright (magnification: 5000x), which highlights the two different microregions of the corresponding coagulum. The glass surface presents some background noise probably due to a thin layer of osmium deposited on the support. (c) Magnified SE and (d) BSE views of the NR-NR homoaggregation corresponding to the red-squared zones in (a and b). (e) Magnified SE and (f) BSE views of the yellow-boxed regions shown in (a and b), composed of the CB filler and NR particles (magnification: 40000x). (g) Magnified SE and (h) BSE views corresponding to the blue-boxed region in (e and f, magnification: 80000x). Red arrows indicate regions in which the CB aggregates seem to sink into the NR globule.

The comparison of the SE and BSE microstructures in Figure 3a and b reveals regions composed of homoaggregated NR particles that maintain their original colloidal structure, which is clearly visible in the magnified images of Figure 3c and d. Outside these regions, NR particles are essentially dispersed together with large agglomerates of CB filler. This general dominance of homoaggregation can be related to the mixing strategy. CB agglomerates are present in the aqueous slurry, and their size depends on various parameters, such as the shear stress during mixing. Standard mixing using a simple bench-top stirring device leads to object sizes ranging from 1 to 5 μm , with a minor population of objects ranging from 100 to 300 nm. This is confirmed by a control sample of CB slurry prepared and imaged with the same protocol as that used when in the presence of NR globules (Figure S1), thus revealing the formation of CB agglomerates. Despite the dominance of CB agglomerates, we can point out localized regions having particular morphological characteristics. First, some persisting small CB aggregates ($\sim 100\text{-}300$ nm) are in close contact with NR globules and can be covered by the rubber material (Figure 3e and f). Additionally, some of them seem to sink into the surface of the globule, as indicated by the red arrows in Figure 3g and h. These local morphological features suggest a specific interaction between the small CB aggregates and NR globules. Similar observations are reported for a coagulum made of DPNR latex and CB filler (Figure S2), indicating that lipids may play an important role in the nanomechanism responsible for the abovementioned morphological characteristics; this phenomenon will be further discussed later. The mass percent ratio between the CB filler and NR was also drastically decreased to 5 wt% and 1 wt% (by maintaining a constant NR concentration) to assess whether the interaction of NR globules with small CB aggregates was dependent on the CB concentration (Figure S3).

At $t=4$ h, the distribution of CB and NR particles is similar to that observed for the coagulum at $t=1$ h (Figure 4a and b compared with Figure 3a and b), with domains composed of only NR-NR homoaggregation and other domains consisting of large agglomerates of CB filler with scattered NR particles. The most striking difference in the structure of the coagulum between $t=4$ h and $t=1$ h is in the elongation of all the NR globules. Such elongation was quantified by the increase of 200-250 nm in the average Feret diameter (Figure 4c and d). A similar elongation of the NR particles is also found for the sample composed of only NR latex (Figure 4d). At $t=5$ h, as more of the solvent has evaporated, we observe a clear destabilization in the whole population of NR globules in the NR-CB sample: NR globules lose their spherical shape (Figure 4e and f). Again, similar results are found for a sample composed of only NR latex (Figure 4g). After 24 h and the complete evaporation of solvent in both samples, NR globules completely lose their shape (Figure 4h and i and Figure 4j), resulting in a polymer film. In summary, the structural evolution of the NR-CB coagulum can generally be attributed to a typical film formation process of NR due to solvent evaporation. This process is composed of the elongation and coalescence between rubber globules along with the diffusion of the polymer chain, thereby giving rise to a polymer film¹⁷. More interestingly, some NR globules in contact with small

CB aggregates lose their original colloidal shape at earlier stages than those deformed due to solvent evaporation (Figure 3g).

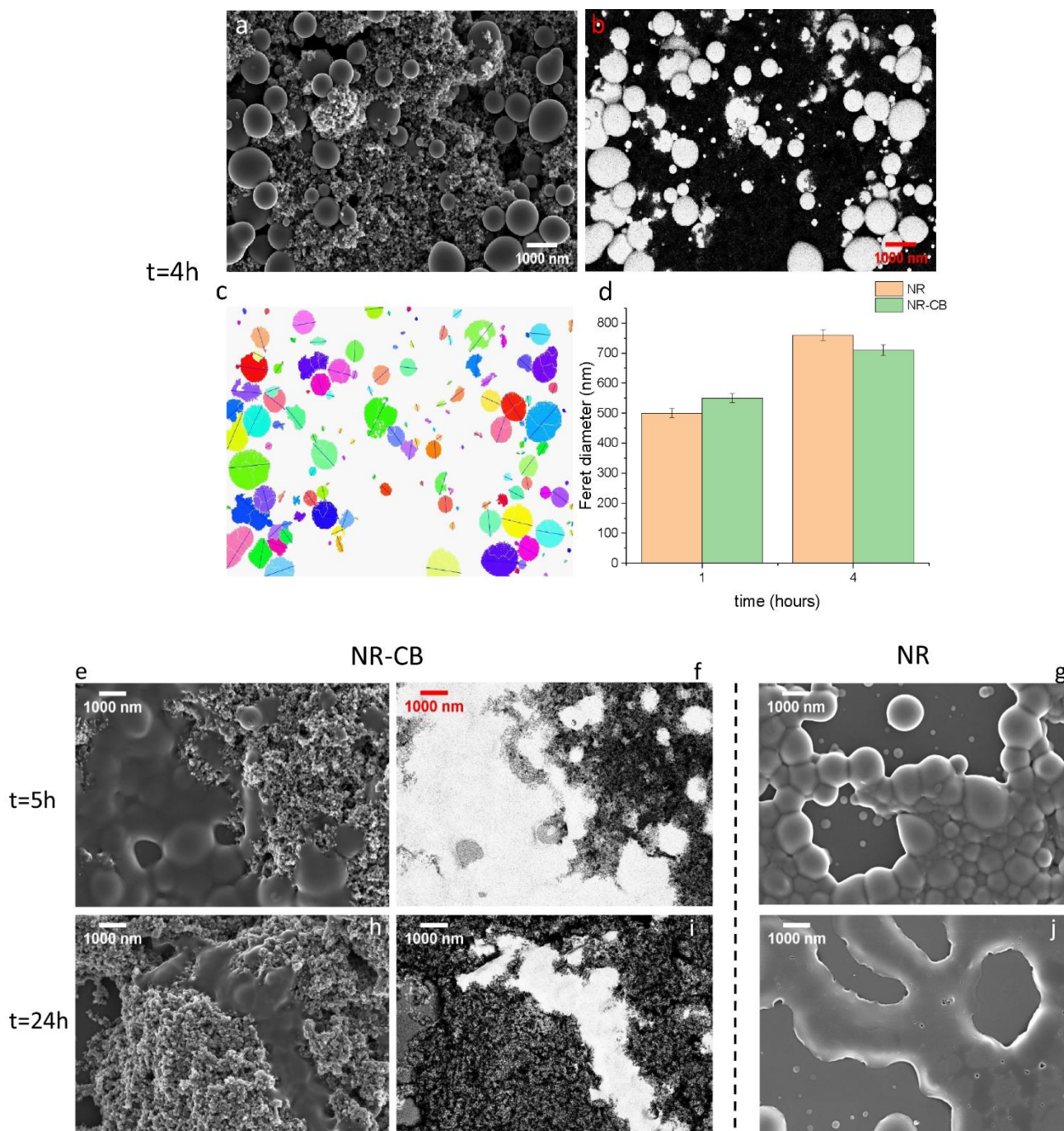


Figure 4. Typical FESEM micrographs of the NR-CB coagulum and NR latex over time. SE images and corresponding BSE micrographs of the NR-CB coagulum at t=4 h (a and b), t=5 h (e and f), and t=24 h (h and i). SE images recorded on a sample composed of only NR latex: t=5 h (g) and t=24 h (j). All images were taken with a magnification power corresponding to 10000x. (c) Illustration of the Feret diameter determination of NR particles in image (a). (d) Histogram showing the elongation of NR particles in terms of the average Feret diameter between t=1 h and t=4 h.

We hypothesize that this deformation at an early stage may be related to an interaction with the small CB filler that is capable of inducing the destabilization of the globule surface. To assess this hypothesis, we tried to boost the contact between the surface of NR globules and CB filler by the application of physical stress, thus aiming to reduce CB agglomeration.

3.2 Effect of shear stress in the liquid suspension

Controlled mechanical shear stress was employed to reduce CB agglomeration. The mechanical forces were initially applied using the RheOptiCAD module right after the deposition of the NR-CB suspension on the coverslip ($t=0$) (Figure 2a). Light transmission images recorded during the applied oscillation cycles highlight the formation and combination of irregular flocs, growing in size and quickly leading to a macroscopically visible phase-separated coagulum at the end of 10 oscillation cycles (~ 10 min) (Figure S4). On the other hand, approximately 1 h is needed to macroscopically observe phase separation without the application of shear. Such behaviour is typical of a shear-induced aggregation mechanism, where the applied shear forces can increase NR-CB contact and drive the particles to overcome the interaction energy barrier¹⁸. Prior to the observation of the NR-CB coagulum structure, a control sample was imaged attesting that the confinement between the parallel plates does not induce any deformation of the NR globules, as shown in Figure S5. Figure 5a illustrates the structure of the coagulum formed under shear. We can observe that the distribution of CB filler is not improved when shear is applied; the large CB agglomerates are not broken down by the applied force. Furthermore, in zones where NR-NR homoaggregation is dominant, no shear effect on the original form of the NR globules is highlighted (see the red boxed region in Figure 5b). Interestingly, regions of the sample where NR globules are in contact with small CB aggregates exhibit different structures. In these zones, the original spherical form of NR globules appears flattened upon the application of shear stress. Polymer leakage and diffusion is increased toward the surrounding CB aggregates (Figure 5c and d). Additional experiments were performed by applying shear on the floating NR-CB coagulum formed at $t=1$ h (Figure 2b). In this case, the shearing effect shows remarkable distortion of the NR globules in contact with the CB filler (Figure 5e and f). In summary, we can state that in our experimental conditions, the applied shear did not improve the dissociation of CB agglomerates. However, it accelerated the formation of a phase-separated NR-CB coagulum together with NR particle distortion in regions where they are in close proximity to CB aggregates, thus leading to polyisoprene diffusion through the sample. In an attempt to improve CB distribution and favor its interaction with NR globules, the two components were then mixed under sonication.

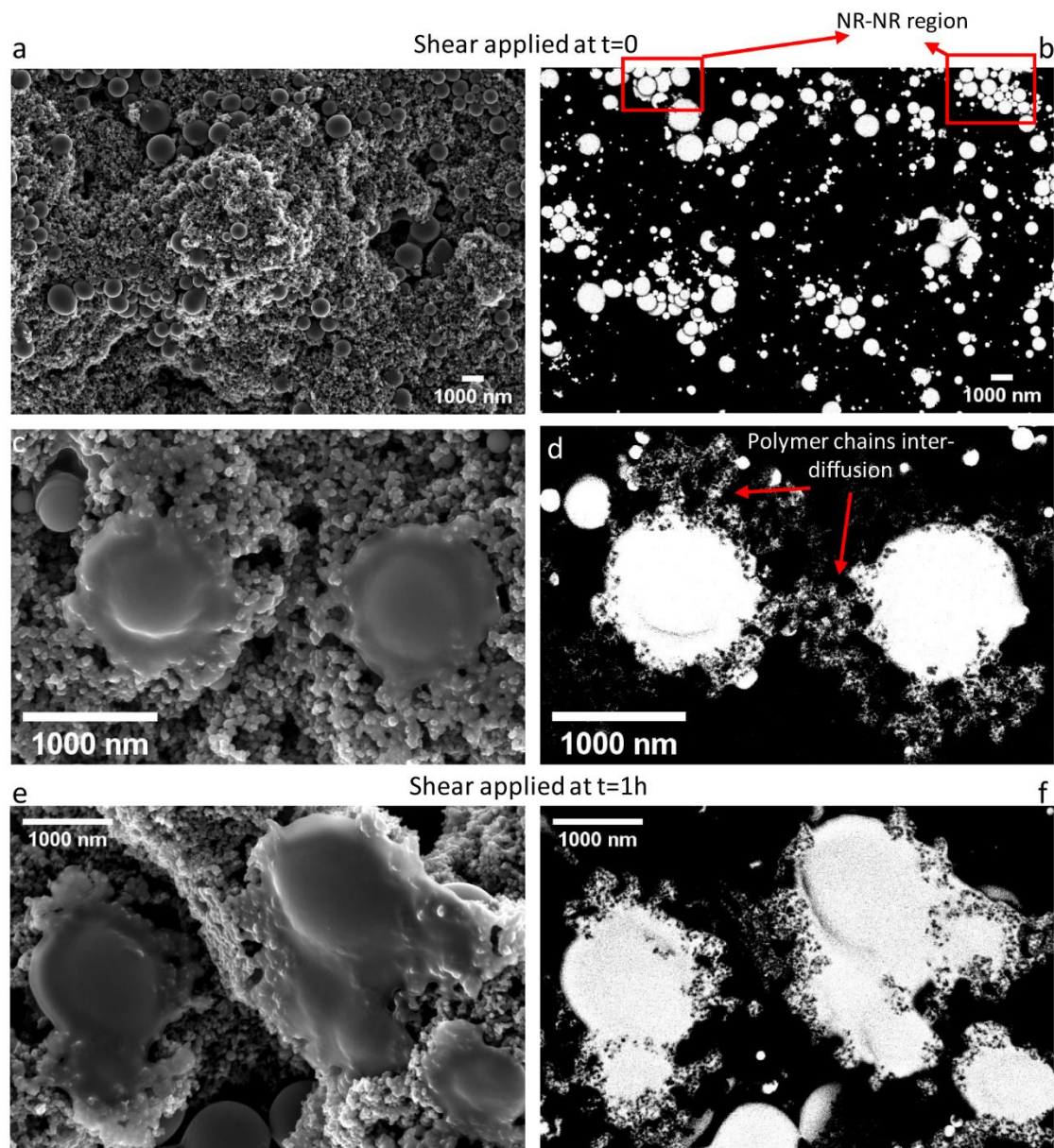


Figure. 5. FESEM micrographs of NR-CB coagulum formed under the application of mechanical shear-stress at $t=0$ or formed during 1h and then subjected to shear-stress. (a) Large view SE and (b) BSE images of the NR-CB hetero-coagulum formed after the application of 10 shearing cycles at $t=0$ (magnification: 5000x), showing large areas of CB agglomerates. The red boxed area highlights domains of NR-NR aggregation (c) Magnified SE and (d) BSE views of NR globules deformation in the NR-CB coagulum formed under shear applied at $t=0$, highlighting polymer diffusion into the surrounding CB filler (magnification: 20000x). (e) SE and (f) BSE images recorded on the NR-CB coagulum subjected to shear applied at $t=1h$ (magnification: 20000x), thus showing similar result as those in (c) and (d).

3.3 NR-CB mix under sonication: effect on the structure of the formed coagulum

Sonication is known to break down CB agglomerates into smaller objects, down to a size that depends on the energy and on the sonication time. Our experimental conditions were defined so that sonication applied on only NR globules does not affect their structure (Figure 6g and h). When sonication is applied during mixing of NR globules with CB slurry, the formed coagulum has remarkable properties compared with those obtained from the previously used conditions: neither CB micrometer-sized agglomerates nor NR-NR homoaggregated regions are observed. Small CB aggregates (20-200 nm) and NR globules are homogeneously distributed. This leads to a coagulum mainly formed through heteroaggregation (Figure 6a and b). Additionally, SE and BSE images recorded with high magnification (Figure 6c and d) highlight the partial coalescence between the NR globules, which are this time surrounded by several small CB aggregates (20-200 nm). These aggregates establish notable contact with the globule surface (Figure 6e), and some of them are found to partially sink into the globule, as indicated by the red arrows in Figure 6f. Thus, what is locally observed without sonication (Figure 3g and h) is here extended to the whole coagulum. These morphological features confirm a specific interaction between the small CB aggregates and NR globules. This interaction induces the destabilization of the colloidal form of NR particles and results in the ability of the polyisoprene chains confined in the inner part of the globule to diffuse toward the outside, thus leading to partial coalescence.

Altogether, these results indicate (i) that the size of CB aggregates is a key parameter in the binary colloidal dispersion pathway controlling the structure of the formed NR-CB coagulum and (ii) that the hydrophilic character of proteins and lipid head groups at the surface of NR globules (in contrast to the hydrophobic nature of CB) does not prevent the two particles from interacting. These important indications allow us to formulate hypotheses on the microscopic mechanisms involved in the interaction between the NR particles and CB filler. In a previous study on the interfacial structure of NR globules, it has been reported that the hydrophilic heads of lipids protrude toward the solvent phase, forming a very thin second layer (~ 0.6 nm) above the mixed protein and lipid layer that has a thickness of ~ 3.5 nm³. Thus, we can reasonably presume that small CB aggregates can reach the hydrophobic alkyl chain of lipids located on the biomembrane. This can subsequently result in lipid reorganization and adsorption on the hydrophobic domains of CB. The biomembrane being partially shared with the CB aggregates will leave small and transiently uncovered patches on the globule surface, leading to the observed coalescence between them. The aforementioned hypothesis is also supported by a recent study on the efficiency of carbon nanotubes to penetrate phospholipid bilayers¹⁹. The researchers used single-chain mean field theory to report a possible migration of the phospholipid tails on the surface of hydrophobic nanotubes¹⁹. Moreover, the work of Amornwachirabodee et al.²⁰ on the penetration of oxidized carbon black (OCBs) (prepared from commercially available CB) into cell-sized liposomes also reported the adsorption of phospholipids on OCBs. Additionally, a study on the effect of CB incubated with giant unilamellar phospholipid vesicles (GUV) reported a decreasing number of GUV over time²¹, thus supporting our hypothesis.

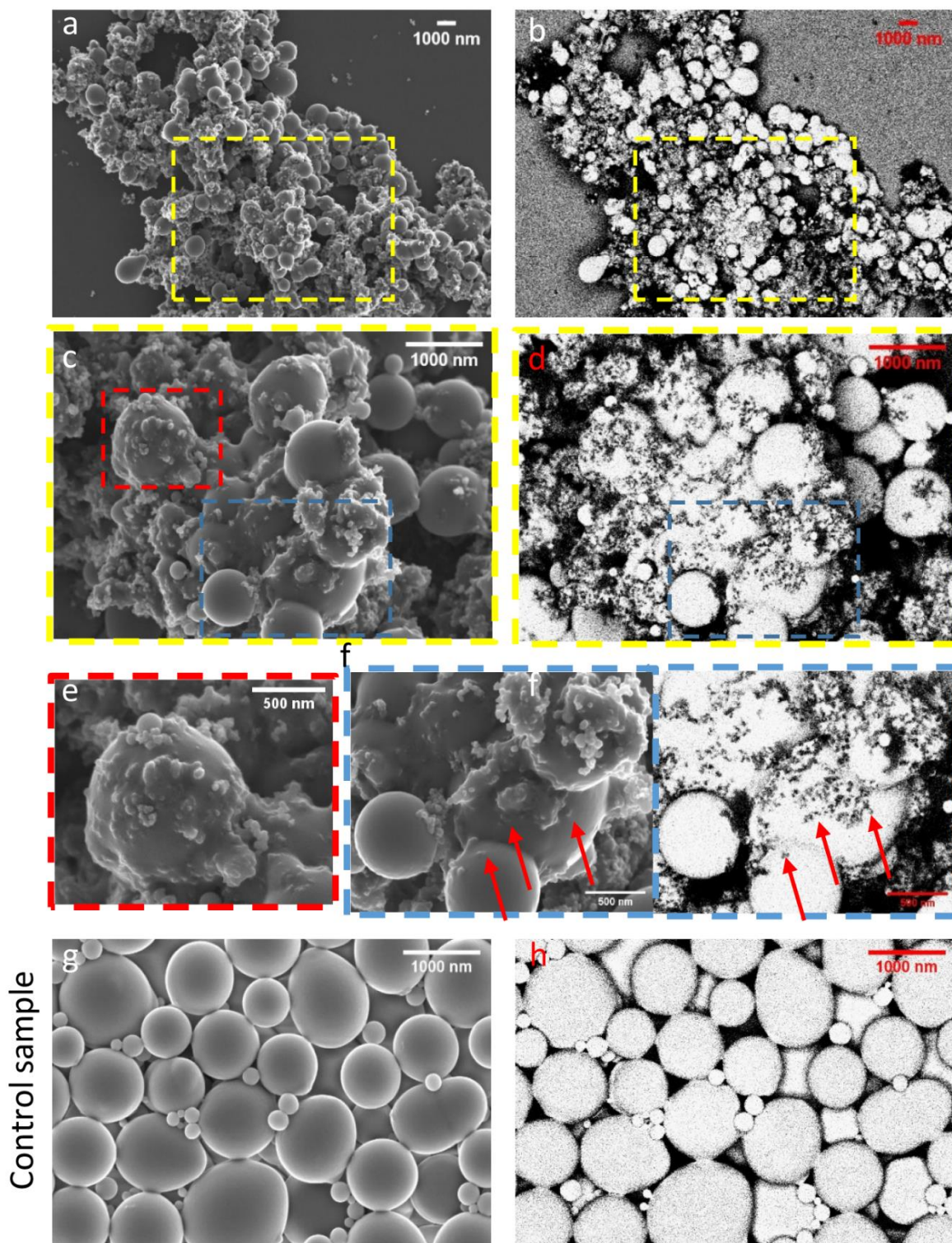


Figure 6. FESEM micrographs of the NR-CB heterocoagulum obtained with sonication during mixing: mass ratio in the liquid suspension = 40% CB/rubber and the structure was fixed at $t=1$ h. (a) Large view SE and (b) BSE images of the same region showing the homogeneous distribution of NRs and CB filler (magnification: 5000x). (c) Magnified SE and (d) BSE views corresponding to the yellow-squared region in (a and b) (magnification: 10000x), highlighting the partial coalescence between the NR globules that are surrounded by several small CB aggregates. (e) Magnified SE of the red boxed region in (c) (magnification: 80000x). (f) Magnified SE and BSE views of the blue-boxed region shown in (c and b) (magnification: 40000x), showing that the CB filler partially sinks toward the inner part of

the NR globules. (g) Magnified SE and (h) BSE views corresponding to the control sample composed only of sonicated NR globules.

4. CONCLUSION

This study reports new insights into the processes occurring during the coagulation between NR latex and a CB slurry. The structural evolution dynamics at the nm scale were investigated, and the impacts of external physical stresses (shear and sonication) were tested.

We highlighted the dependence of NR-CB heteroaggregation vs NR-NR or CB-CB homoaggregation based on the way the filler and NR particles came into first contact. Mixing the two components in colloidal suspensions under sonication maintained CB filler in the form of small aggregates (20-200 nm), resulting in the good homogenization of filler around the NR globules. When small CB aggregates were in contact with NR particles, a structural modification of the NR colloidal form was observed. We hypothesize a local membrane destabilization induced by the adsorption of lipids on the hydrophobic domains of CB, thus leading to the coalescence between the NR globules. To our knowledge, this is the first time that the nanoscopic mechanism that rules NR-CB heteroaggregation has been described, with the visualization of the high reactivity between the CB filler and NR globules.

REFERENCES

1. Salomez, M. *et al.* Micro-organisms in latex and natural rubber coagula of *Hevea brasiliensis* and their impact on rubber composition, structure and properties. *Journal of Applied Microbiology* **117**, 921–929 (2014).
2. Gaboriaud, F., de Gaudemaris, B., Rousseau, T., Derclaye, S. & Dufrêne, Y. F. Unravelling the nanometre-scale stimuli-responsive properties of natural rubber latex particles using atomic force microscopy. *Soft Matter* **8**, 2724 (2012).
3. Rochette, C. N. *et al.* Shell Structure of Natural Rubber Particles: Evidence of Chemical Stratification by Electrokinetics and Cryo-TEM. *Langmuir* **29**, 14655–14665 (2013).
4. Nawamawat, K. *et al.* Surface nanostructure of *Hevea brasiliensis* natural rubber latex particles. *Colloids and Surfaces A: Physicochemical and Engineering Aspects* **390**, 157–166 (2011).
5. Thomas, S., Chan, C. H., Pothen, L. A., Joy, J. P. & Maria, H. J. *Natural Rubber Materials: Volume 2: Composites and Nanocomposites*. (Royal Society of Chemistry, 2013).
6. Goudarzi, T., Spring, D. W., Paulino, G. H. & Lopez-Pamies, O. Filled elastomers: A theory of filler reinforcement based on hydrodynamic and interphasial effects. *Journal of the Mechanics and Physics of Solids* **80**, 37–67 (2015).
7. *Encyclopedia of materials: science and technology*. (Elsevier, 2001).
8. Rubber Division, ACS Liquid Phase Mixing: The Future of Natural Rubber Compounding for Productivity and Performance. <http://rubber.docegon.com/papers/2637-Liquid-Phase-Mixing-The-Future-of-Natural-Rubber-Compounding-for-Productivity-and-Performance->.
9. Martínez-Pedrero, F. *et al.* Making an elastomeric composite material via the heteroaggregation of a binary colloidal dispersion. *Soft Matter* **8**, 8752 (2012).
10. Wang, T. *et al.* CEC and its application in off-the-road tires. 6 (2003).

11. Lin, Y., Zhang, A., Wang, L., Pei, C. & Gu, Q. Carbon Black Filled Powdered Natural Rubber. *Journal of Macromolecular Science, Part B* **51**, 1267–1281 (2012).
12. Santipanusopon, S. & Riyajan, S.-A. Effect of field natural rubber latex with different ammonia contents and storage period on physical properties of latex concentrate, stability of skim latex and dipped film. *Physics Procedia* **2**, 127–134 (2009).
13. Boitte, J.-B. *et al.* A novel rheo-optical device for studying complex fluids in a double shear plate geometry. *Review of Scientific Instruments* **84**, 013709 (2013).
14. Boitte, J.-B., Hayert, M. & Michon, C. Observation of wheat flour doughs under mechanical treatment using confocal microscopy and classification of their microstructures. *Journal of Cereal Science* **58**, 365–371 (2013).
15. Hennig, P. & Denk, W. Point-spread functions for backscattered imaging in the scanning electron microscope. *Journal of Applied Physics* **102**, 123101 (2007).
16. Mazzoli, A. & Favoni, O. Particle size, size distribution and morphological evaluation of airborne dust particles of diverse woods by Scanning Electron Microscopy and image processing program. *Powder Technology* **225**, 65–71 (2012).
17. Butt, H.-J., Kuropka, R. & Christensen, B. Latex film formation studied with the atomic force microscope: Influence of aging and annealing. *Colloid & Polymer Science* **272**, 1218–1223 (1994).
18. Meng, X., Wu, H. & Morbidelli, M. Kinetics and Cluster Morphology Evolution of Shear-Driven Aggregation of Well-Stabilized Colloids. *Langmuir* **31**, 1113–1119 (2015).
19. Pogodin, S. & Baulin, V. A. Can a Carbon Nanotube Pierce through a Phospholipid Bilayer? *ACS Nano* **4**, 5293–5300 (2010).
20. Amornwachirabodee, K. *et al.* Oxidized Carbon Black: Preparation, Characterization and Application in Antibody Delivery across Cell Membrane. *Sci Rep* **8**, (2018).

21. Pajnič, M. *et al.* Effect of carbon black nanomaterial on biological membranes revealed by shape of human erythrocytes, platelets and phospholipid vesicles. *Journal of Nanobiotechnology* **13**, (2015).

Supporting information

Natural Rubber - Carbon Black coagulation: following the nanostructure evolution from a colloidal suspension to an elastomeric composite

Gianluca Cattinari ^{*}, [§], Karine Steenkeste [§], Catherine le Bris [§], Alexis Canette [‡], Matthieu Gallopin [†], Marc Couty [†], Marie-Pierre Fontaine-Aupart [§]

[§] Université Paris-Saclay, CNRS, Institut des Sciences Moléculaires d'Orsay, 91405, Orsay, France

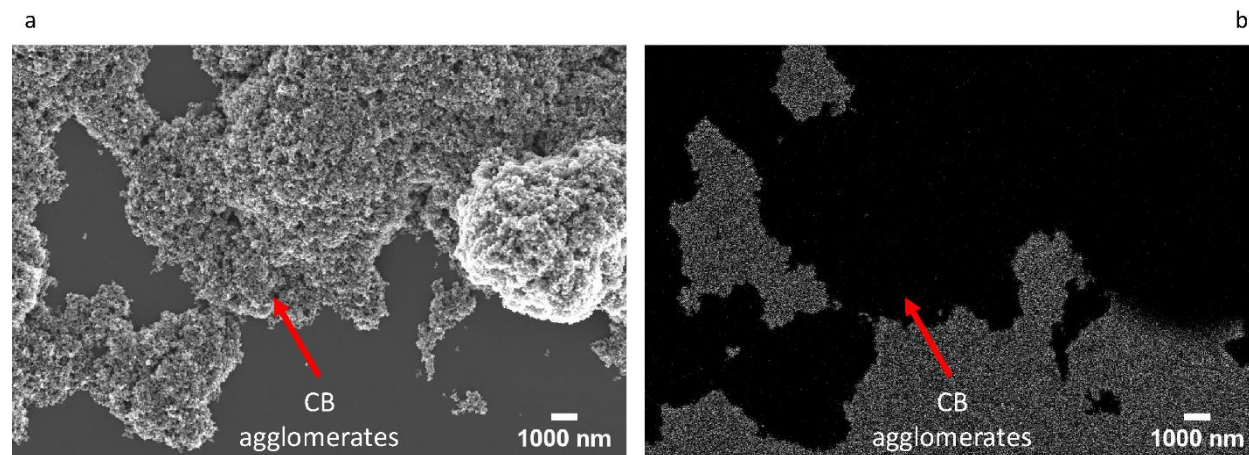
[‡] Sorbonne Université, CNRS, Institut de Biologie Paris-Seine, 75005, Paris, France

[†] Manufacture Française des Pneumatiques Michelin, Clermont Ferrand, France

* Corresponding author

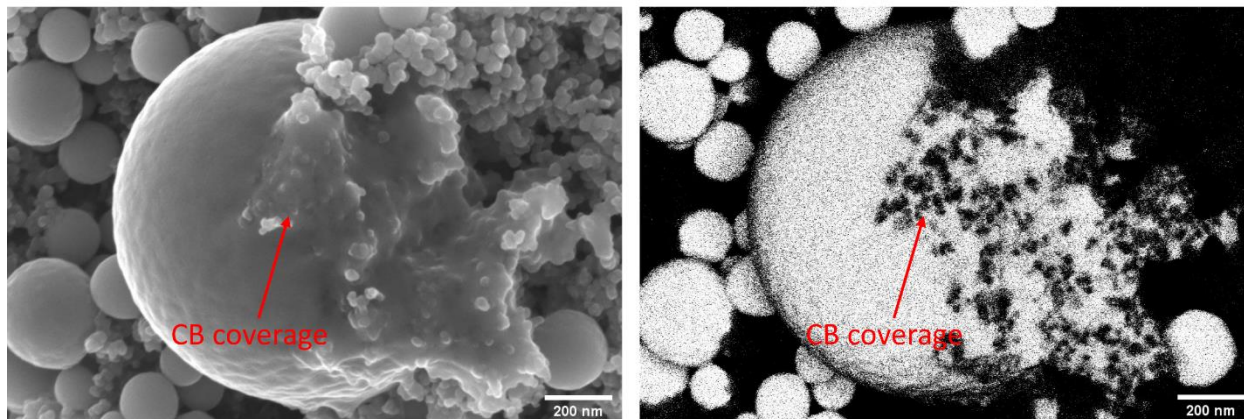
E-mail: gianluca.cattinari@u-psud.fr

Supporting Information 1 (S1): FESEM images of the CB slurry showing the agglomeration of CB in the liquid medium. (a) SE image. (b) BSE image.

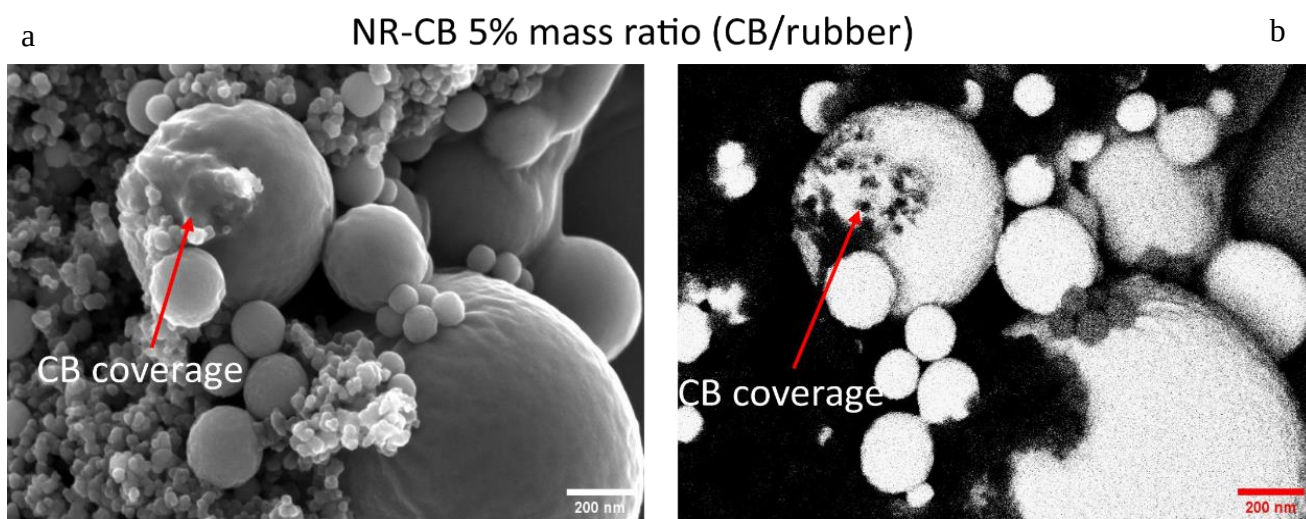


Supporting Information 2 (S2): (a) SE and (b) BSE image showing CB aggregate in interaction with a DPNR globule. DPNR latex was produced via treatment of highly ammoniated NR latex with a bio-enzyme (proteinase), which hydrolyzes the proteins into a water soluble forms. It was subsequently mixed with CB in the same way as for NR latex.

DPNR-CB

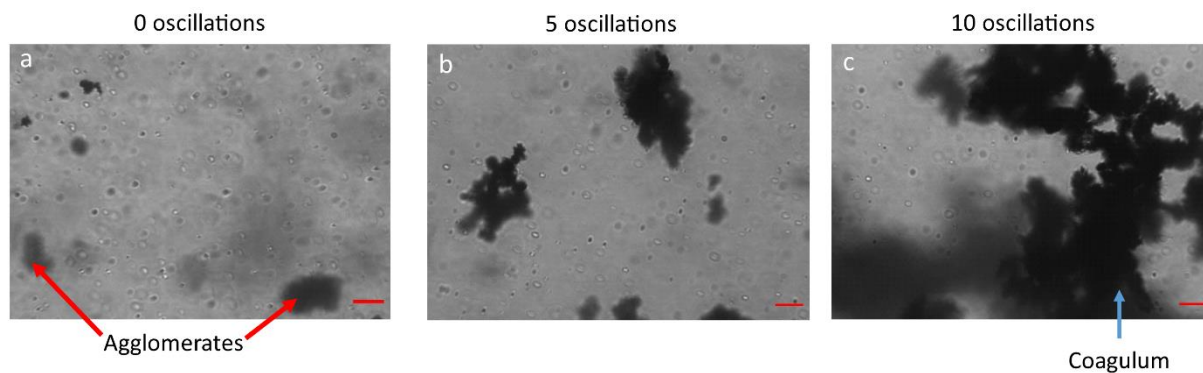


Supporting Information 3 (S3): (a) SE and (b) BSE images showing CB aggregate in interaction with a NR globule - mass ratio in liquid suspension = 5% CB/rubber

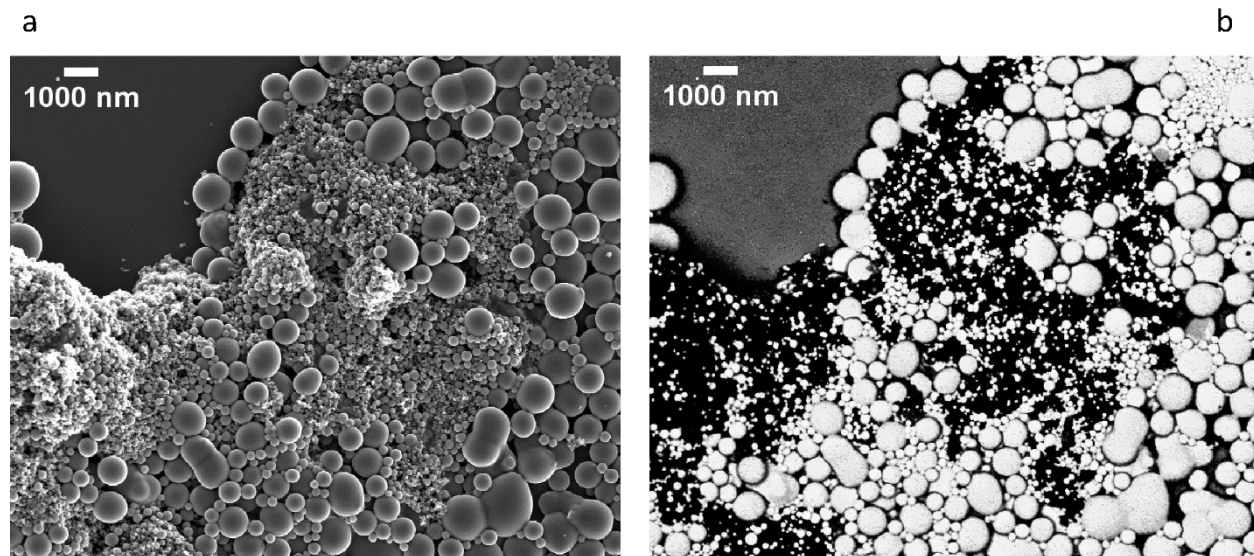


Supporting Information 4(S4): Transmission images recorded along with oscillation cycles for the NR-CB binary colloidal suspension. Mechanical forces were applied using the RheOptiCAD module right after the deposition of the sample on the coverslip ($t=0$). The parameters of each oscillation correspond to 10 Hz frequency; total displacement of 1 μm displacement; 500 μm of gap; and 60s of application. Scale bar corresponding to 10 μm .

$t=0$



Supporting Information 5(S5): FESEM micrograph of NR-CB coagulum formed at $t=1$ h inside the shearing module without the application of mechanical shear. It shows the maintenance of NR globular structure, attesting that the parallel plate geometry used for the application of shear does not influence the NR-CB coagulum structure as well as the NR globular form. (a) SE and (b) BSE images.



Chapter 4: Natural rubber-silica coagulation: structural characterization and evolution towards an elastomeric composite

Introduction

Another important filler used in rubber technology refers to silica (Si). The main drawback often associated to the use of Si as filler concerns its hydrophilic nature, which often limits its dispersion state in a non-polar rubber matrix. In natural rubber (NR) technology, methods for efficient dispersion of Si are still continuously being improved. The previously described liquid phase mixing seems an interesting method to possibly obtain NR-Si composite with good dispersion of the filler. This approach could take advantage of the globular structure of NR latex to allow interaction in liquid and thus possibly achieve a good dispersion in resulting composite. However, contrarily to CB, bringing NR latex in contact with a slurry of Si does not allow spontaneous coagulation. Hence, various solutions have been proposed to achieve this coagulation. For example, incorporating silica into the rubber latex by treating the Si with a coupling agent and mixing the resulting treated Si with conventional coagulants such as polyamine. Another possible solution to achieve coagulation relies on the combined action of divalent ions and/or the coupling with the shearing of the binary colloidal suspension. The latter protocol is very promising, but the structural characterization of the formed coagulum and its evolution dynamics towards the formation of a composite, as well as the distribution of Si fillers has never been described. The first part of this chapter focuses on these issues employing a similar FESEM approach as the one described for a NR-CB system, together with measurements of AFM-IR. This multimodal microscopy approach allowed us to structurally characterize the formed coagulum and follow its evolution with specific attention to the nanodistribution of Si fillers.

Subsequently we pursued the structural characterization by investigating on the spatial arrangements of proteins and lipids of NR, during coagulation and drying. In particular, we studied their arrangement in respect to the Si fillers distribution, locating both biomembrane components and Si from the early stage of mixing until the formation of a composite after solvent evaporation at room temperature. This allowed us to unravel microscopic mechanism occurring during the liquid phase mixing, involving Si, proteins and lipids of NR. To do so, we performed experiments using mainly dual color dSTORM imaging. Additionally, the latter technique was combined with FESEM measurements for a more complete structural characterization.

Results are presented in the form of two articles in preparation, the first one entitled “*Structural evolution dynamics of a Silica-Natural Rubber hetero-coagulum, towards an elastomeric composite*“, and the second one “*Nanosopic spatial arrangement of silica fillers with proteins and lipids of natural rubber: from a colloidal suspension to an elastomeric composite*“.

Article 2: Structural evolution dynamic of a Silica-Natural Rubber heterocoagulum, towards an elastomeric composite

Gianluca Cattinari^{*1}, Karine Steenkeste¹, Catherine le Bris¹, Alexis Canette², Ariane Deniset³,
Matthieu Gallopin⁴, Marc Couty⁴, Marie-Pierre Fontaine-Aupart¹

¹ Université Paris-Saclay, CNRS, Institut des Sciences Moléculaires d'Orsay, 91405, Orsay, France

² Institute de biologie Paris Seine (IBPS), Sorbonne Université, CNRS service de microscopie électronique, 75005 Paris

³ Université Paris-Saclay, CNRS, Institut Chimie Physique (LCP), Université Paris-Saclay, 91405, Orsay, France

⁴ Manufacture Française de Pneumatiques Michelin

Article in preparation

Structural evolution dynamics of a Silica-Natural Rubber heterocoagulum, towards an elastomeric composite

Gianluca Cattinari*¹, Karine Steenkeste¹, Catherine le Bris¹, Alexis Canette², Ariane Deniset³, Marc Couty⁴, Matthieu Gallopin⁴, Marie-Pierre Fontaine-Aupart¹

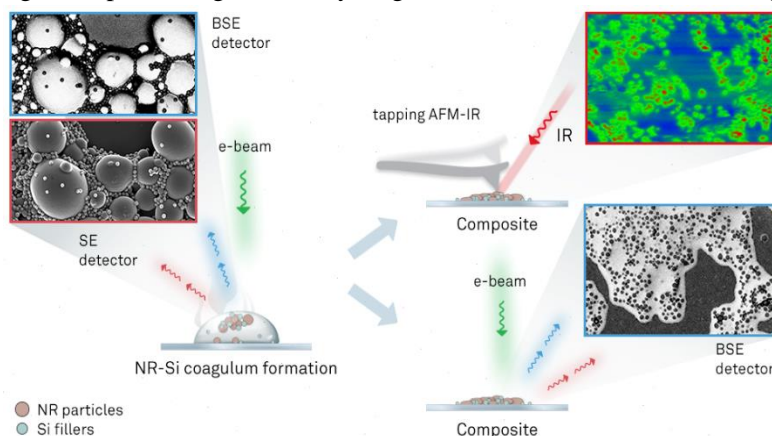
¹ Université Paris-Saclay, CNRS, Institut des Sciences Moléculaires d'Orsay, 91405, Orsay, France

² Institute de biologie Paris Seine (IBPS), Sorbonne Université, CNRS service de microscopie électronique, 75005 Paris

³ Université Paris-Saclay, CNRS, Institut Chimie Physique (LCP), 91405, Orsay, France

⁴ Manufacture Française des Pneumatiques Michelin, Clermont Ferrand, France

ABSTRACT: Natural rubber (NR) latex extracted from *Hevea brasiliensis* is an essential raw material used in the manufacturing of elastomeric composites. In the tire industry, NR is mixed with fillers, in particular with silica (Si) particles to obtain tires with more versatile properties and above all more ecological. The “liquid route” consisting in the mixing of NR latex with a colloidal suspension of Si to give rise to a coagulum that is further dried seems a promising method to obtain a composite. In this context, this study aims to provide a fundamental knowledge of the formation and of the structural evolution dynamics of a NR-Si heterocoagulum coagulum efficiently formed by addition of Mg^{2+} ions. For this purpose, we employed an original field emission scanning electron microscopy (FESEM) approach combining a specific chemical fixation method with the backscattered electron (BSE) and secondary electron (SE) imaging modes. Moreover, FESEM was supported by atomic force microscopy coupled to infrared spectroscopy (AFM-IR) to reveal the nanoscopic distribution of Si fillers in the depth of the obtained composite. The results highlight the presence of the Si fillers surrounding the colloidal NR particles in the heterocoagulum, preventing their early stage deformation. This occurs along with solvent evaporation, leading to the formation of a composite composed of a polymer film with embedded Si particles. The latter remain homogeneously dispersed throughout the film thickness, organized in interconnected individual particles or small aggregates. Regularly, ellipsoidal-ring like structures of Si fillers can be observed, as if Si particles remained frozen in their initial interaction with the NR globules. Our shear stress application does not modify the Si filler distribution within the heterocoagulum but strongly increases its dynamics of formation and evolution.



1. INTRODUCTION

Rubber polymers, with both synthetic or Natural Rubber (NR), need to be reinforced with fillers to achieve necessary strength for most applications¹⁻³. The use of silica (Si) as filler has become of growing importance for certain applications, especially in the tire industry^{4,5}. It has been found that their introduction into rubber blends has allowed to improve the rolling-resistance of tires with related

benefits such as fuel saving and less negative effect on the environment⁶. Different procedures have been developed to incorporate Si fillers in NR (milling, sol-gel techniques, etc)⁷. Among those, the “liquid route” is interesting approach that relies on the colloidal mixture of NR latex with an aqueous suspension of Si, and further drying. Different options are also available: the mixture can be directly dried to form a continuous polymer film with embedded fillers⁸ or it can be first coagulated by chemical or mechanical actions⁹ before drying. These coagulation methods allow to quickly obtaining a composite that could be advantageous at the industrial level. Preliminary studies highlighted the role of divalent cations to promote NR-Si interaction in liquid suspension^{10,11}. However, the structural characterization of the resulting coagulum and the distribution of Si fillers has never been described. To reach this goal, imaging techniques giving access to nanoscopic resolution are required. In this work, we employed field emission scanning electron microscopy (FESEM) in an original approach that lies both on the specific chemical sample’s fixation as well as on the electron multi-detecting modes: backscattering electron imaging (BSE) and secondary electron (SE). Additionally, FESEM was supported by atomic force microscopy coupled to infrared spectroscopy (AFM-IR) to reveal the nanoscopic distribution of Si fillers in the depth of the rubber matrix. By using this multimodal microscopy approach, it was possible to image for the first time the nanostructure of the NR-Si heterocoagulum but also to follow its structural evolution dynamics along drying with a specific attention on the nanodistribution of the Si filler. Additionally, shear-stress applied on NR-Si suspension was investigated in terms of shear-driven aggregation and impact on the structural evolution dynamic.

2. MATERIAL AND METHODS

2.1. Sample Preparation and characterization

High ammonia NR latex concentrate (~60 wt %, HA latex) (Michelin, Clermont Ferrand, France) was used for most of the experiments. It was obtained by centrifugation of field NR latex containing 0.7 wt% ammonia to eliminate free components and nonrubber particles as well as to preserve the colloidal structure of NR globules (a polyisoprene core surrounded by a thin bioshell of proteins and phospholipids). Some experiments were also realized with deproteinized natural rubber (DPNR) latex obtained via treatment of HA latex with a proteinase enzyme. Regardless of the type, the obtained latex is a colloidal dispersion of only NR globules in aqueous phase. Both rubber lattices were diluted to 0,075 wt% rubber content using distilled water and mixed with 100 nm diameter plain Si particles (Kisker Biotech, Steinfurt, Germany) to obtain a binary colloidal suspension. Using dynamic light scattering method (DLS), the size distribution of both NR and Si particles before mixing was controlled. NR latex corresponds to a bimodal distribution of particles with ~90% of globules belonging to small rubber particles (SRPs) (size < 500 nm) and ~ 10% belonging to large rubber particles (LRPs) (size > 500 nm), in agreement with previous results¹² (Figure S1). As expected for the hydrophilic Si particles in suspension, a major peak centered at ~ 100 nm was observed confirming

that the fillers are monodispersed (Figure S1). The mass percent ratio between Si and rubber was kept constant in all the samples and fixed at 40% in colloidal mixture. It was further controlled that this protocol led to a coagulum having $\sim 20\%$ mass ratio of Si/rubber (data not shown). Unless otherwise mentioned, the experiments were conducted in an aqueous medium composed of magnesium sulfate 0.025M (Sigma-Aldrich) corresponding to 100 mM ionic strength and adjusted at pH of ~ 6.5 , a prerequisite to induce a phase-separation and formation of a NR latex or NR-Si coagulum (Figure S2) as previously reported¹¹. The zeta potential of NR and Si particles in solution was determined, both in the presence and in the absence of Mg^{2+} ions (ionic strength = 0.1 M) using a Zetasizer Nano ZS (Malvern Paranalytical) apparatus. The global negative charge of NR globules (due to the presence of proteins and lipids on their surface) was found to decrease following the addition of the ions, while the global negative charge of Si particles (due to the silanol groups) remained unchanged (Table S3). For imaging experiments, 100 μ L of the binary colloidal suspension was deposited on a rounded glass coverslip (coverslip thickness of 170 μ m (MENZEL-GLASER), resulting in a casted drop with a spherical cap shape as illustrated in Figure 1 (drop diameter ~ 1 cm). A phase-separation was macroscopically visible at $t=1$ h, with the formation of a floating object corresponding to the “heterocoagulum” (Figure 1). After $t=4$ h, when most of solvent evaporated, the heterocoagulum adhered on the glass surface. After complete evaporation of the solvent ($t=24$ h) the material referred to a composite. Similar sample preparation was used for suspension composed of only NR latex. Some experiments were also performed to delay solvent evaporation. In this case, the sample was placed in a humidity controlled chamber.

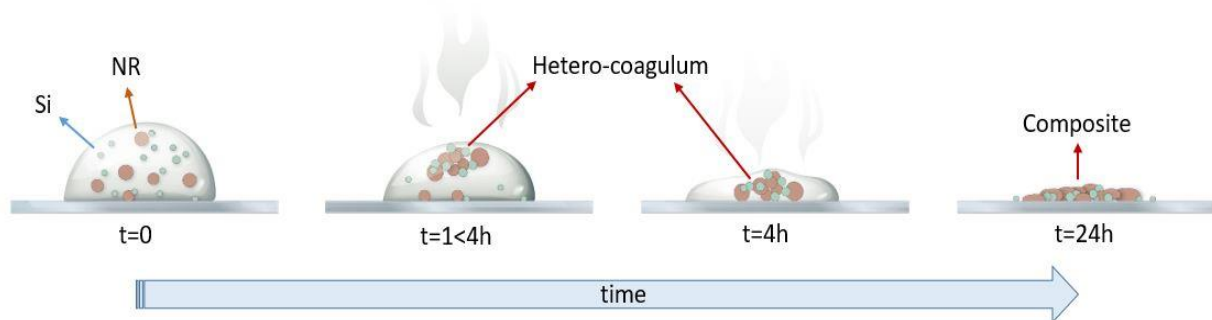


Figure 1. Schematic illustration of the dynamics of heterocoagulum and composite formation after deposition on the glass coverslip of a NR-Si binary colloidal suspension.

2.2. Application of controlled shear-stress

The sample preparation and description of the shearing module used in these experiments were described in details elsewhere¹³. Briefly, the NR-Si binary colloidal suspension was placed between two microscopy coverslips (with a controlled gap width of 500 μ m) well suited for the application of controlled shear. We have controlled that such intercalation of the colloidal suspension between the two glass slides does not induce any deformation on the NR globular structure (Figure

S4). Shear application was obtained using a commercial device called RheOptiCAD^{14,15} (CAD instrument). It consisted in 10 cycles of oscillations during a total of 10 min. Each oscillation corresponds to the displacement of the upper plate of 1 mm (500 μm on either side from a central position) at a frequency of 10Hz during 60s. It was verified on a sample of colloidal NR particles that the shearing conditions did not alter the NR globular form (Figure S5). This shearing device was designed to fit on an inverted microscope (Axiovert, ZEISS) equipped with an Olympus 60x water immersion objective having 1.1 N.A. and a CCD camera (UCBO, Olympus) allowing to acquire transmission imaging of the sample during shear.

2.3. FESEM

FESEM using both topological contrast by secondary electrons (SE) imaging and chemical contrast by backscattered electron (BSE) imaging was performed on samples chemically fixed using vapor of osmium. This type of fixation allowed to preserve the NR colloidal structure and to exploit BSE imaging distinguishing between NR and Si filler due to a different contrast: Si filler appears dark in comparison to NR globules that are bright (Figure 3b). The chemical fixation protocol was optimized in order to be applied regardless of the amount of solvent still present in the sample. It consists in the deposition of 50 μL drops of osmium tetroxide (EMS, USA) solution (1% in water, prepared extemporaneously) around the cover slip of the sample, in a hermetic box protected from light avoiding immersion of the deposited specimen. After 30 minutes, the fixation was considered as complete and the samples were gently rinsed with ultrapure water to remove the excess of dry salt on the specimen and mounted on 25.4 mm aluminium pin stubs (Micro to Nano, the Netherlands) with double sided sticky and conductive tabs (EMS, USA). Samples were then coated with a 10 nm carbon layer by double thread evaporation in high vacuum (10^{-5} mbar) with an ACE600 device (Leica, Germany). Observations were performed in high vacuum (10^{-6} mbar in the observation chamber) with a FESEM Gemini500 (Zeiss, Germany) driven by SmartSEM (version 6.3) operating at 2 kV, with high current mode, a 20 μm aperture and approximately 2 mm working distance. The SE signal was collected with the corresponding SE in lens detector. The BSE signal was collected with the energy selective in column detector using filtering grid (> 400 V) to filter out the SE signal. Images were acquired with a 1024 x 768 resolution, with a dwell time of 6,4 μs and a line averaging of 25. Both SE and BSE signals are surface selective; the SE images are produced at the extreme surface (depth of few nanometers) while the BSE images are capable of providing information arising from a depth of few tens of nanometers¹⁶. For each sample, at least two different zones were recorded using a range of magnification power spanning from 10000x to 40000x.

2.4. Image treatment for quantitative analysis

The minimum average distance between centroids of nearest NR globules was estimated from the FESEM images of the NR-Si coagulum formed at $t=1$ h. For this calculation, the Nearest Neighbor Distance calculation (NND) plugin of ImageJ was used.

SRPs and LRPs were counted in the BSE images recorded from $t=1$ h to $t=4$ h. To do so, a non-local means filter was first applied to subtract the noise from the BSE images. Subsequently, the MorphoLibJ Plugin (ImageJ) was employed on the binary image with the application of watershed segmentation to detect the max Feret diameter of NR particles. This is often used in microscopy measurements for the size analysis of non-spherical particles, and it refers to the longest direction of the globule¹⁷. A threshold was set at 500 nm to discriminate the NR particles: they were considered as SRPs below this threshold, while above they were considered as LRPs. The counting was performed in three different image planes for each condition at 10000x magnification.

2.5. FTIR Analysis

The infrared spectra of Si fillers and NR were acquired with a Bruker Vertex 70 FTIR spectrometer with a diamond ATR (attenuated total reflection) attachment (PIKE MIRacle crystal plate diamond ZnSe) using an MCT detector with a liquid nitrogen cooling system. Prior to measurements, HA latex 60 wt% or the purchased Si suspension at 5 wt% were dehydrated and subsequently deposited directly on the ATR-crystal for spectra acquisition. Each FTIR spectrum corresponds to an accumulation of 100 scans from 4000 to 600 cm^{-1} and with a resolution of 4 cm^{-1} .

2.6. Atomic Force Infrared Microscopy (AFM-IR)

AFM-based infrared spectroscopy (AFM-IR) is a hybrid technique that combines the spatial resolution of atomic force microscopy (AFM) with the chemical analysis capability of infrared (IR) spectroscopy. The method was described in details in references^{18,19}. The instrument used in this study is a NanoIR2 (Anasys Instrument, Bruker nano Surfaces, California, US) combining an AFM set-up with an IR pulsed tunable laser covering the mid-IR region between 1900 cm^{-1} and 900 cm^{-1} (QLC beam, MIRcat-QT, DAYLIGHT solutions; peak powers up to 1 W; average powers up to 0.5 W, wavelength repeatability < 0.1 cm^{-1} and a tunable repetition rate of 1-2000 kHz). The sample were deposited on CaF_2 coverslips (Crystal GmbH, Berlin). The system is used in tapping AFMIR mode²⁰. Simultaneous acquisition of topographic images and IR maps at a specific wavenumber are acquired in tapping mode by means of a Au-coated silicon probe (scan rate 0,2 Hz, driving strength 16%, Power 5,77%, tapping AFM-IR cantilever, Anasys Instruments – spring constant 1–3 nN.m^{-1}). In tapping mode, the lever is forced to oscillate constantly at a given amplitude and frequency. To perform AFM-IR measurements in this mode, it is therefore essential to detect the oscillation generated by the photo-thermal expansion,

whereas the cantilever is already oscillating. Here is the strategy: the oscillation frequency of the tapping cantilever is mixed with the photothermal expansion frequency of the object. While the cantilever is driven at a certain frequency for the tapping mode (here 1430 kHz), the frequency of the laser repetition rate is chosen so that the difference of these two frequencies corresponds another eigenmode of the cantilever (here around 230 kHz, second mode). The nonlinear interaction produced is therefore directly related to the photothermal expansion and will contain all the information related to the IR absorption of the object. Please note that, the IR mapping is capable of providing information arising from a depth $> 1 \mu\text{m}$, while classic topography images are surface selective as FESEM. Topography and IR maps were treated using MountainsMap software, while local IR spectra were filtered using a Stavitsky-Golay algorithm.

3. RESULTS and DISCUSSION

A. NR-Si coagulum formation

The coagulum formed in the presence of Mg^{2+} ions (0,1 M ionic strength) from the phase separation of NR-Si binary colloidal suspension was fixed at $t=1$ h, and subsequently analysed by FESEM (Figure 2). The structure of such coagulum highlights NR particles regularly dispersed as single globules, and surrounded by Si fillers which fill the void between (Figure 2a and b). The determination of the minimal average distance between centroids of nearest NR globules (as described in experimental section) resulted to a value of ~ 250 nm, confirming that at least one Si particle is found intercalated between two NR globules both LRPs or SRPs (Figure 2c and d). Thus, we confirmed that the presence of the divalent cations (ionic strength= 0,1 M) is necessary to screen the electrostatic double layer (EDL) and induce the interaction between NR particles (Table S3) and/or to act as electrostatic bridges between the surfaces of adjacent NR and Si particles, allowing the interaction between them. Interestingly, results obtained on the coagulum of only NR latex report differences in comparison to the NR-SI heterocoagulum (Figure 2e and f). In the former case, the Mg^{2+} ions also enable the NR-NR interaction in the liquid phase, but as soon as the NR globules are in contact their deformation and coalescence is observed. We can reasonably hypothesize that the NR particles are close enough to each other, to be able to induce a destabilization of the NR bioshell surface. This results in the ability of the polyisoprene chains confined in the inner part of the NR globules to diffuse toward the outside. By contrast, the presence of Si fillers surrounding the NR particles hinders their contact and prevents them from their destruction.

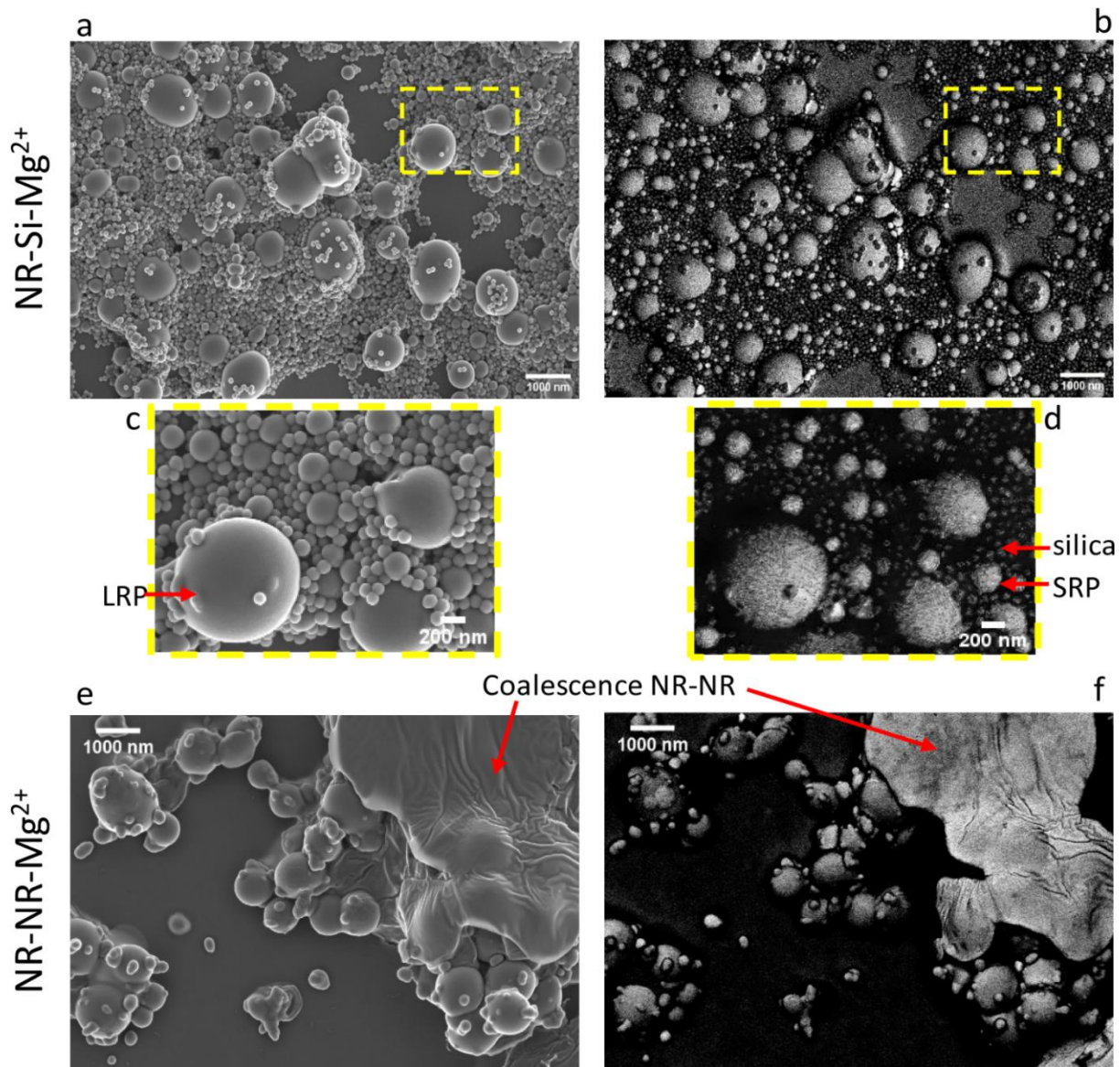


Figure 2. FESEM micrographs of NR-Si heterocoagulum and NR-NR homocoagulum obtained in the presence of Mg^{2+} ions (100 mM ionic strength); structure fixed at $t=1$ h. (a) SE and (b) BSE images of the NR-Si heterocoagulum (magnification: 10000x). (c) Magnified SE and (d) BSE images corresponding to the yellow squared region in (a) and (b), showing silica fillers surrounding NR globules and preventing their contact (magnification: 40000x). (e) SE and (f) BSE images of the NR-NR coagulum, showing large zones of coalescence between NR globules (magnification 10000x).

B. Structural evolution dynamics of the NR-Si coagulum

In order to follow the structural evolution dynamics of the NR-Si heterocoagulum throughout solvent evaporation, until the formation of a composite, FESEM images were performed at different

times from $t=1$ h to $t=24$ h. At $t=2$ h the NR globules still maintain their original colloidal structure (Figure S6a). From $t=3$ h and along with the solvent evaporation, the sample becomes structurally heterogeneous. Regions where the colloidal structure of NR globules is preserved as well as domains characterized of a polymer film covering parts of the sample can be observed (Figures S6b and Figure 3a). This last region is the result of polyisoprene chains, previously confined in the inner part of the globules and diffusing across the NR particle interfaces filling the regions occupied by Si fillers. To verify if the loss of the NR globular structure was due to their interaction with the Si fillers and/or to the solvent evaporation, the NR-Si heterocoagulum was formed and maintained in a controlled humidity environment to limit the evaporation. In this condition, at $t=4$ h while the solvent is still largely present, the FESEM images did not reveal any zone of filmification. (Figure S7). Thus, the destabilization of the NR colloidal form is regulated by the solvent evaporation.

To progress in the understanding of the structural evolution of the NR-Si heterocoagulum, counting of LRPs and SRPs has been carried out on the structures recorded from $t=1$ h to $t=4$ h (Figure 3b). Interestingly, the heterocoagulum at $t=1$ h is found to be composed of $\sim 85\%$ of SRPs and 15% of LRPs (Figure 3c), a ratio between the two types of NR particles similar to the one established by DLS measurements (Figure S1). This reveals that both LRPs and SRPs are included in the heterocoagulum. However, during evaporation, the globular form of LRPs was retained for longer time than that of SRPs, (Figure 3c). This is consistent with the NR particles size: the specific surface area of SRPs is greater than the one of LRPs and thus assuming similar polymer inter-diffusion rates, we expect the loss of the colloidal structure of SRPs at earlier stage than that of LRPs. This observation is in agreement with a previous Atomic Force Microscopy (AFM) study²⁰ on latex films containing mostly LRPs and SRPs, respectively. Films formed from SRPs are smooth and show no sign of individual particles, while the ones containing LRPs are rough and the topology of individual particle is conserved. Another parameter that affected the structural evolution dynamics of the heterocoagulum containing Si fillers is the surface composition of NR globules. Indeed, using a DPNR in place of NR, a faster filmification process was observed (Figure S8) suggesting that proteins might contribute to the rigidity of the biomembrane of the NR globules, retaining their spherical form for longer time.

At $t=24$ h, after complete evaporation of the solvent, a composite was obtained. FESEM images show that the memory of the original colloidal form of NR globules was mostly lost to give rise to a film with a very smooth surface where Si fillers were embedded (Figure 3c and d). The fillers appear quite homogeneously dispersed but also regularly organized as ring-ellipse like structures (such as the ones circled by an orange circle on Figure 3d), with sizes ranging between 250- 2000 nm, similar to those of the NR particles in their initial colloidal form. To further investigate the Si fillers arrangement inside the composite, AFMIR measurements were performed.

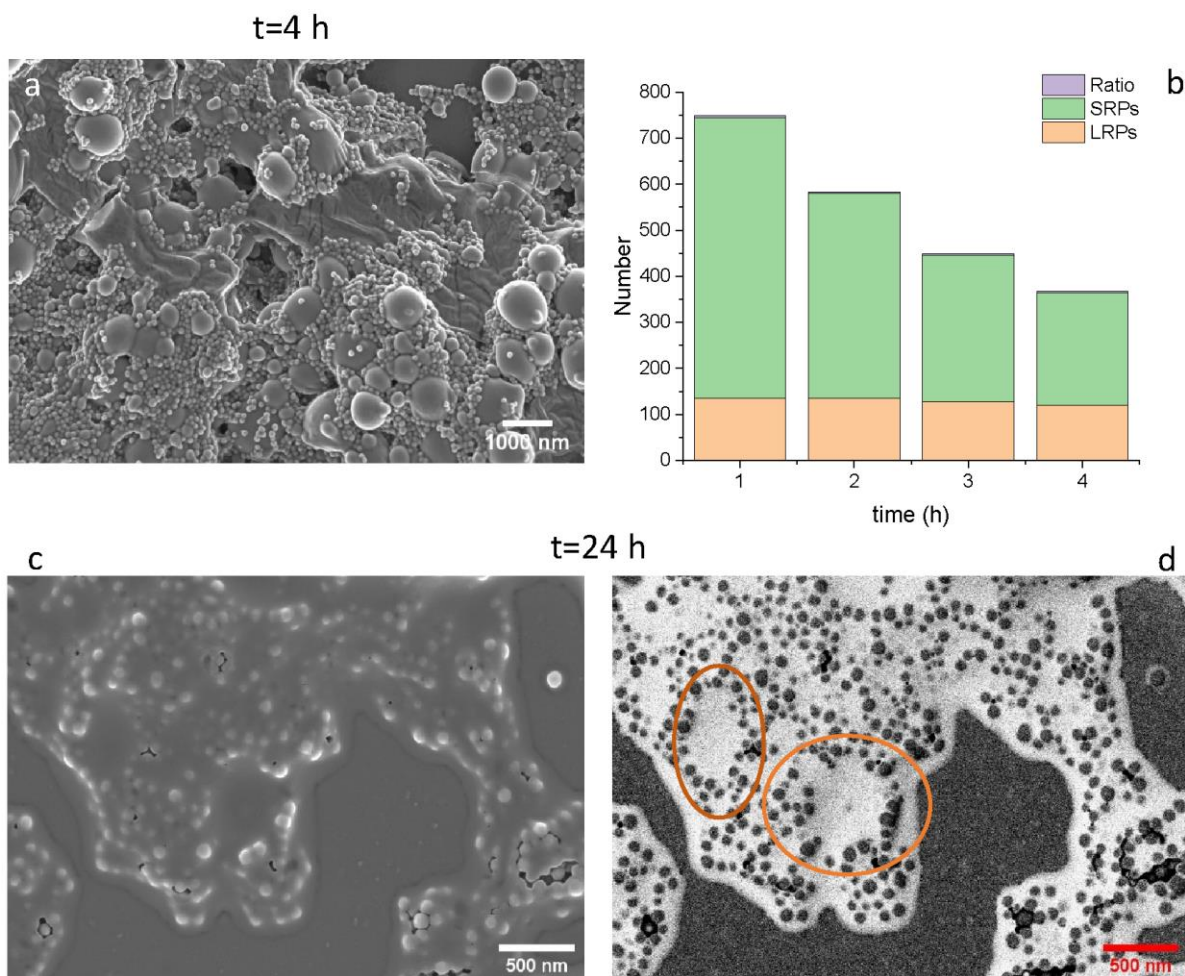


Figure 3. Structural evolution dynamics of NR-Si heterocoagulum, and Si filler distribution in the obtained composite. (a) SE micrographs showing the structure at t=4 h of the (a) NR-Si heterocoagulum (magnification 10000x). (b) Histogram grouping the SRPs and LRPs counts and the ratio (SRPs/LRPs) between t=1h and t=4h. (c) SE and (d) BSE images showing the distribution of Si filler in the obtained composite, t=24h (magnification 20000x). The orange circles highlight a ring-distribution of Si fillers.

Classical tapping-AFM measurements combining topography, amplitude and phase contrast informations (Figure S9) are in line with FESEM images. They show the presence of a NR film (Figure S9a) covering embedded Si fillers that are better discern on the amplitude and phase contrast images (Figure S9b and c). The coupling of AFM with the IR spectroscopy allows to investigate the arrangement of Si fillers with deeper axial depth ($>1\mu\text{m}$). A first IR map was recorded at 1100 cm^{-1} , corresponding to the asymmetric Si-O-Si stretching as illustrated on the FITR spectra (insert in Figure 4d). The IR map confirms their distribution in ring-ellipse structures and revealed their possible interconnection forming a network (Figure 4b). AFM-IR also allows the local acquisition of IR spectra by positioning the AFM tip on domains of interest (grey and orange arrow in Figure

4b). The local IR spectra showed minor peaks between 1300 cm^{-1} and 1800 cm^{-1} and a major peak at 1100 cm^{-1} (Figure 4d). This confirms that the absorbing structure on the IR map recorded at 1100 cm^{-1} refers to Si fillers which are at least partially covered by the NR film as revealed by the minor absorption bands between 1300 cm^{-1} and 1800 cm^{-1} . The presence of such film was also confirmed by acquiring the IR map at 1450 cm^{-1} , a wavelength related to the CH_2 bending, typical of polyisoprene (Figure 4d). The latter represents the negative image of the one recorded at 1100 cm^{-1} . Interestingly, the local IR spectra recorded on a large area NR film (blue arrow Figure 4c) reveals an intense absorption at 1100 cm^{-1} , proving the presence of Si fillers arising from deeper layers.

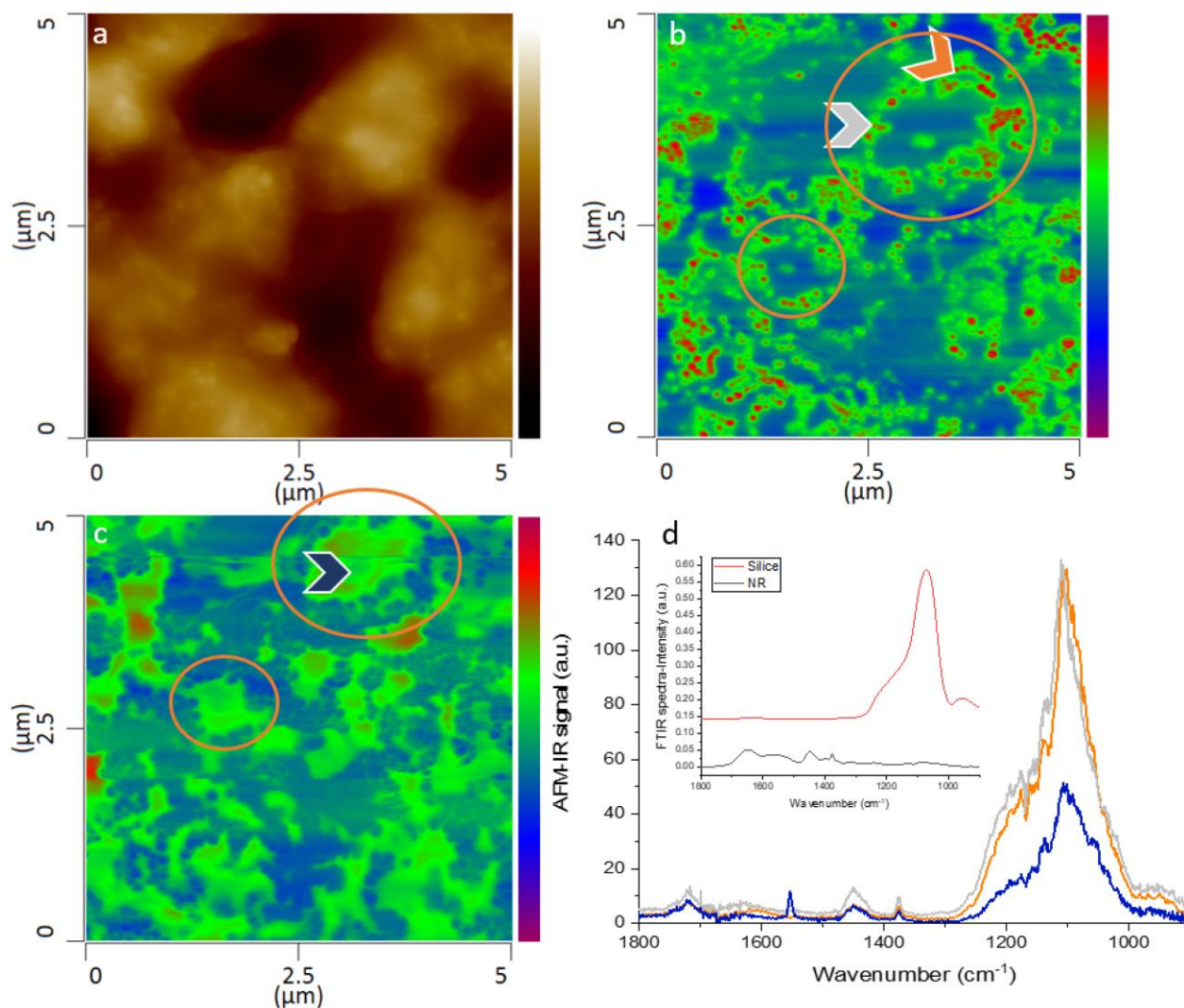


Figure 4. Si fillers distribution on obtained composite at $t= 24\text{ h}$. AFM (a) height image. (b) IR map at 1100 cm^{-1} of the corresponding region referring to Si-O-Si asymmetric stretching. (c) IR map at 1450 cm^{-1} referring to the CH_2 bending. In both cases, the red and blue colours correspond respectively to high and low level of IR absorption, respectively. The orange circles highlight a specific arrangement of Si fillers. (d) Local IR spectra acquired in specific location indicated by arrows in (c) and (d), and corresponding FTIR spectra of individual Si and NR.

In summary, Si fillers are scattered throughout the thickness of the latex film. When they appear embedded in ring-like structure of similar sizes as the diameter of NR particles, we can reasonably assume that the distribution of Si fillers in the obtained composite might be link to the early stage interaction with the globules. Therefore, along with the solvent evaporation NR globules lose their colloidal form while Si fillers remain frozen in their initial position.

C. Effect of shear-stress on the colloidal suspension

Mechanical shear was applied right after the deposition of the NR-Si suspension on the coverslip, to assess its impact on the coagulation and filmification process. Light transmission images recorded during the applied oscillation cycles, highlight the formation and combination of aggregates, growing in size and quickly leading to a macroscopically visible phase-separated coagulum at the end of 10 min (end of the oscillation cycles) (Figure S10a). By comparison, approximately 1 h was needed to macroscopically observe phase separation without the shear application. It was controlled that in the absence of Mg^{2+} ions, the formation of the coagulum under shear was not observed (Figure S10b). This demonstrates that in our conditions, such mechanical constraint was not sufficient for NR globules and Si particles to overcome the interaction energy barrier¹⁸, mainly due to the electrostatic repulsion between particles. The more rapid formation of the NR-Si coagulum under shear application is due to the increasing number of encounters between particles. Figure 5a illustrates the nanostructure of the NR-Si heterocoagulum formed under shear application. As observed macroscopically, the structural evolution kinetics of this heterocoagulum is significantly speed-up: the FESEM image at 10 min is comparable to that obtained at $t=4$ h without shearing (Figure 3a) with no perceptible structural difference. The influence of the applied shear on the distribution of Si fillers in the final composite ($t=24$ h) was also controlled by combining SE (Figure 5b) and AFM-IR (Figure 5c and d) measurements. A similar distribution and arrangement, with no more aggregation of the fillers are observed as the one obtained without shear application (Figure 3c and 4c). Thus, the application of the shear on the binary colloidal suspension greatly accelerates the formation of a phase-separated NR-Si heterocoagulum together with boosting coalescence between NR globules, without influencing the Si fillers distribution.

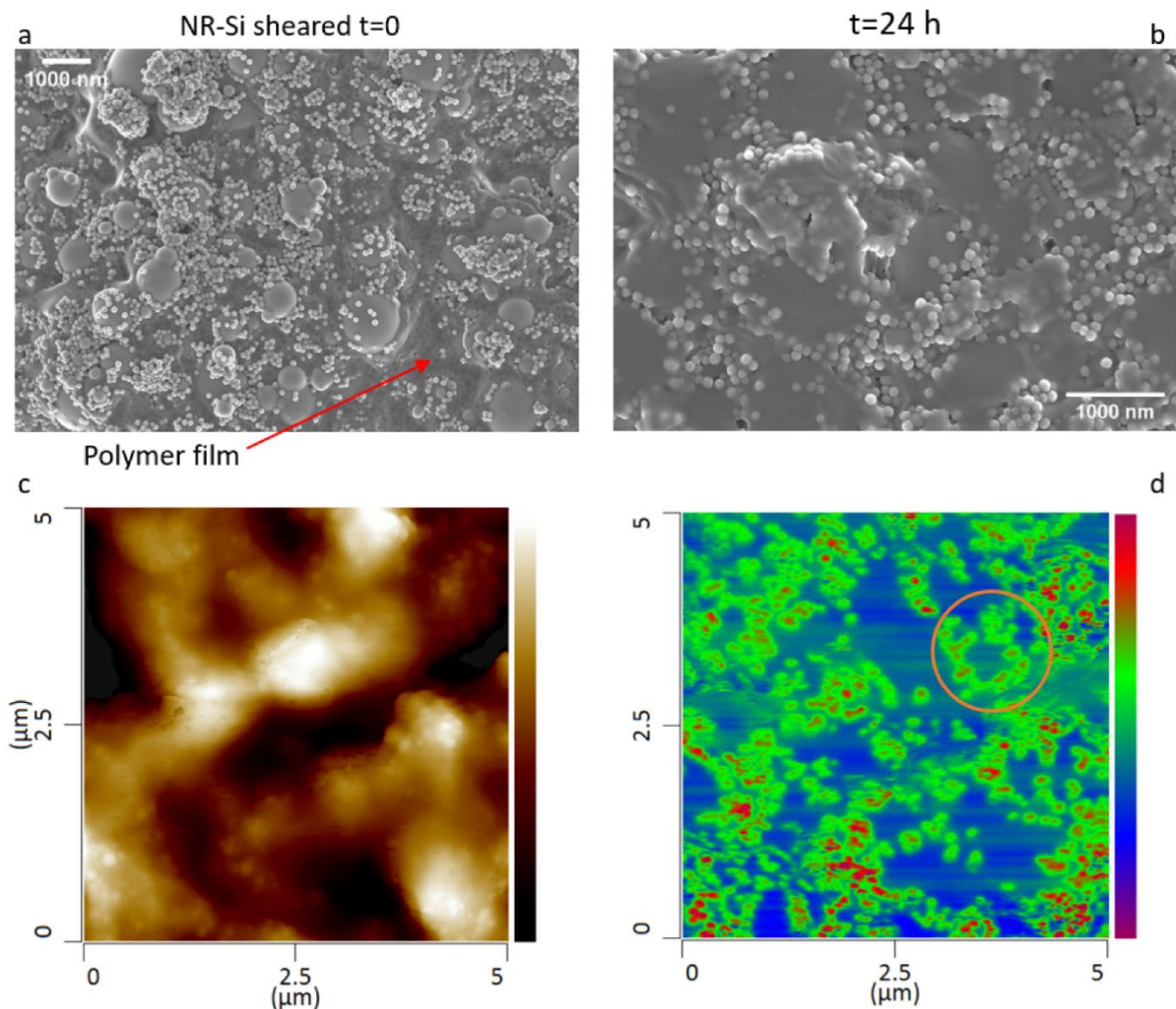


Figure 5. Effect of shear on the structure of the NR-Si hetero-coagulum and on the distribution of Si in the obtained composite. Mechanical shear was applied using the RheOptiCAD module. SE images showing the structure of (a) the heterocoagulum at the end of the 10 oscillation cycles (10 min) (magnification 10000x). (b) SE micrograph showing the distribution of Si fillers in the composite at $t=24$ h when shear-stress was applied (magnification 20000x). (c) AFM height and (d) corresponding IR map at 1100 cm^{-1} of the composite at $t=24$ h. The red colour refers to high adsorption, whereas the blue to low adsorption. The circled regions highlight a ring-distribution tendency in the arrangement of Si fillers.

4. CONCLUSION

In this study, we report new insights on the nanoscale structural characterization and evolution of a NR-Si heterocoagulum made by coagulation of NR latex with an aqueous suspension of Si fillers in presence of Mg^{2+} ions (ionic strength= 0,1 M). The impact of mechanical shear applied in the binary liquid suspension was also tested.

The obtained coagulum is characterized by the presence of Si fillers surrounding NR globules and establishing contact with their surface. Their contact does not itself trigger any deformation of the globule. However, along with solvent evaporation, the NR globules deform giving rise to a composite consisting of a polymer film with embedded Si fillers homogeneously distributed. The latter are found organized in ellipsoidal-ring like structures with size ranging from 250-1000 nm in the obtained composite, as if they remained frozen in their initial localization surrounding the NR globules. The application of mechanical shear applied in the binary liquid suspension greatly accelerates the dynamic of coagulum formation as well as boosting coalescence between NR globules without any effect on the distribution of Si fillers. To our knowledge, this is the first time that the structural evolution dynamics of a NR-Si heterocoagulum is reported, with particular focus on the distribution of the fillers. One of the open questions to be addressed concerns the role of the bio-membrane components of NR globules in the reported structural evolution, as well as their distribution in the filled rubber matrix. We believe that such structural characterization studies enrich the knowledge of nanoscale processes occurring during fabrication of elastomeric composite materials through the liquid route.

REFERENCES

1. *Encyclopedia of materials: science and technology*. (Elsevier, 2001).
2. Sahakaro, K. Mechanism of reinforcement using nanofillers in rubber nanocomposites. in *Progress in Rubber Nanocomposites* 81–113 (Elsevier, 2017). doi:10.1016/B978-0-08-100409-8.00003-6.
3. Donnet, J.-B. & Custodero, E. Reinforcement of Elastomers by Particulate Fillers. in *Science and Technology of Rubber* 367–400 (Elsevier, 2005). doi:10.1016/B978-012464786-2/50011-0.
4. Sarkawi, S. S., Dierkes, W. K. & Noordermeer, J. W. M. Elucidation of filler-to-filler and filler-to-rubber interactions in silica-reinforced natural rubber by TEM Network Visualization. *European Polymer Journal* **54**, 118–127 (2014).

5. Dierkes, W. & Blume, A. Silica Reinforcement. in *Encyclopedia of Polymeric Nanomaterials* (eds. Kobayashi, S. & Müllen, K.) 1–7 (Springer Berlin Heidelberg, 2014). doi:10.1007/978-3-642-36199-9_307-1.
6. Kaewsakul, W. Silica-reinforced natural rubber for low rolling resistance, energy-saving tires: aspects of mixing, formulation and compatibilization. (2013).
7. Thomas, S., Chan, C. H., Pothen, L. A., Joy, J. P. & Maria, H. J. *Natural Rubber Materials: Volume 2: Composites and Nanocomposites*. (Royal Society of Chemistry, 2013).
8. Oberdisse, J. Aggregation of colloidal nanoparticles in polymer matrices. *Soft Matter* **2**, 29–36 (2006).
9. Wang, T. *et al.* CEC and its application in off-the-road tires. 6 (2003).
10. Chan, A. J. *et al.* Natural Rubber–Filler Interactions: What Are the Parameters? *Langmuir* **31**, 12437–12446 (2015).
11. Berriot (Michelin), US. Patent 9,175,144B2, November, 2015.
12. Santipanusopon, S. & Riyajan, S.-A. Effect of field natural rubber latex with different ammonia contents and storage period on physical properties of latex concentrate, stability of skim latex and dipped film. *Physics Procedia* **2**, 127–134 (2009).
13. Natural rubber-carbon black coagulation: following the nanostructure evolution from a colloidal suspension to an elastomeric composite (article currently submitted to journal of Applied Polymer science).
14. Boitte, J.-B. *et al.* A novel rheo-optical device for studying complex fluids in a double shear plate geometry. *Review of Scientific Instruments* **84**, 013709 (2013).
15. Boitte, J.-B., Hayert, M. & Michon, C. Observation of wheat flour doughs under mechanical treatment using confocal microscopy and classification of their microstructures. *Journal of Cereal Science* **58**, 365–371 (2013).

16. Hennig, P. & Denk, W. Point-spread functions for backscattered imaging in the scanning electron microscope. *Journal of Applied Physics* **102**, 123101 (2007).
17. Mazzoli, A. & Favoni, O. Particle size, size distribution and morphological evaluation of airborne dust particles of diverse woods by Scanning Electron Microscopy and image processing program. *Powder Technology* **225**, 65–71 (2012).
18. Dazzi, A. & Prater, C. B. AFM-IR: Technology and Applications in Nanoscale Infrared Spectroscopy and Chemical Imaging. *Chemical Reviews* **117**, 5146–5173 (2017).
19. Pancani, E. *et al.* High-Resolution Label-Free Detection of Biocompatible Polymeric Nanoparticles in Cells. *Particle & Particle Systems Characterization* **35**, 1700457 (2018).
20. Mathurin, J. *et al.* How to unravel the chemical structure and component localization of individual drug-loaded polymeric nanoparticles by using tapping AFM-IR. *Analyst* **143**, 5940–5949 (2018).
21. Rippel, M. M., Lee, L.-T., Leite, C. A. P. & Galembeck, F. Skim and cream natural rubber particles: colloidal properties, coalescence and film formation. *Journal of Colloid and Interface Science* **268**, 330–340 (2003).

Supporting information

Structural evolution dynamics of a Silica-Natural Rubber heterocoagulum, towards an elastomeric composite

Gianluca Cattinari ^{*}, [§], Karine Steenkeste [§], Catherine le Bris [§], Alexis Canette [‡], Ariane Deniset ^{**},

Matthieu Gallopin [†], Marc Couty [†], Marie-Pierre Fontaine-Aupart [§]

[§] Université Paris-Saclay, CNRS, Institut des Sciences Moléculaires d'Orsay, 91405, Orsay, France

[‡] Sorbonne Université, CNRS, Institut de Biologie Paris-Seine, 75005, Paris, France

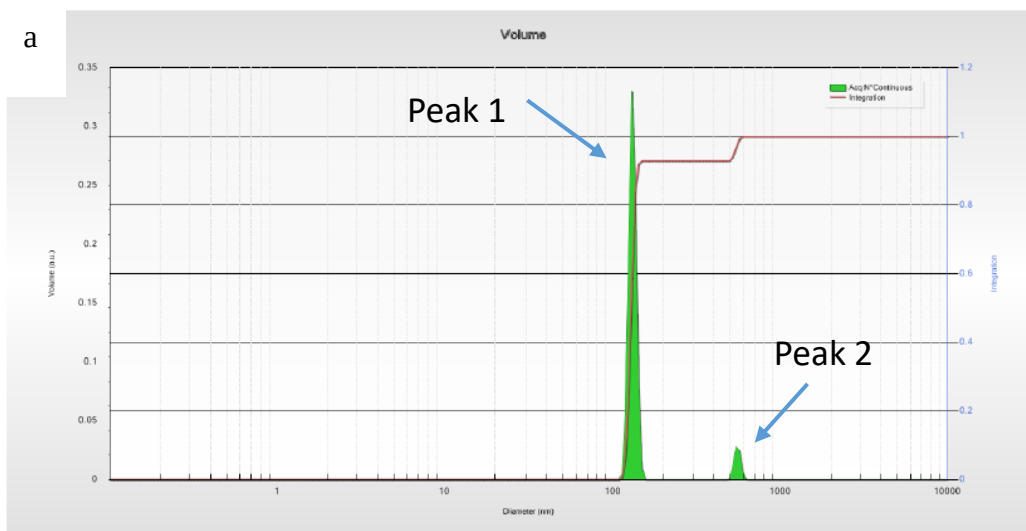
^{**} Université Paris-Saclay, CNRS, Institut Chimie Physique (LCP), 91405, Orsay, France

[†] Manufacture Française des Pneumatiques Michelin, Clermont Ferrand, France

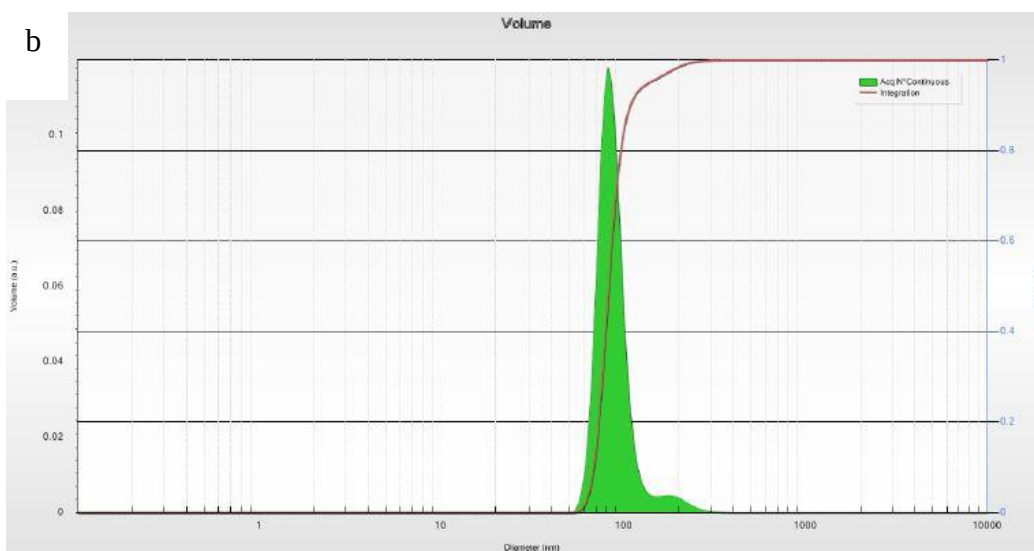
* Corresponding author

E-mail: gianluca.cattinari@u-psud.fr

Supporting Information 1 (S1): DLS measurement of (a) NR particles (0,075 wt%) and (b) silica particles recorded using a DLS Cordouan Vasco Flex apparatus. The particle size and distribution are based on volume.

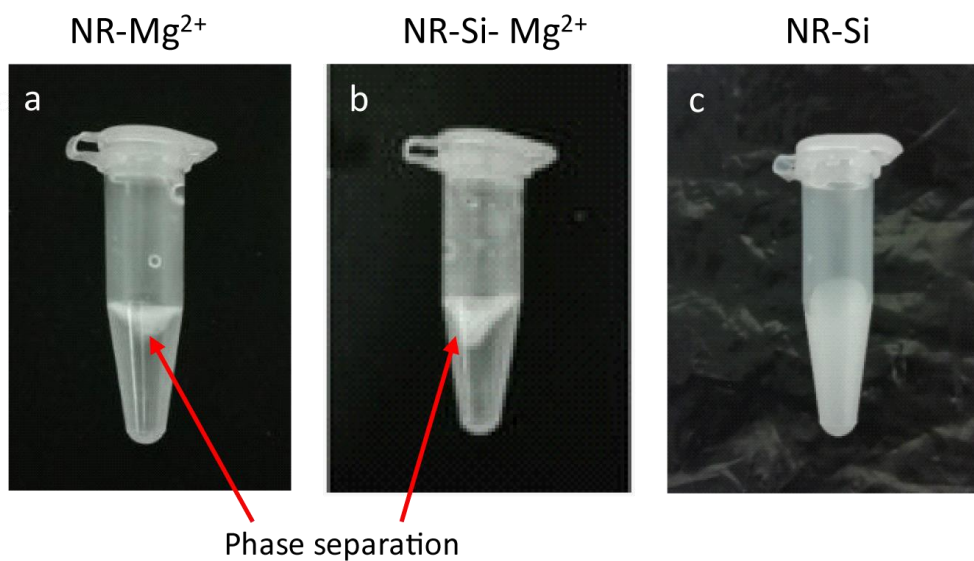


Peak1	Mean:130,60 nm	Std Dev: 6,29%	Intensity: 92,9%
Peak2	Mean: 554,27 nm	Std Dev: 5,59%	Intensity: 7,1%



Peak1	Mean:86 nm	Std Dev: 18	Intensity: 96%
Peak2	Mean:180 nm	Std Dev: 19	Intensity: 4%

Supporting Information 2 (S2): Coagulation assays. NR concentration ~ 0.075 wt%; mass percent ratio $\sim 40\%$ (silica/rubber); pictures were taken after 24h from the mixture (a) Photograph of NR latex in presence of presence of Mg^{2+} ions (100 mM ionic strength). (b) Photograph of NR-Si binary colloidal dispersion in presence of Mg^{2+} ions (100 mM ionic strength). (c) Photograph of NR-Si dispersion in absence of ions.

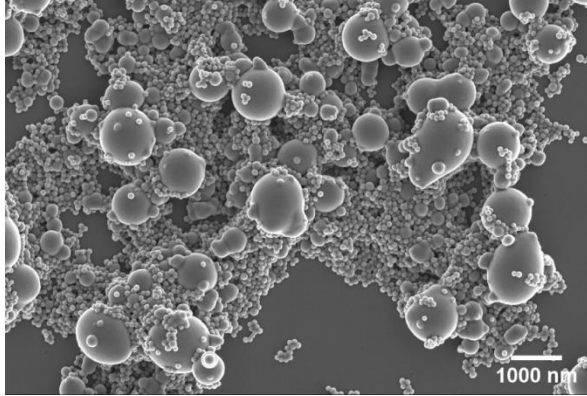


Supporting Information 3 (S3): Zeta potential average values of NR and Si particles in absence and presence of MgSO₄, (Ionic strength =0,1M; pH=6.5) recorded using Zetasizer Nano ZS (Malvern Paranalytical) apparatus

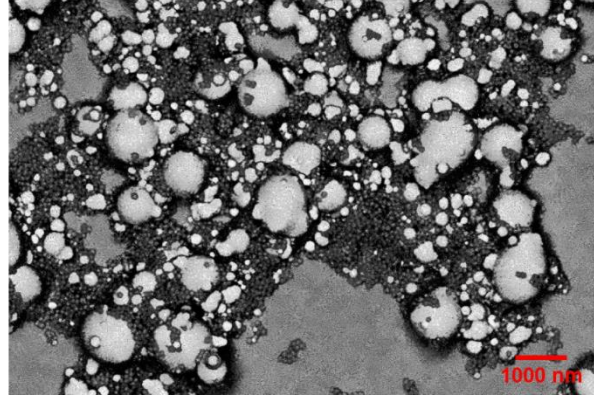
Sample	Zeta Average (mV)	Standard deviation (%)
NR	-57,9	1,1
NR + Mg ²⁺	-28,8	0,5
Si	-12,2	1,4
Si - + Mg ²⁺	-12,2	0,6

Supporting Information 4 (S4): FESEM micrograph of NR-Si hetero-coagulum formed at $t=1h$ inside the shearing module without the application of mechanical shear. The NR globular structure is maintained, attesting that the insertion of the bicolloidal suspension between two parallel plates does not induce any deformation effect. (a) SE and (b) BSE images. Magnification $\times 10000$.

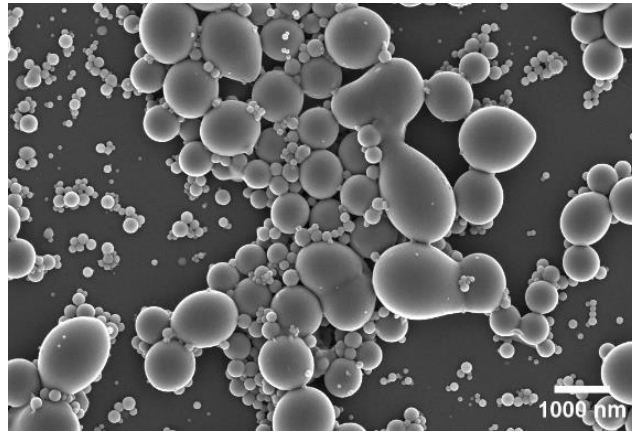
a



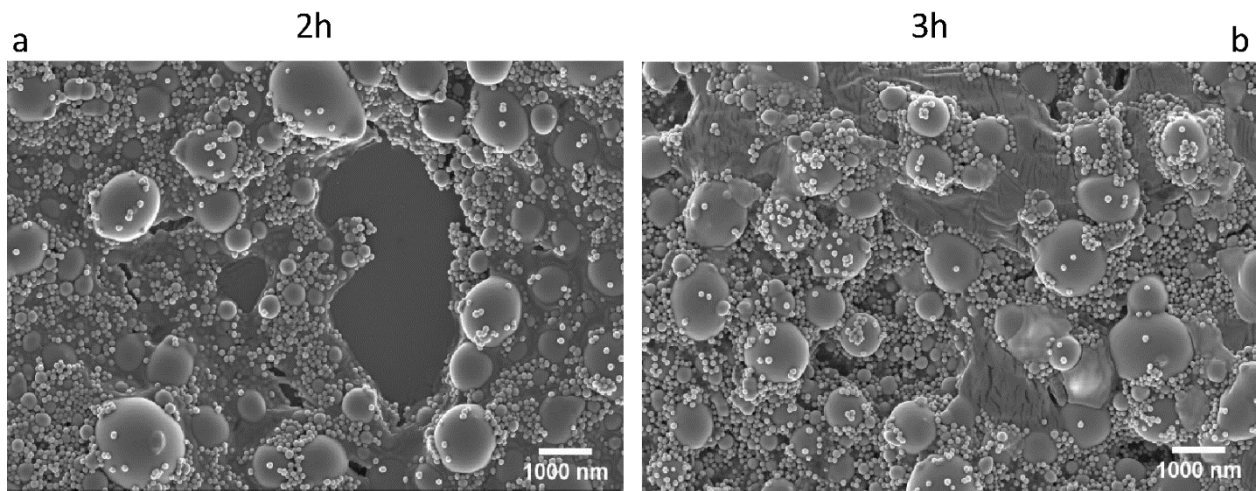
b



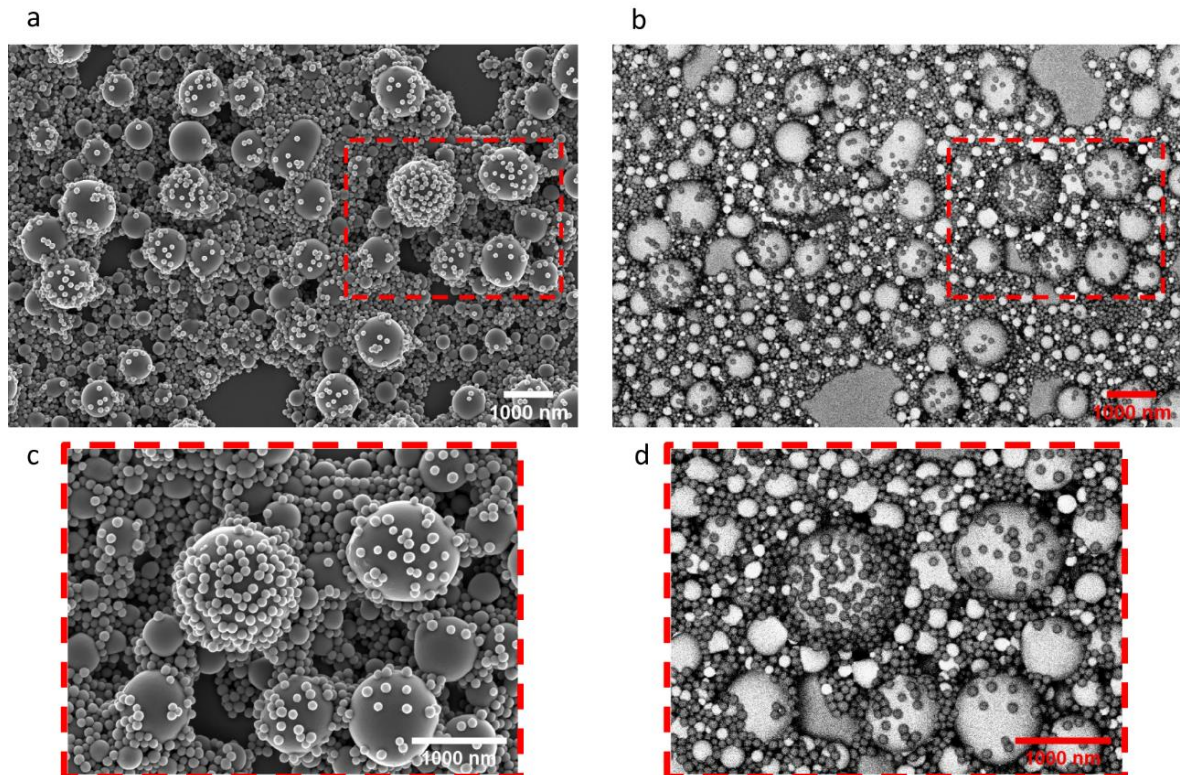
Supporting Information 5 (S5): SE micrograph on NR latex (without Mg²⁺ ions) at the end of 10 oscillation cycles of shear. The NR globular structure is maintained attesting that the shear conditions used does not induce any NR structural deformation on the NR globules in absence of Mg²⁺ ions. Magnification 10000x.



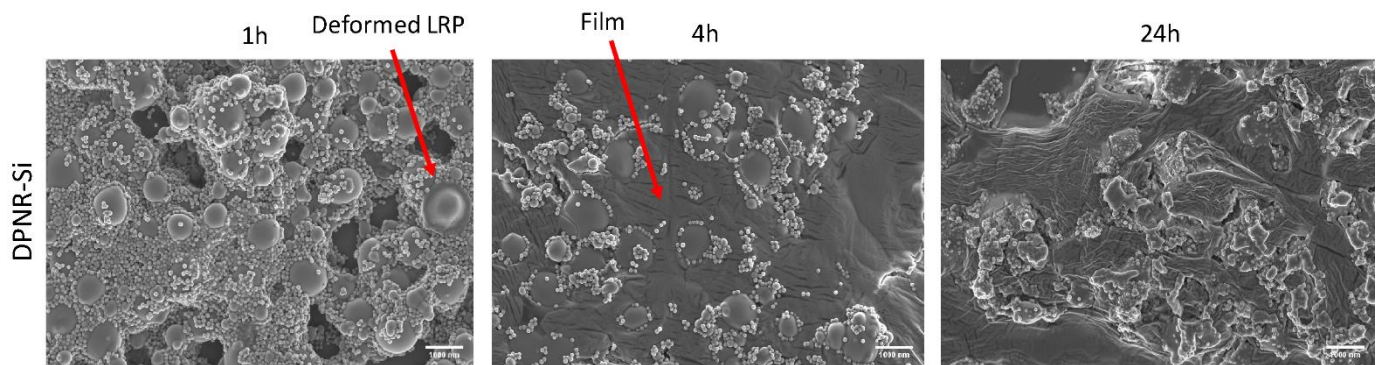
Supporting Information 6 (S6): Structural evolution dynamics of the NR-Si hetero-coagulum at (a) $t=2$ h and (b) $t=3$ h. Magnification 10000x.



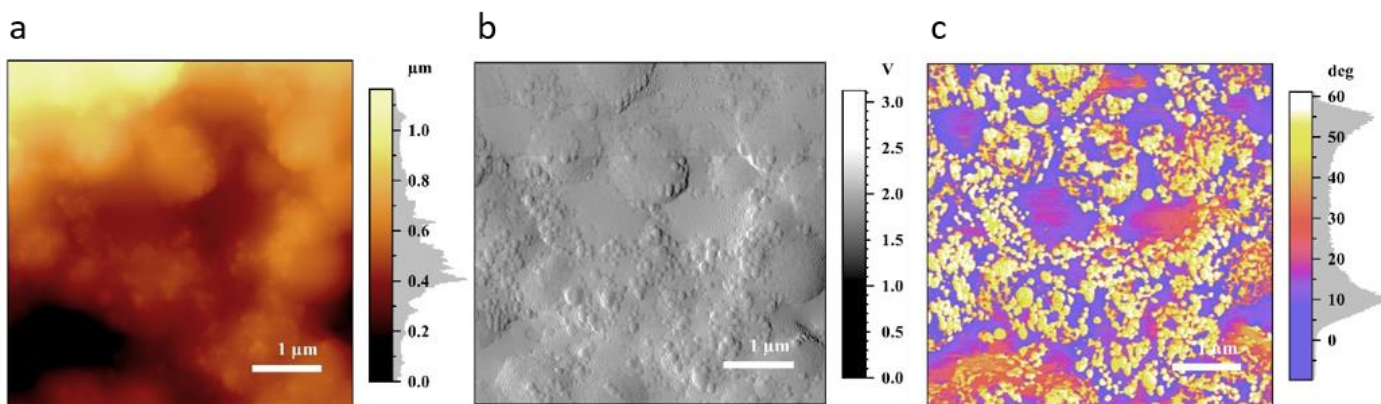
Supporting Information 7 (S7): FESEM micrographs of NR-Si heterocoagulum when the sample was maintained in a humidity controlled environment, highly limiting solvent evaporation. (a) SE micrograph showing the structure at $t=4\text{h}$, (b) the corresponding BSE micrograph. The original spherical form of NR globules is maintained. Magnified (c) SE and (d) BSE images corresponding to the red boxed zone in (a) and (b).



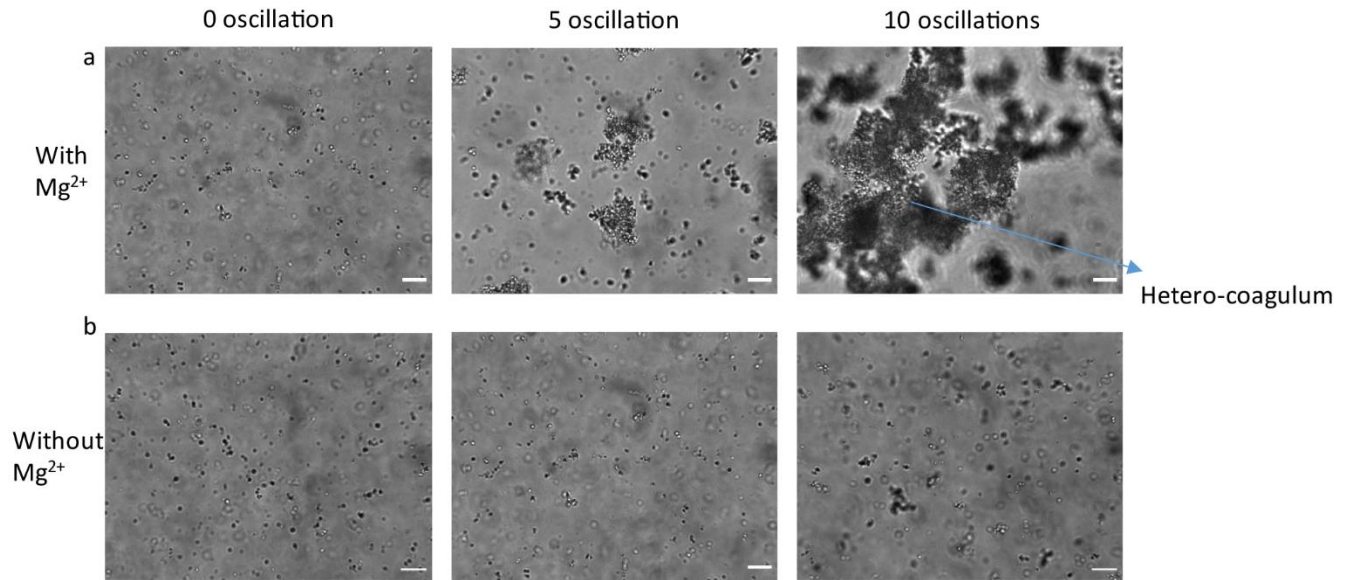
Supporting Information 8 (S8): SE micrographs of the DPNR-Si; structure fixed at (a) $t=1$ h, (b) $t=4$ h and (c) $t=24$ h after deposition of the sample on the cover slip. Magnification 10000x, and scale bar corresponding to 1000 nm.



Supporting Information 9 (S9): Figure S10. AFM imaging on NR-Si composite obtained at $t=24$ h. Typical (a) height, (b) amplitude and (c) phase contrast imaging. Changes in the amplitude signal and phase contrast imaging reveal the presence of embedded Si fillers.



Supporting Information 10 (S10): Transmission images recorded along with oscillation cycles for the NR-Si binary colloidal suspension in presence (a) and absence of ionic medium (b). Mechanical forces were applied using the RheOptiCAD module. The parameters of each oscillation correspond to 10 Hz frequency; total displacement of 1 μm displacement; 500 μm of gap; and 60s of application. Scale bar corresponding to 10 μm .



Article 3: Nanoscopic spatial arrangement of silica fillers with proteins and lipids of natural rubber: from a colloidal suspension to an elastomeric composite

Gianluca Cattinari^{*1}, Karine Steenkeste¹, Clément Cabriel¹, Sandrine Leveque-Fort¹, Alexis Canette², Matthieu Gallopin⁴, Marc Couty⁴, Ariane Deniset³, Marie-Pierre Fontaine-Aupart¹

¹ Université Paris-Saclay, CNRS, Institut des Sciences Moléculaires d'Orsay, 91405, Orsay, France

² Institute de biologie Paris Seine (IBPS), Sorbonne Université, CNRS service de microscopie électronique, 75005 Paris

³ Université Paris-Saclay, CNRS, Institut Chimie Physique (LCP), Université Paris-Saclay, 91405, Orsay, France

⁴ Manufacture Française de Pneumatiques Michelin

Article in preparation

Nanoscopic spatial arrangement of silica fillers with proteins and lipids of natural rubber: from a colloidal suspension to an elastomeric composite

Gianluca Cattinari^{*1}, Karine Steenkeste¹, Clément Cabriel¹, Sandrine Leveque-Fort¹, Alexis Canette², Matthieu Gallopin⁴, Marc Couty⁴, Marie-Pierre Fontaine-Aupart¹

¹ Université Paris-Saclay, CNRS, Institut Sciences Moléculaires d'Orsay, 91405, Orsay, France

² Sorbonne Université, CNRS, Institut de Biologie Paris-Seine, 75005, Paris, France

³ Université Paris-Saclay, CNRS, Institut Chimie Physique (LCP), Université Paris-Saclay, 91405, Orsay, France

⁴ Manufacture Française des Pneumatiques Michelin, Clermont-Ferrand, France

ABSTRACT: Producing an elastomeric composite material through coagulation of a binary colloidal suspension composed of Natural Rubber (NR) latex and particulate fillers is a novel production method of interest in rubber technology. The applicability of this process using silica (Si) as fillers is particularly interesting, especially in the tire industry. If the technological process parameters are quickly developing at engineering level, the fundamental knowledge of nanoscale structural characterization during coagulation and drying is still at its infancy. In particular, the spatial arrangement of proteins and lipids of NR and their localization in respect to the fillers is not known, and if solved it could enrich the knowledge on the role of those biomolecules during coagulation and drying. To this aim, we used dual colors direct stochastic optical reconstruction microscopy (d-STORM) as super resolution fluorescent microscopy technique to unravel the spatial distribution of lipids and proteins of NR from the early stage of mixing of NR latex with Si fillers, until the formation of a composite obtained after evaporating the solvent at room temperature. The combination of d-STORM and field emission scanning electron microscopy (FESEM) was exploited to localized proteins and lipids with regards to Si fillers. We report that the presence of Si influences the distribution of proteins and lipids of NR. When Si fillers surround NR globules at the early stage of mixing, proteins and lipids of NR are found forming large domains (~300 nm) in the NR-Si composite, while smaller proteins and lipids aggregates are present in absence of Si. Subsequently, the large proteins and lipids domains formed in presence of Si are found either co-localized or in close proximity to filler structures in the composite. We conclude suggesting a Si-induced aggregation mechanism of the biomolecules.

1. INTRODUCTION

Making elastomeric composite materials *via* coagulation of a binary colloidal suspension of natural rubber (NR) and silica (Si) fillers is a novel strategy in rubber technology¹. Preliminary studies highlighted the importance of divalent ions present in suspension in order to achieve the desired coagulation². Additionally, a recent study by our group focused on the structural characterization and evolution of such hetero-coagulum along drying, reporting the presence of Si fillers surrounding NR globules and indicating an interaction between the two components in liquid suspension. However, the spatial arrangement of proteins and lipids of NR and their localization in respect to the filler during coagulation and drying remains unknown, and if solved it could enable more insights on the role of those biomolecules in the nanoscopic processes occurring during the coagulation and drying. To explore the spatial distribution of such biomolecules and precisely localize Si fillers, high resolution imaging techniques are necessary. Fluorescence microscopy techniques have been extensively used to visualized proteins and lipids in cell membranes³. However, conventional fluorescence microscopy cannot differentiate proteins from lipids in NR⁴. Only the recent advances on single molecule localization microscopy (SMLM) enabled specific

recognition of these bio-molecules with resolution down to several dozens of nanometers⁵. These techniques have mostly seen applications in the life sciences, but they are recently gaining interested in the field of materials⁶. In particular, direct stochastic optical reconstruction microscopy (d-STORM) has been recently used for NR reporting the presence of proteins and lipids at the chain-end of polyisoprene⁷. In this work, dual color d-STORM imaging is employed to investigate on the spatial arrangement of proteins and lipids of NR from the early stage of contact between NR globules and Si occurring during hetero-aggregation until the formation of a composite obtained after drying. In addition, the combination of d-STORM with field emission scanning electron microscopy (FESEM) was also exploited recovering the same exact region of the sample and precisely localize proteins and lipids in respect to Si fillers in the composite material obtained after evaporation of the solvent at room temperature.

2. MATERIAL AND METHODS

2.1 Sample Preparation and materials

High ammonia concentrated NR latex (~60 wt %, HA latex) (Michelin, Clermont Ferrand, France) was used diluted at a concentration of 0,075 wt% in distilled water and used for the experiments. The obtained suspension is a colloidal dispersion of only NR globules. Their typical structure refers to a polyisoprene core surrounded by a thin biomembrane primarily made of lipids and proteins⁸, and their size varies between ~100-1000 nm⁹. This NR latex suspension was mixed with 100 nm Si fillers (when fluorescent, the corresponding spectra is reported in Figure S1) (Kisker Biotech, Steinfurt, Germany) at a concentration adjusted to have a final volume percent ratio of 40%. It was further controlled that this protocol leads to a coagulum having ~20% mass Si/NR ratio (data not shown). The suspension medium was composed of a magnesium sulfate solution (MgSO₄) (Sigma-Aldrich) adjusted to a concentration of 0.025M (pH of ~6,5) corresponding to 100 mM ionic strength when mixed with NR latex. Immediately after mixing, 100 μL of the binary colloidal suspension were deposited on a rounded glass coverslip (coverslip thickness of 170 μm (1.5H, MENZEL-GLASER)), resulting in a casted drop with a spherical cap shape as illustrated in Figure 1 (drop diameter ~ 1 cm). A phase-separation was macroscopically visible at t=1 h, with the formation of a floating object corresponding to the “heterocoagulum” but also some NR and Si particles adhering on the coverslip. After t=4 h, when most of solvent evaporated, the heterocoagulum adhered on the glass surface. Under complete solvent evaporation (t=24 h) the material referred to a composite.

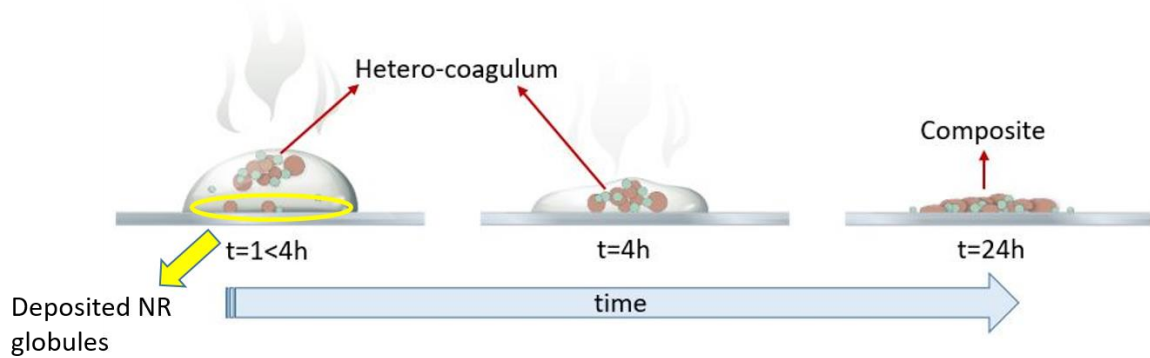


Figure 1. Schematic illustration of the kinetics of the hetero-coagulum and composite formations after deposition on the glass coverslip of a NR-Si binary colloidal suspension.

2.2 direct Stochastic Optical Reconstruction Microscopy (dSTORM)

d-STORM relies on the reconstruction of a nanoscale image after recording the stochastic pinpointing of fluorophores that undergo an on-off switching mechanism, also known as blinking¹⁰. To achieve such temporal signal separation, addition of a chemical imaging buffer to the sample is necessary. The one used herein contained PBS, β -mercaptoethylamine and an oxygen scavenger enzymatic system composed of glucose oxidase and catalase (Smart kit, Abbelight, Paris, France). Such buffer performs better in a poor oxygen environment. Thus, the samples were further sealed using twinstil paste.

To allow the proteins and lipids localization both on the NR globules and in the composites, the biomolecules were fluorescently labelled with Cy5-NHS (100 μ M, incubation time 1h) and Dil (25 μ M, incubation time 10 minutes) respectively. Labelling occurred directly in liquid suspension. When fluorescent Si fillers were mixed with NR globules, Dil was replaced by DID as lipid probe to prevent any spectral interference between the probes (Figure S1). Moreover, we controlled that nor Cy5-NHS, Dil and DID have interactions with the fluorophore of Si fillers: no change in the Si emission spectra was observed (Figure S2).

Fluorescence images were acquired using a Nikon Eclipse Ti-E microscope equipped with two laser lines. A 532 nm (Verdi G5, 5W, Coherent) was used to excite the fluorescence of both Dil and fluorescent Si fillers, while a 637 nm (Obis 637LX, 140mW, Coherent) line was employed to excite Cy5-NHS as well as DID. Firstly, we used a weak laser power to illuminate the sample and record a conventional diffraction-limited epifluorescence image. Afterwards, the laser power intensities were increased to induce the stochastic photo-switching of the fluorophores. Two different modes of excitation were used: a total internal reflection fluorescence (TIRF)¹¹ and a highly-inclined and laminated optical sheets (Hilo)¹² configurations as illustrated in Figure S3. In TIRF illumination, the generated evanescent wave is limited to 300-400 nm from the glass surface, reducing the background noise for a better signal quality. However, when a deeper sample penetration was required Hilo became the preferred excitation mode: the incident laser beam is highly inclined by a large refraction and is laminated as a thin optical sheet at the specimen site allowing image acquisition through a depth of several micrometers.

In both cases, the laser light was focused through a high numerical aperture and magnification objective (APO TIRF x100 1.49NA, Nikon). Images were acquired using a complementary metal oxide semiconductor camera (CMOS) with 50 ms exposure time. Appropriate band pass filters were placed in front of the camera to separate the emission signals of the different fluorophores. A single d-STORM image is generated by the accumulation ~6000 fluorescence images. The images were acquired and processed using NEO (Abbelight, Paris, France), a commercial software allowing live image reconstruction as well as treatment, drift corrections and analysis in terms of spatial descriptive statistic and clustering. Furthermore, images were processed removing the pixel per pixel temporal median in order to get rid of background noise without altering the number of photons in the PSFs. Each PSF was characterized using a Gaussian fit, and potential drift between sequential acquisition was corrected using a cross correlation algorithm.

2.3 Cluster Analysis

Density based spatial clustering of application with noise (DBSCAN) was employed as algorithm for cluster analysis. DBSCAN looks for clusters, by looking for the number of localizations within a circle defined by its radius (ϵ) and its center (p). If the area of the circle contains more than a minimum number of points (MinPts), a new cluster with p as a core object is created. We chose $\epsilon=50$ nm and MinPts=50 as input parameters in order to detect clusters that would allow high density areas of proteins and lipids in a circle having diameter of 100 nm. This method has been applied on two ROI regions of the acquired d-STORM images for each condition.

2.4 Field Emission Scanning Electron Microscopy (FESEM)

FESEM using both topological contrast by secondary electrons (SE) imaging and chemical contrast by backscattered electron imaging (BSE) was performed on samples fixed using vapor of osmium as described in details in reference¹³. This type of fixation allowed us to preserve the colloidal structure of NR globules as well as to exploit both SE and BSE imaging based on chemical contrast. Indeed, the high affinity of osmium for NR particles results in an important differentiation between NR and Si in BSE images: Si particles appears dark while NR appears bright. The fixed coverslips were mounted on 25.4 mm aluminium pin stubs (Micro to Nano, the Netherlands) with double sided sticky and conductive tabs (EMS, USA). Samples were then coated with a 10 nm carbon layer by double thread evaporation in high vacuum (10^{-5} mbar) with an ACE600 device (Leica, Germany). Observations were performed in high vacuum (10^{-6} mbar) with a FESEM Gemini500 (Zeiss, Germany) operating at 2kV, with high current mode, a 20 μ m aperture and around 2 mm of working distance. SE were collected with the corresponding SE in lens detector. BSE were collected with the energy selective in column detector using filtering grid > 400 V to filter out SE signal. Please note that both SE and BSE signals are surface selective, but while SE images are produce at the extreme surface (depth of few nanometers), BSE images are capable of providing information arising from a depth of few tens of nanometers¹⁴. Images were acquired with a 1024 x 768 definition, a pixel dwell time of 6,4 μ s (scan speed "7") and a line averaging of 25.

FESEM was also performed after d-STORM measurements recovering the same region of acquisition. The re-location of the same area of the sample by both methods has been achieved through the use of patterned glass coverslips (also of thickness 170 μm (1.5H)) (Ibidi GmbH); they are composed of 400 numbered micro-squares of 50 μm (Figure S4), as well as the use of Si as bi-functional probe visible by both methods. Due to strong quenching of the fluorescence signal after fixation with vapors of osmium tetroxide¹⁵, d-STORM acquisitions using Hilo illumination were performed prior FESEM measurements.

3. RESULTS AND DISCUSSION

A. Spatial distribution of proteins and lipids on NR globules: the interaction with Si fillers

The distribution of proteins and lipids on NR globules using d-STORM measurements was first approached by Wu and al⁷. In their conditions, the NR globules were spin coated on a slide and were thus analysed without solvent environment. Here, we controlled the proteins and lipids distribution in our ionic medium conditions (Mg^{2+} , ionic strength=0,1 M) (Figure 3) using both TIRF and Hilo illumination. In each case, both biomolecules appear quite homogeneously distributed all around the NR surface. However, some segregated domains randomly interdispersed can be observed in particular for proteins, in agreement with previous observations⁷. Additionally, when two different NR globules come into contact, proteins and lipids are observed in the “bridging zone” connecting the two NR particles. This same condition was also analysed by FESEM (Figure 3e), showing polymeric material in the area connecting rubber globules.

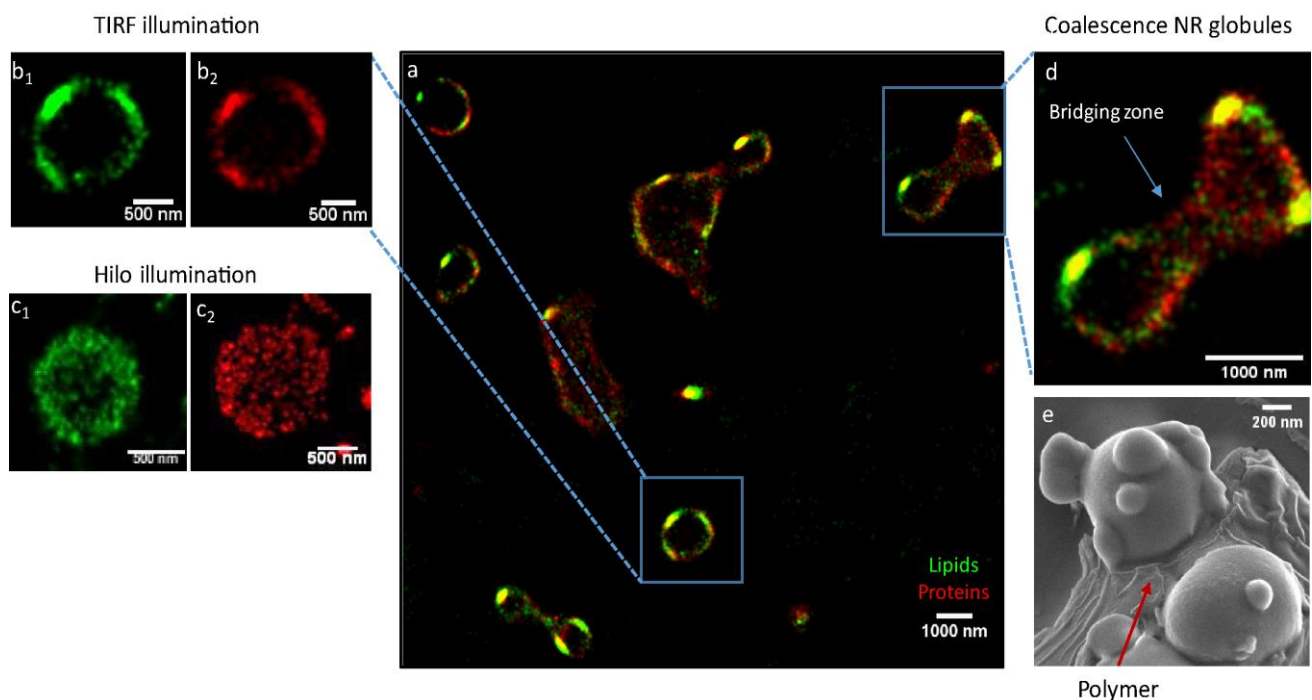


Figure 3. d-STORM microscopy on NR globules, in presence of Mg^{2+} ions (ionic strength=0,1 M), at $t=1$ h. The localization of proteins and lipids is indicated with red and green respectively. (a) Dual color d-STORM micrograph using TIRF illumination on NR globules deposited on the coverslip. (b₁) Lipids and (b₂) proteins distribution on a single NR globule when using TIRF illumination. (c₁) Lipids and (c₂) proteins distribution on a single NR globule when using Hilo illumination. (d) Coalescence between NR globules illustrating the presence of proteins and lipids acting as bridges between them. (e) Corresponding SE image revealing the presence of polymeric material between two NR globules.

Combining the information between the two techniques we can state that during coalescence the polyisoprene chains are diffusing across the particle-particle interface, while at the same time proteins and lipids are also moving filling up the same region. This is an indication that at least part of the lipids and the proteins composing the bio-membrane of NR are linked with the inner polymer

core and are involved in the coalescence between rubber globules.

To investigate on the interaction between Si fillers and NR globules, dual color d-STORM images labelling Si particles and one of the biomembrane components (either proteins or lipids) were performed (Figure 4). In both cases, we highlighted the presence of Si fillers in contact with the surface of the NR globules (Figure 4a and Figure 4b), indicating an interaction. This result is in line with FESEM measurements highlighting the presence of Si fillers surrounding NR globules and preventing their direct contact¹⁶. However, no particular changes concerning the distribution of lipids and proteins on the globules surface were highlighted when Si establishes contact. This indicated that at early stage of mixing, when the solvent is still largely present, Si fillers do not seem to trigger any modification on the arrangement of proteins and lipids on the biomembrane. The latter result is in agreement with our previous work demonstrating that Si fillers do not induce any deformation on NR globules¹⁶.

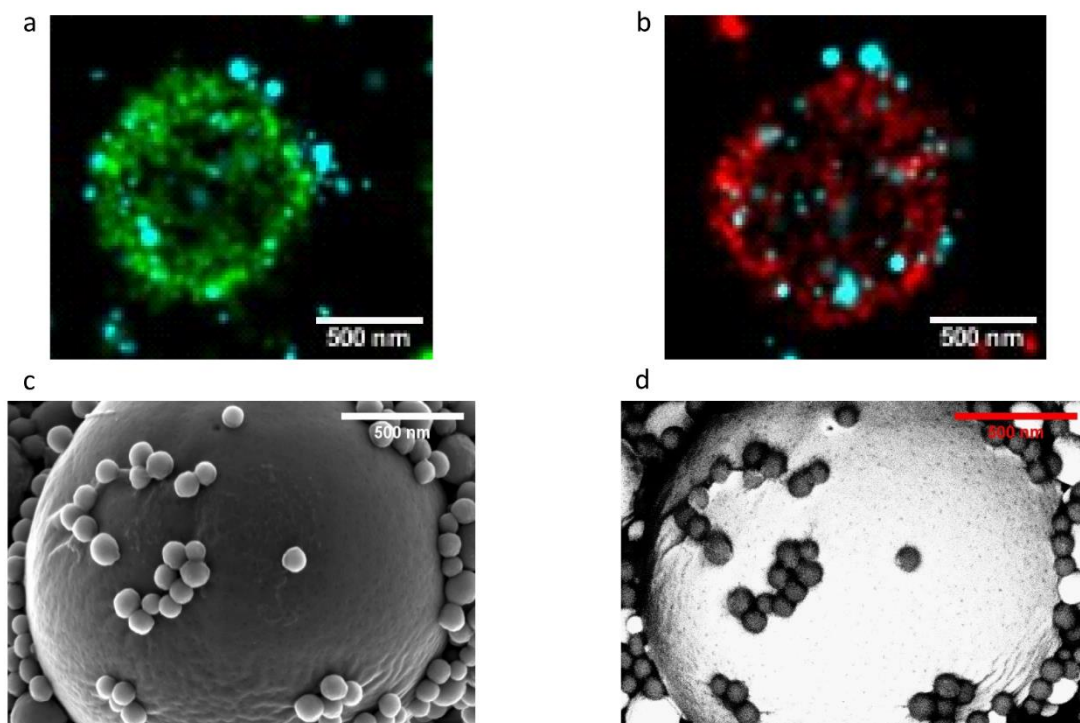


Figure 4. Dual color d-STORM micrographs on a NR globule in contact with Si fillers in presence of Mg^{2+} ions (ionic strength=0,1 M), using Hilo excitation. (a) Dual color image labelling lipids (green) and Si (cyan). (b) Dual color image labelling proteins (red) and Si fillers (cyan). (c) SE and (d) BSE on a NR globule surrounded by Si fillers.

B. Reorganization of proteins and lipids distribution during coalescence

Regardless of the presence of Si, it was previously demonstrated that NR globules lose their original colloidal form along with solvent evaporation, giving rise to a NR film generated from their coalescence. Typically, at $t=4$ h, when most of the solvent is evaporated, the NR-Si coagulum is structurally heterogeneous. A part of the sample is covered by a NR film, while some NR globules

still maintained their colloidal structure. To investigate on the distribution of proteins and lipids of NR along with the aforementioned film formation process, dual color d-STORM imaging was performed at this stage on the NR-Si coagulum, focusing on the leftover colloidal form of NR globules (Figure 5). Results indicate the formation of clusters of proteins and lipids, with size ranging between 250-350 nm. Additionally, these clusters tended to be arranged in more circular forms with size ranging within 500-1200 nm, a similar range as the one referring to the diameters of LRPs (200-1000 nm) (Figure 5b, c and d).

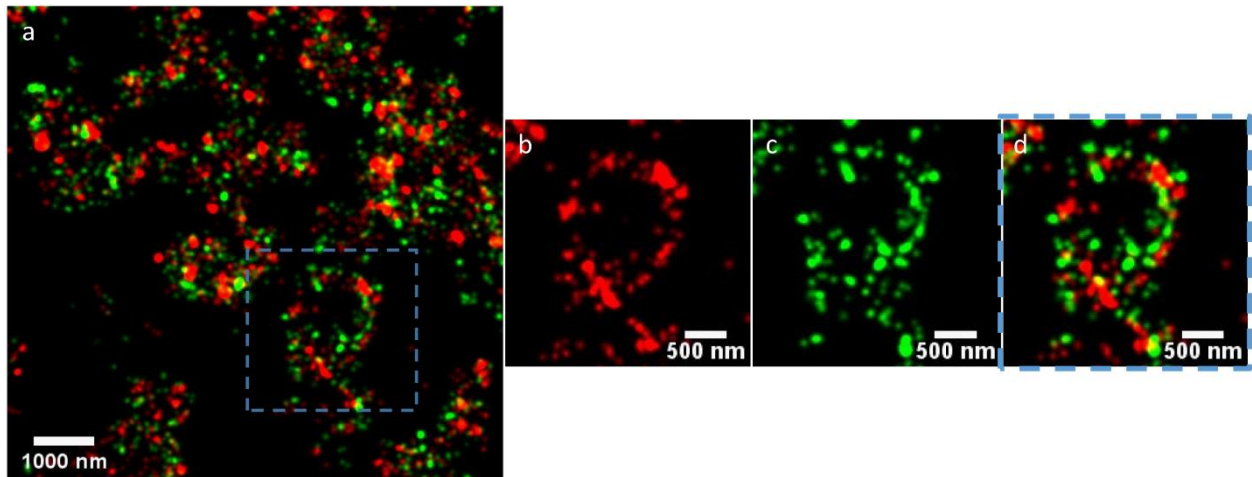


Figure 5. Distribution of proteins and lipids in NR-Si coagulum at $t=4$ h, when the solvent is majorly evaporated. (a) Dual color d-STORM fluorescence image of proteins (red) and lipids (green) showing the organization of the bio-molecules into clustered domains. Magnified views of the boxed region in (a) showing a tendency of (b) proteins and (c) lipids cluster to be organized into circular arrangements. (d) Superposed image of (b) and (c).

The spatial distribution of proteins and lipids was then studied after complete evaporation of the solvent, when the memory of the original colloidal form of NR globules is completely lost ($t=24$ h), in both presence and absence of Si fillers (Figure 6). A very different behavior was observed. In absence of Si fillers, proteins (red) and lipids (green) were organized in very small domains with very few aggregate structures with size of approximately 100-150 nm. The presence of very small proteins and lipids aggregates in absences of Si is in line with previously reported SAXS measurement where their characteristic size was evaluated to be ~ 25 nm¹⁷. Despite this morphology, we find a rather homogenous distribution of the bio-components throughout the NR film (Figure 5c). On the other hand, when Si fillers are embedded in the NR film the biomolecules showed a marked clustering behavior, forming relatively large domains of similar size as the ones reported at $t=4$ h (250-350 nm). Additionally, clusters of proteins and lipids overlapping with each other are also present, suggesting possible co-assembly.

To verify on the accentuated clustering of the biomolecules when in presence of Si, we employed density based spatial clustering of application with noise (DBSCAN) algorithm. Typical example of cluster analysis on different ROIs comparing the level of proteins and lipids clustering between the NR film obtained in absence of Si and the NR-Si composite are shown in Figure S5 and S6, confirming a higher clustering level of the bio-molecules when in presence of Si. To control that the presence of the sole ionic medium could not influence the clustering behavior of bio-membrane

components, the spatial distribution of lipids and proteins and related DBSCAN analysis have been studied on a NR film prepared without coagulation, by simply drying the NR latex in absence of Mg^{2+} (Figure S7 and S8). The analysis resulted in a distribution of proteins and lipids very comparable to the one referred to the NR film obtained after coagulation and solvent evaporation in the absence of Si fillers. Altogether, these results point in the direction of a Si- induced clustering mechanism of proteins and lipids. However, the marked clustering of the biomolecules is not directly related to the liquid state interaction of Si with the surface of NR globules, but it seems to start along with their destabilization carried by solvent evaporation ($t=4$ h). To further investigated whether Si could be responsible for proteins and lipids clusters, we localized the fillers in respect to the bio-molecules on the NR-Si composite combining dual color d-STORM with FESEM experiments recorded on exactly the same sample.

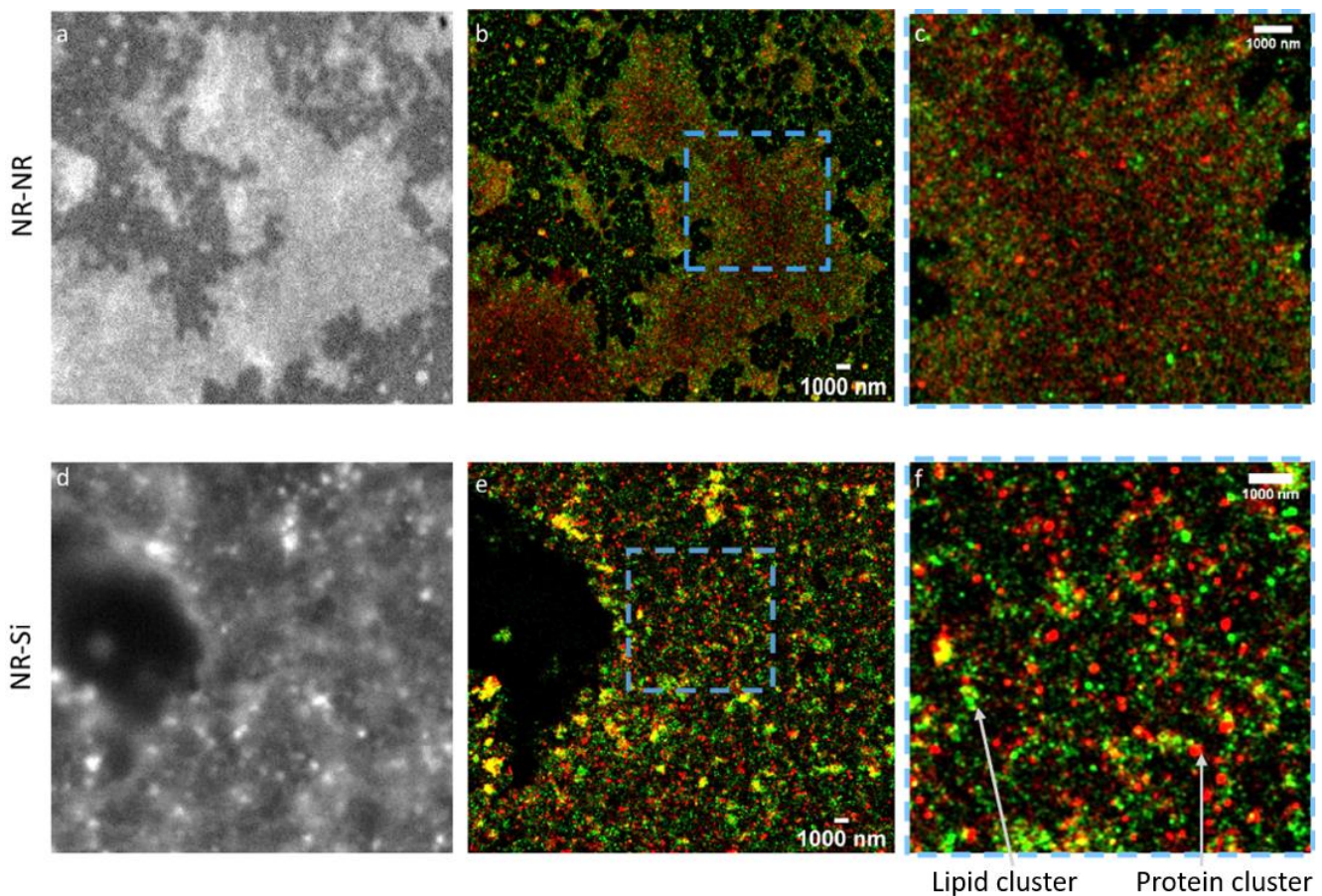


Figure 6. Distribution of proteins and lipids in NR film and NR-Si composite at $t=24$ h, formed by coagulation in presence of Mg^{2+} (ionic strength =0,1 M), and drying. Epifluorescence images of (a) NR film and (d) NR-Si composite. Dual color d-STORM fluorescence image of proteins (red) and lipids (green) of the corresponding (b) NR film and (e) NR-Si composite. (c), (f) Magnified view of the boxed region (image size: $\sim 10 \times 10 \mu m$) in (b), and (e), respectively, showing a difference in the distribution of proteins and lipids between the NR film and the NR-Si composite. Proteins and lipids show a marked clustering in the NR-Si composite.

C. Distribution of Si fillers with regards to proteins and lipids in the composite

Typical d-STORM micrographs labelling lipids and Si fillers and the corresponding FESEM image recorded on the same region of the sample are shown in Figure 7. The large view SE image shows the overall structure of the NR-Si composite (Figure 7a), confirming a complete loss of the original spherical form of the NR globules in favour of film formation process. The alignment of the detected Si fillers on the BSE image and on the d-STORM micrograph of the same region is shown in Figure 7b and c, respectively. Please note that, although shrinkage effect induced by the vacuum condition of FESEM experiments cannot be excluded, common structures are shown by both micrographs. From the magnified BSE image, we can confirm the presence of Si fillers embedded in the rubber film (Figure 7b). It is possible to distinguish ring-ellipse like structures of Si fillers (red circles in Figure 7b). These structures are also clearly observed by d-STORM imaging (Figure 7c). In both cases, this type of observation is in line with previous results describing the distribution of Si fillers in the NR-Si composite¹⁶. The fluorescence signal recorded for lipids and proteins certified the presence of clustered domains of ~ 250-350 nm, (Figure 7d,e and Figure S9). Interestingly, the dual colour d-STORM micrograph superposing lipids with Si fillers shows that the biomolecules clustered domains can be found in close proximity to structures of Si. In particular, when considering Si ring-ellipse structure, the clustered domains of lipids and proteins are found often co-localized (Figure 7d and Figure S9). This suggests that the presence of proteins and lipids clusters is strongly related to the presence of Si fillers.

Altogether, these results allow to propose a possible nanoscopic mechanism responsible for the highlighted clustering behaviour. Thus, since affinity between Si and biomembrane components is highlighted from the early stage of particles contact ($t=1$ h), while clusters of proteins and lipids are found either co-localized or in very close proximity to Si fillers in the composite, we hypothesized a Si-induced clustering mechanism occurring during the process of NR globules deconstruction and polyisoprene chain inter-diffusion. At this stage, the visualized clustering of proteins and lipids might be caused by adsorption of these components onto the Si surface. Adsorptive processes of model phospholipids membranes on the surface of Si nanoparticles have previously been reported in the literature using a set of biophysical methods by Kettiger et al.¹⁸ The researchers have shown that the van der Waals interactions between hydrophilic negatively charged Si particles and phosphatidylcholine membrane lead to formation of lipid clusters on the surface of the particles, thus supporting our hypothesis.

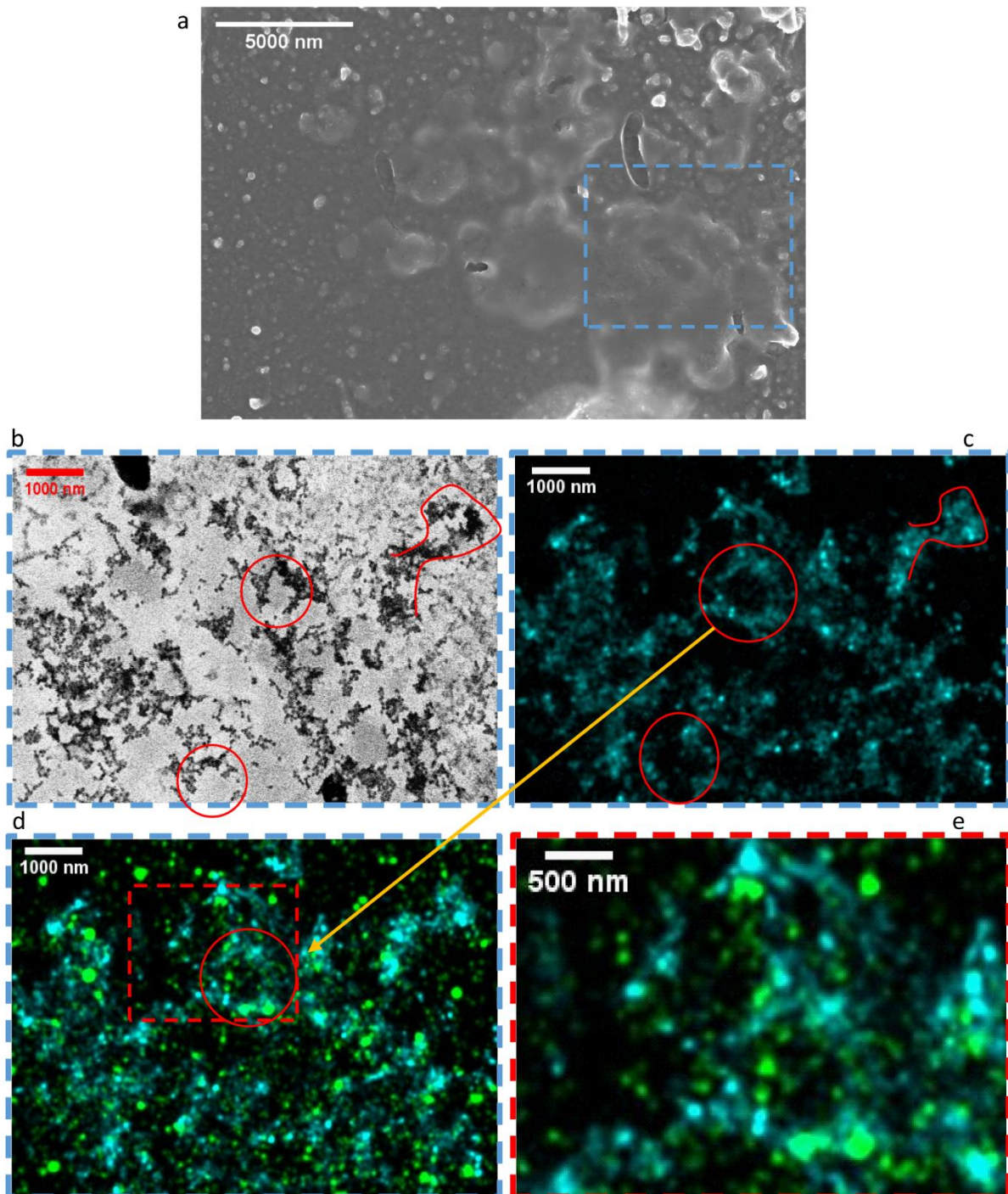


Figure 7. Combined d-STORM and FESEM measurements on the NR-Si composite labelling Si and lipids. (a) SE large view. (b) Magnified BSE image of the blue boxed region in (a). (c) d-STORM micrographs of Si fillers (cyan) showing the presence of ring-ellipse like structure. (d) Dual color d-STORM micrographs combining the fluorescence signals of Si fillers (cyan) and lipids (green), obtained with sequential acquisitions and recorded in the blue boxed region of (a) showing the presence of lipid clusters in close proximity to structures of Si fillers. (e) Magnified view of the red boxed region in (d), showing the presence of lipid clusters in close proximity or co-localised with ring-ellipse like structure of Si fillers.

4. CONCLUSION

This study reports new insights into the spatial distribution of proteins and lipids of NR globules together with Si fillers, during their coagulation and drying processes.

We exploited dual color d-STROM microscopy to report on the impact of Si fillers on the biomolecules distribution, suggesting a Si-induced clustering mechanism of proteins and lipids of NR. In fact, proteins and lipids organized themselves into large domains with sizes of ~300 nm in the NR-Si composite material, while fewer and smaller aggregates were found in absence of Si. Subsequently, the original combination of d-STROM microscopy with FESEM measurements recorded on the same region of the sample highlighted that the clusters of proteins and lipids tend to be located either co-localized or in very close proximity to Si fillers. Thus, we report that the presence of Si is related to the formation of proteins and lipids cluster. In addition, we hypothesize that such proteins and lipids clusters might be formed through adsorptive process occurring during NR globule deconstruction on the surface of Si fillers, which are surrounding the NR particles from the early stage of particles contact. To our knowledge, this is the first time that the spatial arrangement of proteins and lipids of NR is followed from the early stage of mixing with Si fillers, until the formation of an elastomeric composite.

REFERENCES

1. Boonsomwong, K. *et al.* Rejuvenating the structure and rheological properties of silica nanocomposites based on natural rubber. *Polymer* **189**, 122168 (2020).
2. Chan, A. J. *et al.* Natural Rubber–Filler Interactions: What Are the Parameters? *Langmuir* **31**, 12437–12446 (2015).
3. Sezgin, E. & Schwille, P. Fluorescence Techniques to Study Lipid Dynamics. *Cold Spring Harbor Perspectives in Biology* **3**, a009803–a009803 (2011).
4. Sakdapipanich, J. Current Study on Structural Characterization and Unique Film Formation of *Hevea brasiliensis* Natural Rubber Latex. *Advanced Materials Research* **844**, 498–501 (2013).
5. Owen, D. M. & Gaus, K. Imaging lipid domains in cell membranes: the advent of super-resolution fluorescence microscopy. *Front. Plant Sci.* **4**, (2013).
6. Wöll, D. & Flors, C. Super-resolution Fluorescence Imaging for Materials Science. *Small Methods* **1**, 1700191 (2017).

7. Wu, J. *et al.* Super-Resolution Fluorescence Imaging of Spatial Organization of Proteins and Lipids in Natural Rubber. *Biomacromolecules* **18**, 1705–1712 (2017).
8. Rochette, C. N. *et al.* Shell Structure of Natural Rubber Particles: Evidence of Chemical Stratification by Electrokinetics and Cryo-TEM. *Langmuir* **29**, 14655–14665 (2013).
9. Chan, A. J. *et al.* LIPID CONTENT IN SMALL AND LARGE NATURAL RUBBER PARTICLES. *Rubber Chemistry and Technology* **88**, 248–257 (2015).
10. Turkowyd, B., Virant, D. & Endesfelder, U. From single molecules to life: microscopy at the nanoscale. *Analytical and Bioanalytical Chemistry* **408**, 6885–6911 (2016).
11. Total Internal Reflection Fluorescence (TIRF) Microscopy. *Nikon's MicroscopyU* <https://www.microscopyu.com/techniques/fluorescence/total-internal-reflection-fluorescence-tirf-microscopy>.
12. Tokunaga, M., Imamoto, N. & Sakata-Sogawa, K. Highly inclined thin illumination enables clear single-molecule imaging in cells. *Nature Methods* **5**, 159–161 (2008).
13. Bell, S. & Morris, K. *An introduction to microscopy*. (CRC Press, 2010).
14. Hennig, P. & Denk, W. Point-spread functions for backscattered imaging in the scanning electron microscope. *Journal of Applied Physics* **102**, 123101 (2007).
15. Kim, D. *et al.* Correlative Stochastic Optical Reconstruction Microscopy and Electron Microscopy. *PLOS ONE* **10**, e0124581 (2015).
16. Martínez-Pedrero, F. *et al.* Making an elastomeric composite material via the heteroaggregation of a binary colloidal dispersion. *Soft Matter* **8**, 8752 (2012).
17. Karino, T., Ikeda, Y., Yasuda, Y., Kohjiya, S. & Shibayama, M. Nonuniformity in Natural Rubber As Revealed by Small-Angle Neutron Scattering, Small-Angle X-ray Scattering, and Atomic Force Microscopy. *Biomacromolecules* **8**, 693–699 (2007).
18. Kettiger, H., Québatte, G., Perrone, B. & Huwyler, J. Interactions between silica nanoparticles and phospholipid membranes. *Biochimica et Biophysica Acta (BBA) - Biomembranes* **1858**, 2163–2170 (2016).

Supporting information

Nanoscopic spatial arrangement of silica fillers with proteins and lipids of natural rubber: from a colloidal suspension to an elastomeric composite

Gianluca Cattinari^{*1}, Karine Steenkeste¹, Clément Cabriel¹, Sandrine Leveque-Fort¹, Alexis Canette², Matthieu Gallopin⁴, Marc Couty⁴, Ariane Deniset³, Marie-Pierre Fontaine-Aupart¹

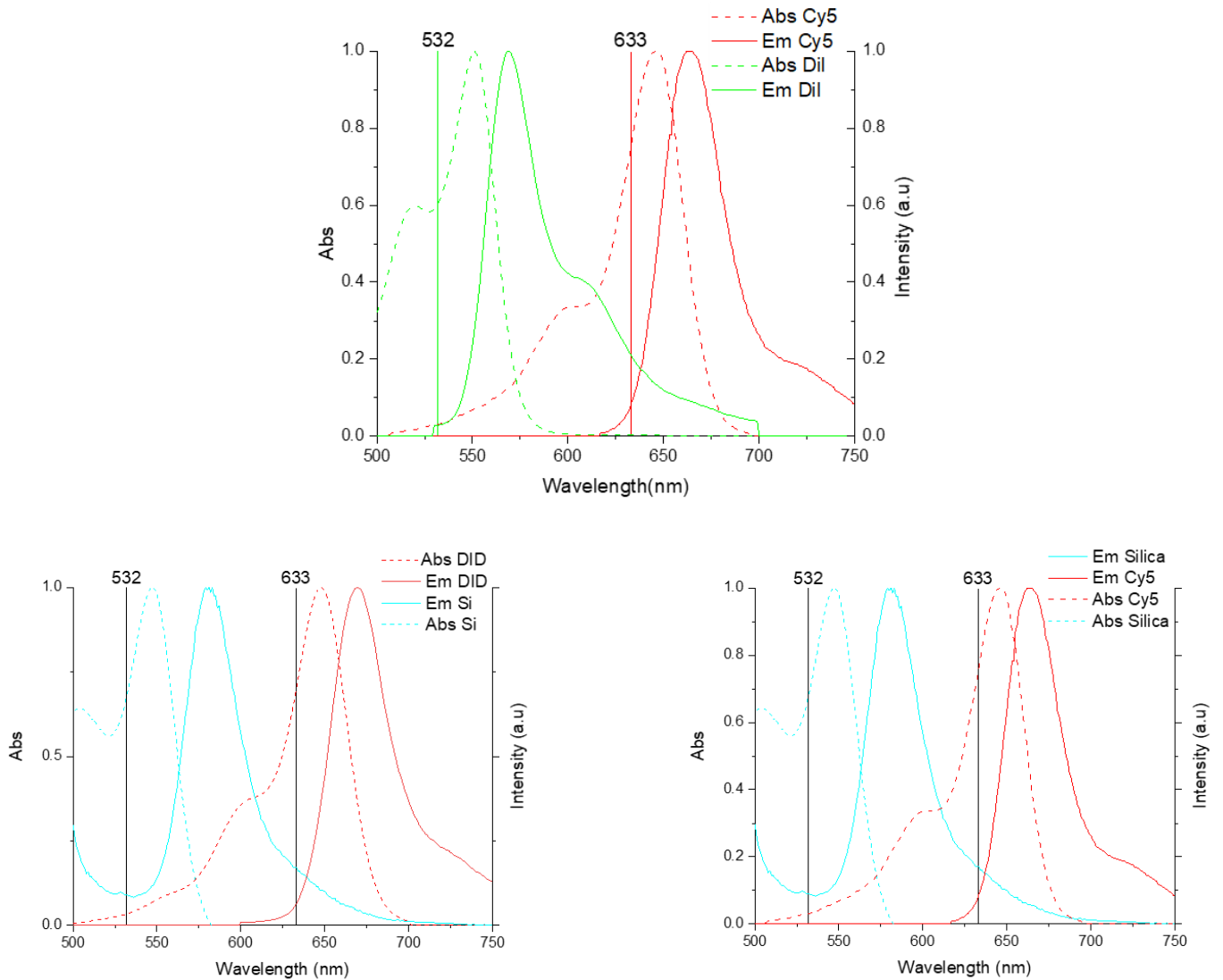
¹ Université Paris-Saclay, CNRS, Institut des Sciences Moléculaires d'Orsay, 91405, Orsay, France

² Institute de biologie Paris Seine (IBPS), Sorbonne Université, CNRS service de microscopie électronique, 75005 Paris

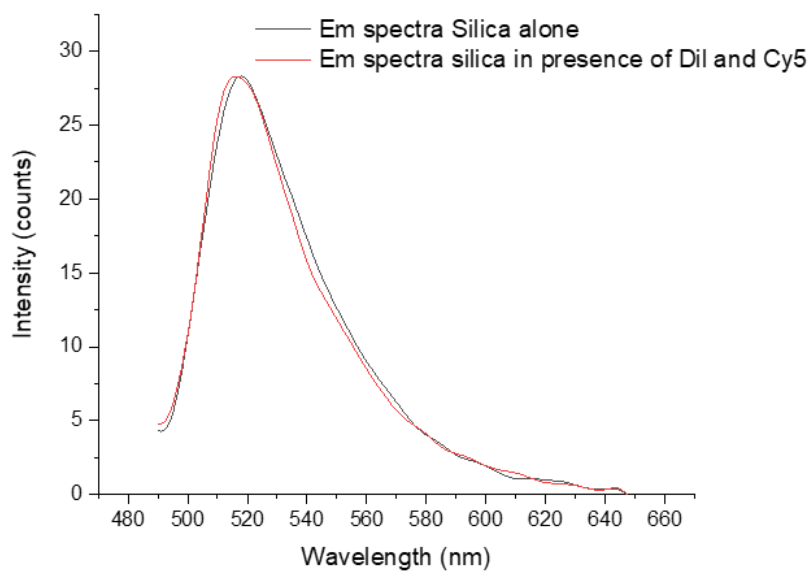
³ Université Paris-Saclay, CNRS, Institut Chimie Physique (LCP), Université Paris-Saclay, 91405, Orsay, France

⁴ Manufacture Française de Pneumatiques Michelin

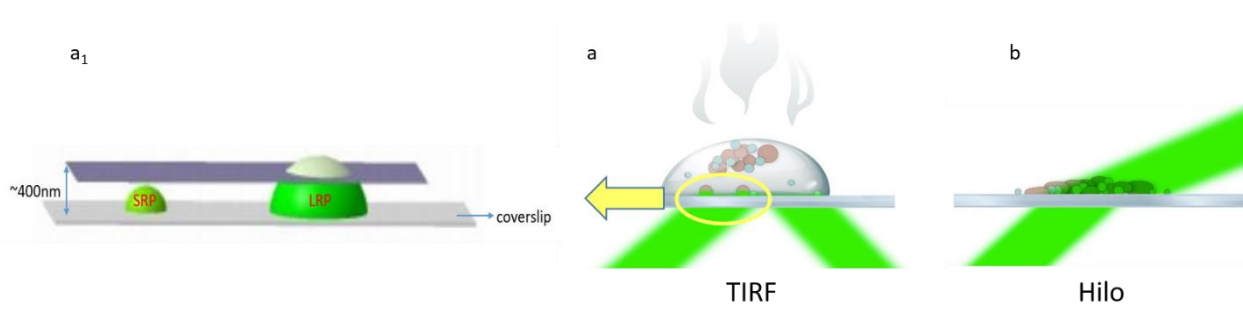
Supporting Information 1 (S1): Fluorescence absorption and emission spectra of the involved fluorophores. Absorption (dashed line) and emission (full line). 532nm and 633nm inserted line represent the respective excitation with the laser. Cy5-NHS is the fluorophore used to label proteins, while either Dil or DID were used as lipid probes. Silica fillers were commercially labeled and no indication on the type of fluorophore was given by the manufacturer (Kisker Biotech, Germany).



Supporting Information 2 (S2): Fluorescence emission spectra of silica particles in absence and presence of Cy5 and Dil. Recorded by Cary Eclipse (Varian, Palo Alto, CA, USA).



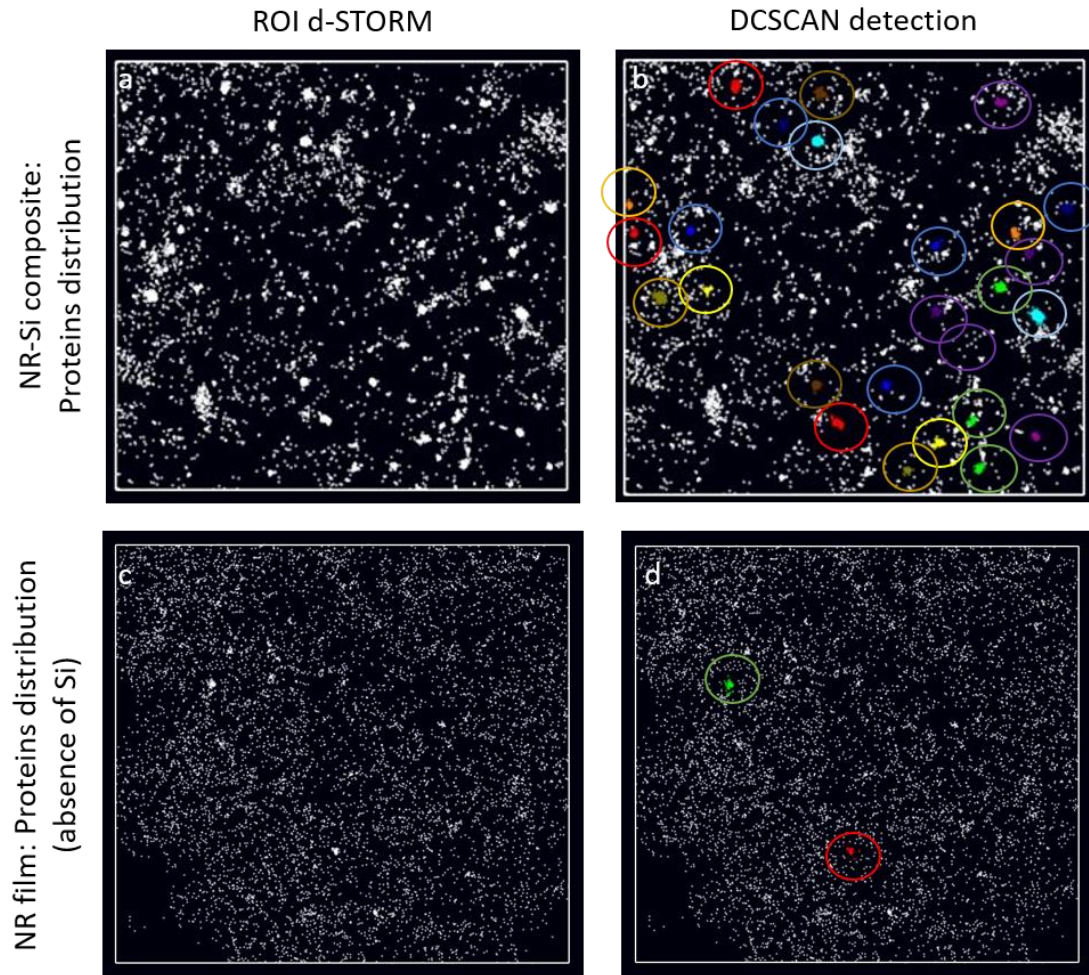
Supporting Information 3 (S3): Schematic illustration of (a) TIRF and (b) Hilo excitation applied to our system. The penetration depth when using TIRF is limited to 300–400 nm so that only a section of LRPs adhered on the coverslip can be excited. Using Hilo excitation, the penetration depth is of several micrometers.



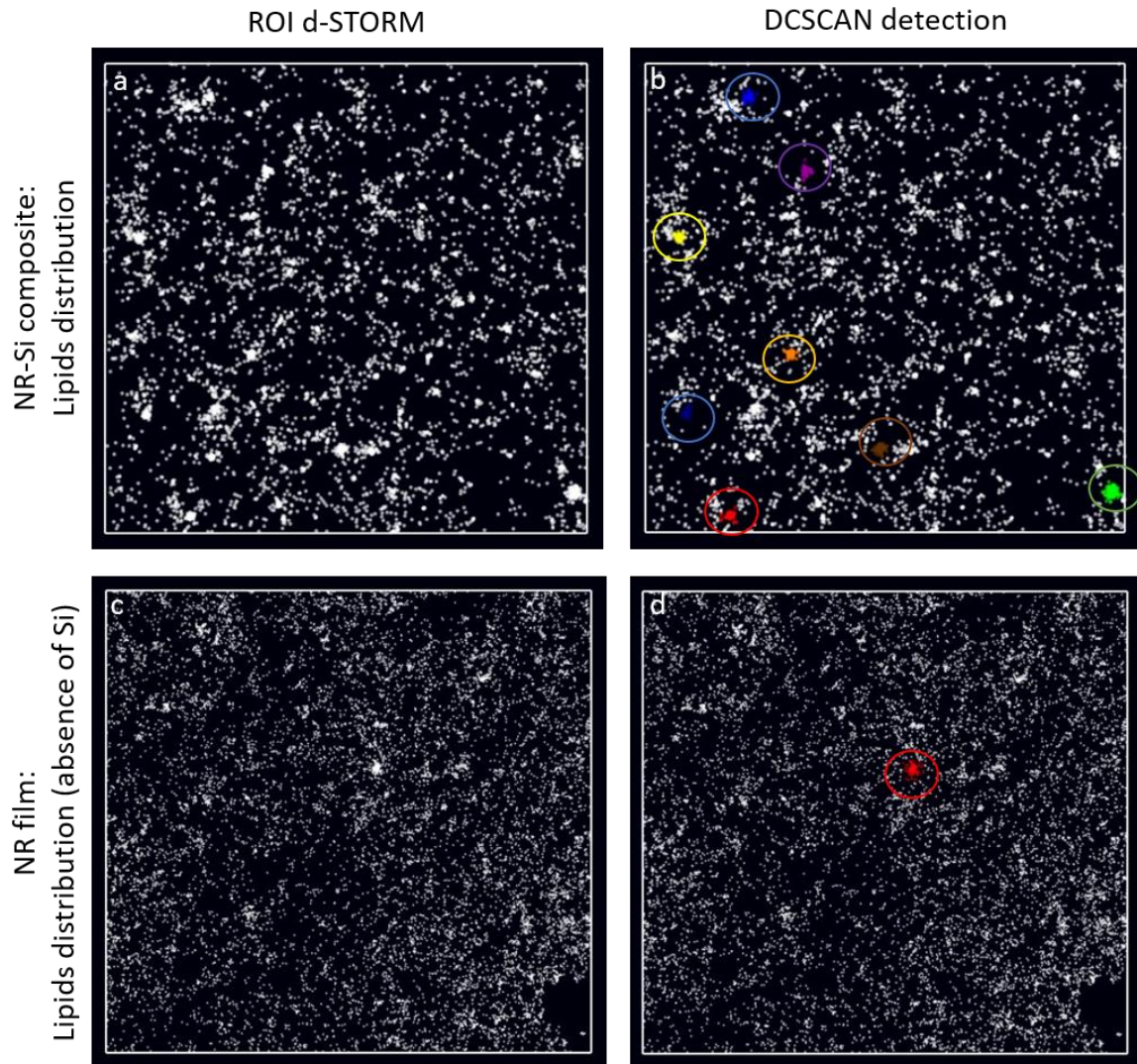
Supporting Information 4 (S4): Large view SE image of the NR-Si composite deposited on an Ibidi correlative support for combining FESEM and d-STORM experiments.



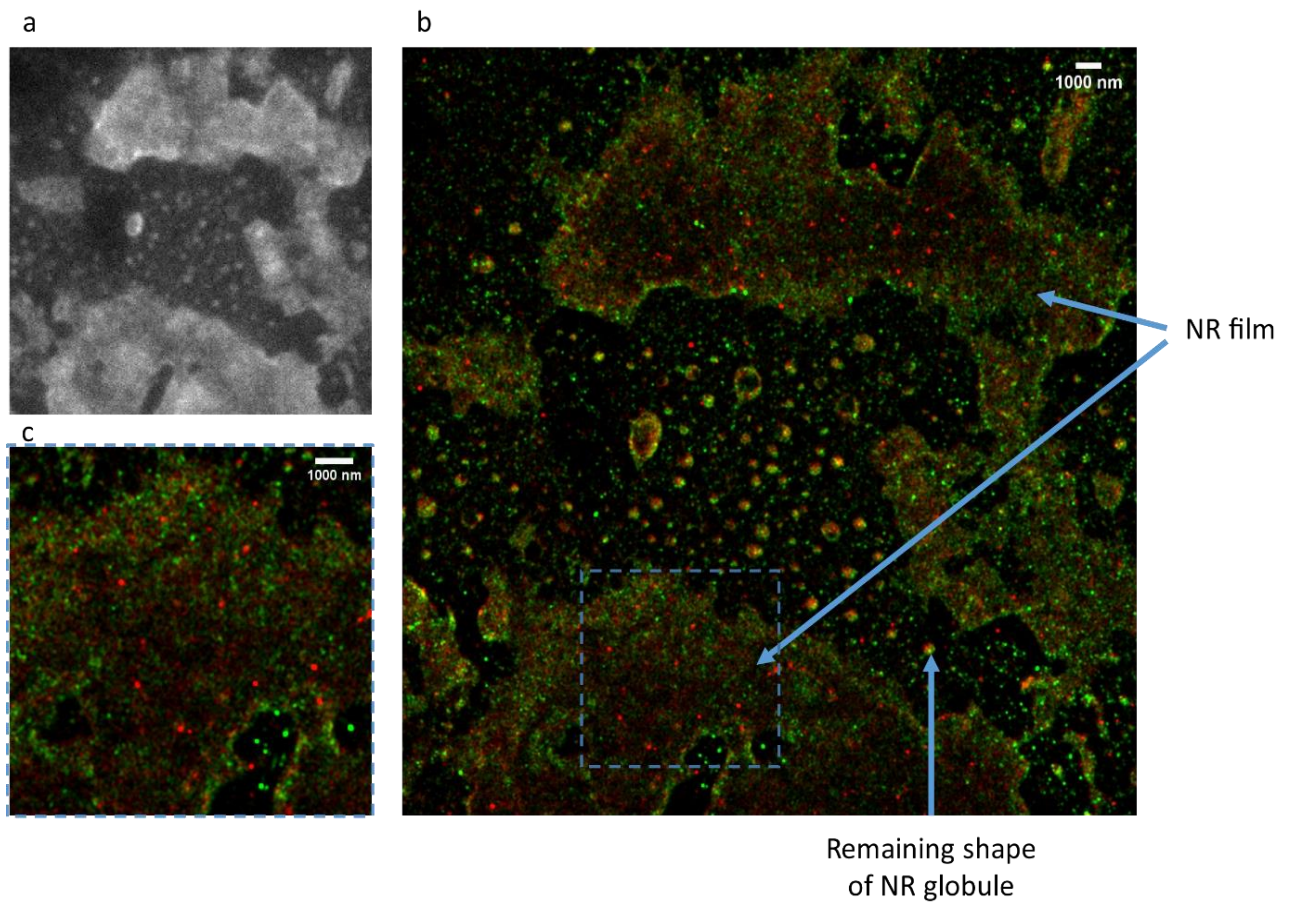
Supporting Information 5 (S5): DBSCAN cluster analysis run on ROI regions of the d-STORM images corresponding to proteins in the NR-Si composite and the NR film. (a and b) d-STORM ROI and DBSCAN detection of proteins clusters in the NR-Si composite. (c and d) d-STORM ROI and DBSCAN detection of proteins clusters in the NR matrix in absence of Si fillers. DBSCAN parameters: $\epsilon=50\text{nm}$ and $\text{MinPts}=50$. The analysis shows a marked clustering of proteins in the NR-Si composite.



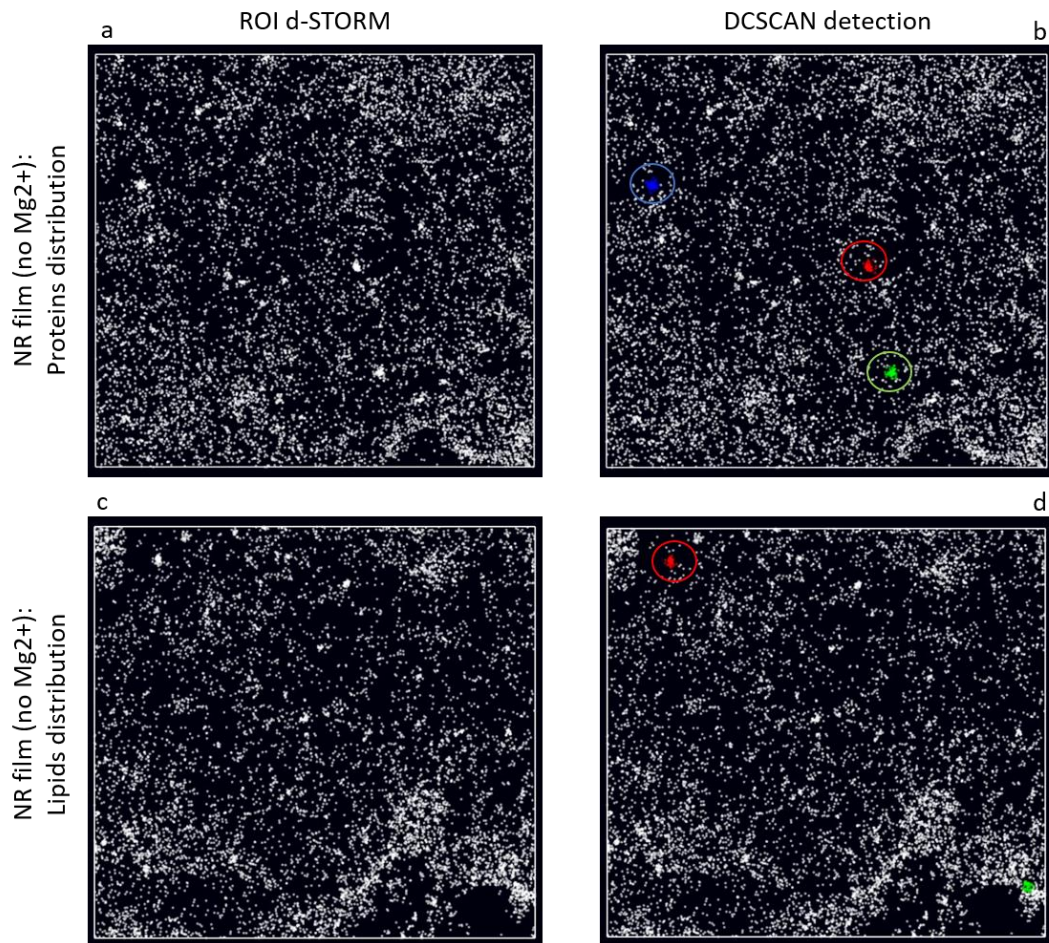
Supporting Information 6 (S6): DBSCAN cluster analysis run on ROI regions of the d-STORM images corresponding to lipids in the NR-Si composite and the NR film. (a and b) d-STORM ROI and DBSCAN detection of lipid clusters in the NR-Si composite. (c and d) d-STORM ROI and DBSCAN detection of proteins clusters in the NR matrix in absence of Si fillers. DBSCAN parameters: $\epsilon=50\text{nm}$ and $\text{MinPts}=50$. The analysis shows clustering of lipid in the NR-Si composite.



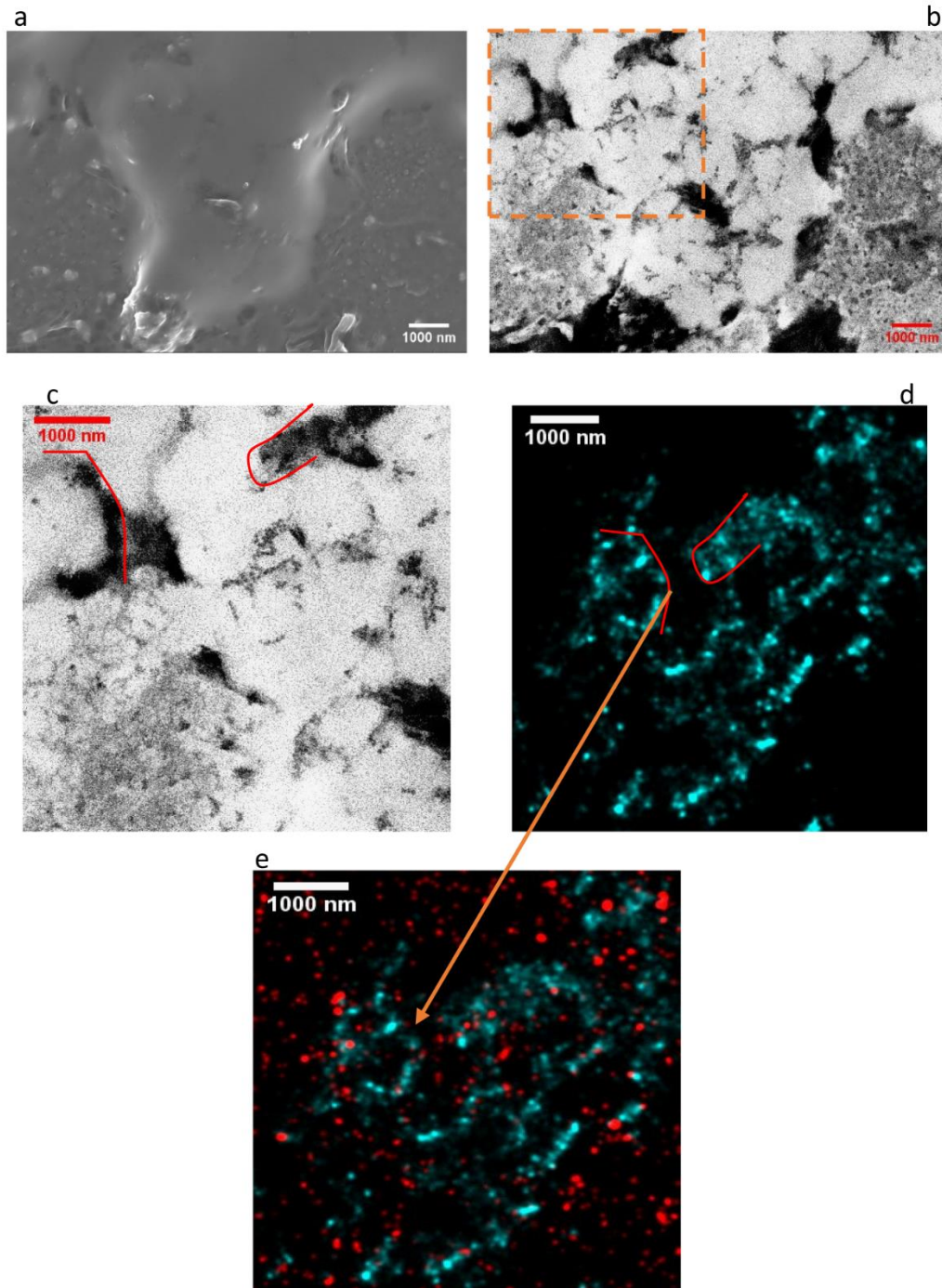
Supporting Information 7 (S7): Distribution of proteins and lipids in NR film formed in absence of the ionic medium, at $t=24\text{h}$. (a) Epifluorescence image (EPI). (b) Dual color d-STORM fluorescence image of proteins (red) and lipids (green) of the same zone. (c) Magnified view of the boxed region in b (image size: $\sim 10 \times 10 \mu\text{m}$).



Supporting Information 8 (S8): DBSCAN cluster analysis run on ROI regions of the d-STORM images corresponding to proteins and lipids in the NR film obtained by simply drying the NR latex in absence of the ionic medium. (a) Proteins distribution and related DBSCAN clustering map. (b) Lipids distribution and related DBSCAN clustering map DBSCAN parameters: $\epsilon=50\text{nm}$ and $\text{MinPts}=50$.



Supporting Information 9 (S9): Combined d-STORM and FESEM measurements on the NR-Si composite labelling Si and proteins. (a) SE large view. (b) Corresponding BSE image. (c) Magnified BSE view of the orange boxed region in (b). (d) Corresponding d-STORM micrographs of Si fillers (cyan) showing the presence of ring-ellipse like structure. (e) Corresponding d-STORM micrographs combining the fluorescence signals of Si fillers (cyan) and lipids (green), showing the presence of lipid clusters either co-localized or in close proximity to structures of Si fillers.



Annex

a) Lipids cluster detection by AFMIR

AFM-IR was also exploited to confirm the presence of lipids cluster on the NR-Si composite. To do so, two IR maps were registered at 1450 cm^{-1} at 1725 cm^{-1} . This last wavenumber is characteristic of the C=O stretching of free fatty acids and its typical absorption band can be detected by the acquisition of local spectra using AFM-IR. On the other hand, the absorption band at 1450 cm^{-1} refers to the CH_2 bending deformation, and it is a typical band of polyisoprene as illustrated in the FTIR spectra of the polymer (Figure 4.1). This last one does not show any absorption at 1725 cm^{-1} .

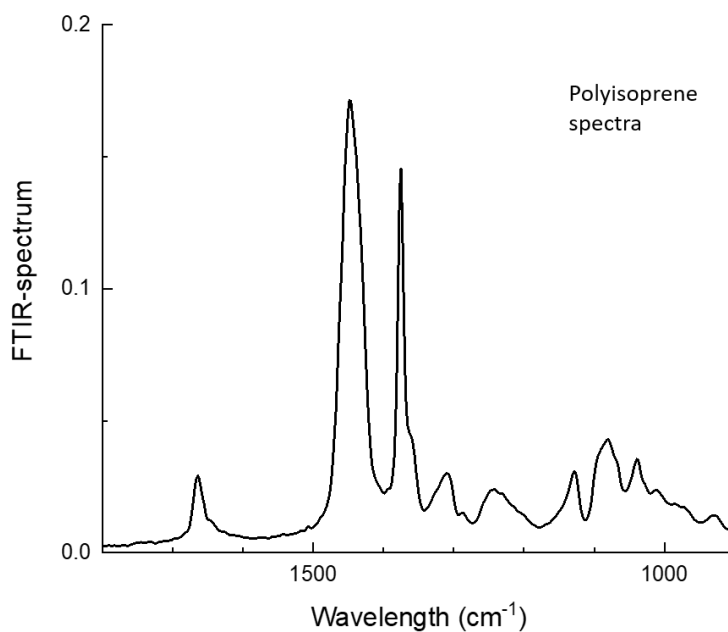


Figure 4.1. FTIR spectra of polyisoprene (IR2200) recorded in attenuated total reflection mode.

The registered IR maps together with the corresponding AFM topography image are shown in Figure 4.2. the IR map at 1725 cm^{-1} shows absorption in equivalent zones as the ones reported in the IR map at 1450 cm^{-1} demonstrating that lipids are surely in very close proximity to polyisoprene chains (Figure 4.2b and c) (the red/yellow colour represent high absorption in the IR maps while the blue colour refers to low absorption, as indicated by the colour bar). Subsequently, the ratio between the IR maps ($1725/1450\text{ cm}^{-1}$) was performed revealing interesting features (Figure 4.2d). In fact, the IR map ratio shows areas of higher intensity (white circles), which strongly suggest the presence of clustered lipid domains. The specific size of these structures ranges between 200 -300 nm, very similarly to the size range detected by d-STORM imaging. This confirmed the possibility to detect lipid clusters using AFM-IR, possibly opening up new possibilities to exploit the techniques to specifically investigate whether lipids are adsorbed on the surface of the fillers.

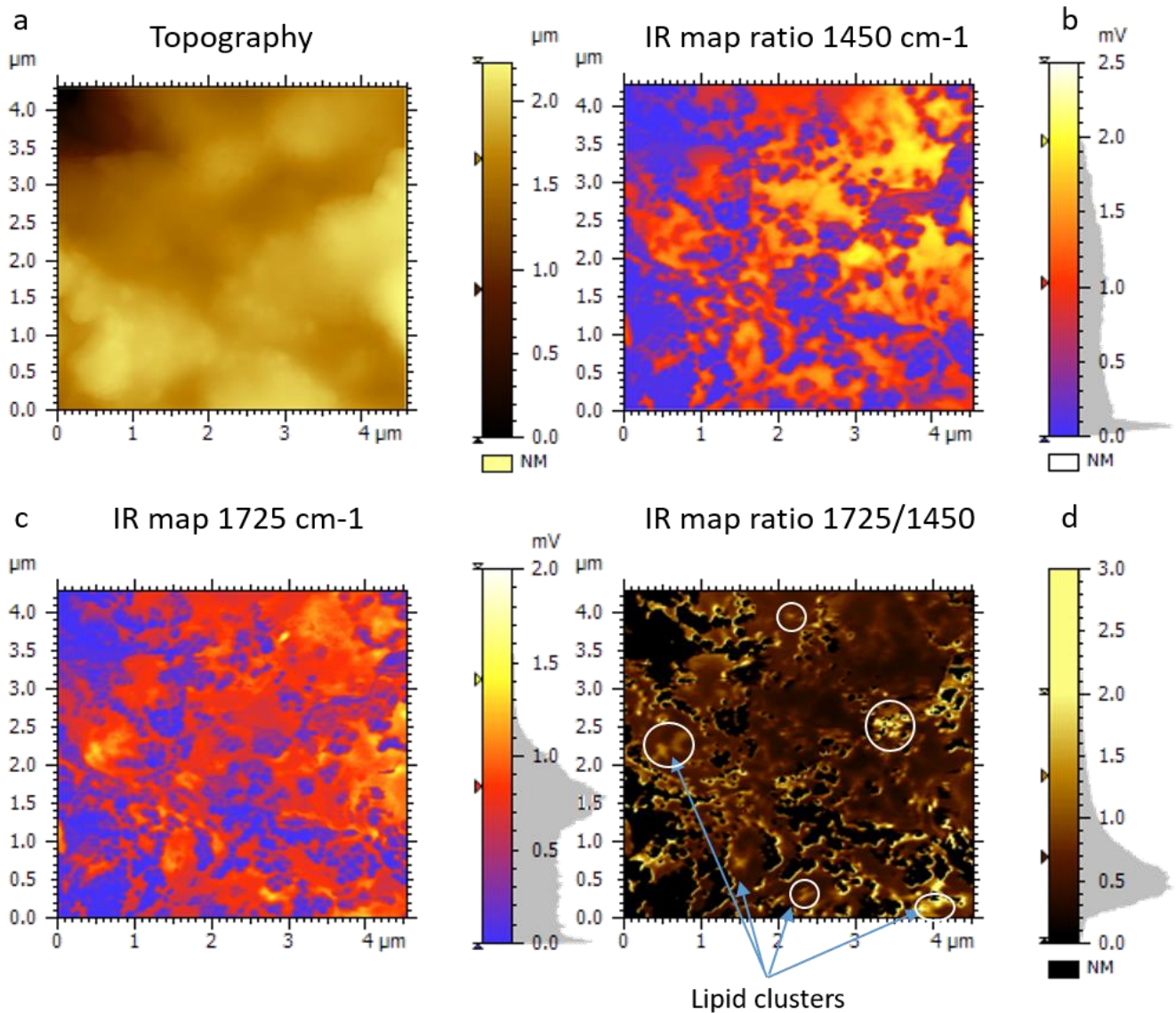


Figure 4.2. Detection of lipids in NR-Si composite by AFM-IR. (a) Topography image. (b) IR map at 1450 cm^{-1} referring to the CH_2 deformation typical of polyisoprene. (c) IR map at 1725 cm^{-1} referring to the $\text{C}=\text{O}$ of fatty acids. (d) IR map ratio between 1725 cm^{-1} and 1450 cm^{-1} highlighting the presence of higher intensity domains probably related to the presence of lipid clusters.

Conclusions and Perspectives

Mixing elastomers in the form of latex with particulate fillers using liquid phase mixing technology is an innovative strategy for the manufacturing of elastomeric composite materials. In the tire industry, this type of mixing is very promising to possibly achieve a successful reinforcement by improving the dispersion and distribution of the fillers. For this reason, liquid phase mixing is central for MICHELIN innovation strategy, especially using NR latex in combination with CB or Si fillers. If the technological process parameters are under control at the engineering level, the fundamental knowledge of the nanoscopic mechanisms and nanoscale processes occurring during hetero-aggregation and drying are unknown. We believe that their understanding might open up new ways of exploiting the liquid phase mixing technology. Thus, the main objectives of this PhD work consisted in the structural characterization of a coagulum made combining NR latex with an aqueous suspension of either Si or CB fillers, and to follow its evolution along drying until the formation of an elastomeric composite.

Because of the nanoscale size of NR globules and fillers, the use of highly resolved imaging techniques was necessary for our investigation. In fact, the beginning of our work consisted in the development of several imaging protocols for the employment of different microscopy techniques comprising: FESEM, d-STORM and AFM-IR. Each one of these techniques allowed to reach innovative and original results.

For a system composed of NR latex and CB fillers in aqueous suspension, we demonstrated that the way NR globules come into first contact with CB fillers is very important in regulating the structure of the formed coagulum. The simple mixture of the two colloidal suspensions without any application of external physical stress leads to a coagulum where CB fillers are not homogeneously distributed nor in contact with NR globules. However, mixing the two components under sonication maintained CB filler in the form of small aggregates (20-200 nm), leading to a good distribution of the filler around the NR globules. Such localization of small CB aggregates in direct contact with the surface of NR globules triggered a structural modification of the latex particles, quickly leading to coalescence and polyisoprene chain diffusing through the sample. The visualization of this phenomena allowed us to formulate hypothesis on the nanoscopic mechanisms causing the destabilization of the globules. We hypothesize a local membrane destabilization induced by the insertion of small CB filler through the lipidic part of the biomembrane of NR globules. This would then cause the adsorption of lipids on the hydrophobic domains of CB, leading to their coalescence.

When CB black is replaced by an aqueous suspension of Si fillers of hydrophilic nature, we confirmed the necessity of ions at sufficient ionic strength to establish interaction between NR globules and Si particles. Due to the hydrophilic nature of the fillers, we find that Si particle establish contact with proteins and lipids of NR globules in the liquid state. In this scenario, sonication was not necessary to form a coagulum where heteroaggregation is dominant over homoaggregation. In fact, when Mg^{2+} ions (ionic strength = 0.1 M) are present in the binary colloidal suspension composed of NR latex and Si fillers, a heterocoagulum is quickly formed having NR globules completely surrounded by Si particles in contact with the biomembrane components of the NR globules. Contrarily to CB, the contact established between Si fillers and

NR globules does not trigger any deformation or distortion of NR particles, but the state of polymer chain interdiffusion is regulated by the evaporation of the solvent. As a matter of fact, along with solvent evaporation the structure of the heterocoagulum changes giving rise to a composite consisting of a NR film with embedded Si fillers. The latter are found quite homogeneously distributed in the composite and regularly arranged into ring-ellipse like structure, probably related to their initial interaction with NR globules. Although Si fillers do not induce deformation of the NR globules, we demonstrated that their presence around the surface of the NR particles has an effect on the spatial arrangement of proteins and lipids of NR. In this scenario, we highlighted a marked clustering behavior of proteins and lipids of NR in the NR-Si composite, in comparison to their distribution in a NR film obtained post coagulation and drying of only NR latex. Additionally, we also reported a higher concentration of proteins and lipid cluster either co-localized or in close proximity to Si fillers structures in the NR-Si composite. Altogether these results allowed us to hypothesize a Si induce clustering mechanism occurring during the destabilization of NR globules mediated by the adsorption of proteins and lipids on the surface of Si fillers. In this context, the size of the fillers might also influence the aforementioned adsorption of proteins and lipids onto the Si particles. Generally, smaller Si particles would have higher specific surface areas and therefore higher adsorption capacity. It would then be interesting to investigate whether smaller Si fillers could trigger a destabilization of NR globules, similarly to what has been reported for CB fillers.

A possible way to quickly trigger the deformation of NR globules and achieve a state of polymer chain interdiffusion lies in the application of mechanical shear-stress on the binary suspension composed of NR latex with either CB or Si fillers. In particular, the application of uniaxial shear used in this study greatly accelerated the formation of a coagulum, together with boosting coalescence between the NR globules. However, in case of NR-Si system, our shearing condition did not allow to bypass the interaction energy barrier without the use of salt.

Despite the extensive effort and the limited time, there are still questions left unanswered. For example, the initiated protocol used for AFM-IR could be further exploited to possibly demonstrate the hypotheses established for both the NR-CB and the NR-Si system. Theoretically, by the analysis of local IR spectra recorded on the surface of either Si or CB fillers, it would be possible to gain information on adsorbed proteins and/or lipids.

Additionally, it would be interesting to explore more the effect that mechanical shear-stress applied in suspension has at molecular level and its role in the coagulation process. As previously mentioned, we demonstrated that our shearing condition led to coalescence between NR globules. At this stage, it would be interesting to control how proteins and lipids of NR are organized during the application of shear. This would give information on the state of the biomembrane of NR globules during shear.

Furthermore, simple shear was applied in our study at early mixing time on an already pre-mixed NR-fillers suspension. However, such shear application does not properly correlate with the one

occurring at industrial level, which is generated by the injection at very high speed of the aqueous filler suspension with NR latex. For this reason, I believe that it would be interesting to build a laboratory device where a stream of NR latex encounters for the first time the aqueous suspension of fillers under controlled and regulated shearing conditions and further exploit microscopy techniques to understand the effect of shear at molecular level.

Other relevant investigations that would allow to approach the industrial protocol refer to the possibility to repeat our study at increased concentration of NR latex and fillers. This would allow to better explore how the results reported here for a diluted system might correlate with a more macroscopic one.

Another continuation of our work is to extend our experimental protocols and approach using field NR latex. This product is the preferred latex type in the industrial protocol. However, it contains luteoids, Frey-Wyssling particles, and free proteins and lipids in addition to NR globules. For this reason, it would be interesting to investigate how the presence of such components might affect the coagulation process or the nanoscale mechanisms proposed here.

I personally find the multimodal microscopy approach undertaken for this project very interesting. It gave the opportunity to work in different laboratories and with people with different scientific backgrounds, in both the academic and the industrial environment. I hope that the experimental imaging protocols developed during our work will be useful for the microscopy team of Michelin R&D.

By way of conclusion, I also hope that this work opened up ideas for future research projects in the field of NR, liquid phase mixing, and composite materials.

Résumé en français

Le latex de caoutchouc naturel (NR) extrait d'*Hevea brasiliensis* est connu pour être utilisé pour la préparation d'une variété de matériaux. L'ajout de charges renforçantes est une méthode bien établie pour augmenter les propriétés mécaniques de la matrice polymère et il est nécessaire pour obtenir la résistance requise par la plupart des applications. Plusieurs stratégies ont été proposées pour mélanger le caoutchouc avec des charges. Parmi les différentes méthodes, le procédé de mélange liquide semble intéressant et il est central dans le cadre de technologie d'innovation Michelin. Dans ce procédé, le latex NR est mélangé à une suspension aqueuse de charges renforçantes (silice (Si)/noir de carbone (CB)) donnant lieu à un hétéro-coagulum, qui est ensuite soumis à un séchage. Si ce processus se développe rapidement au niveau de l'ingénierie, la connaissance structurelle de l'hétéro-coagulum le long du processus ainsi que les mécanismes de régulation de l'agrégation ne sont encore bien connus. Dans ce but, nous avons utilisé une approche de microscopie multimodale comprenant: la microscopie électronique à balayage à émission de champ (FESEM) (avec à la fois l'imagerie électronique à rétrodiffusion et des électrons secondaires), la microscopie à force atomique couplée à la spectroscopie infrarouge (AFM -IR) et la microscopie à super résolution optique (d-STROM) pour étudier la nanostructure de l'hétéro-coagulum et son évolution vers un composite élastomère. En particulier, cette dernière technique est rarement utilisée pour l'étude des matériaux, et représente donc une caractéristique innovante de l'étude. Pour un système composé de latex NR et de charges CB en suspension aqueuse, nous avons démontré que l'application d'une contrainte physique lors du mélange est un paramètre important qui permet d'avoir un matériau homogène en structure avec le CB en contact avec les globules de NR. Ensuite, nous avons aussi montré que l'interaction entre les globules de NR et les charges de CB provoque une déformation des globules et conduit à un état de coalescence. Contrairement, pour une suspension de latex NR et de charges Si, l'ajout d'ions est nécessaire pour créer une interaction entre les globules de NR et les particules de Si. Cette interaction permet de bien répartir la charge mais n'entraîne aucune déformation structurelle. Pour cela, l'application d'une contrainte physique est encore nécessaire, cette fois ci, pour atteindre un état de coalescence des globules de NR. Pour cette dispersion, nous avons aussi démontré que la présence de Si autour de la surface des particules NR a un effet sur la disposition spatiale des protéines et des lipides de NR dans le composite NR-Si. Nous avons mis en évidence un comportement de clustering marqué des protéines et des lipides de NR. Pour compléter l'étude, nous avons également étudié la distribution de charge de Si dans la matrice finale de NR. Ces particules se trouvent répartis de manière homogène dans le composite et régulièrement disposés en structure de type anneau-ellipse, liée à leur interaction en phase liquide avec les globules. En conclusion, c'est la première fois que la caractérisation structurelle de ces systèmes est faite à l'échelle nanométrique, permettant d'indiquer des paramètres importants pour la production de matériaux composites par mélange liquide. Enfin, nous pensons que la compréhension micro / nanoscopiques des mécanismes survenant au cours du processus de mélange des liquides pourrait ouvrir de nouvelles voies pour l'amélioration et l'exploitation de cette technologie.

Titre : Coagulation d'un latex de caoutchouc naturel - noir de carbone / silice : suivi de l'évolution nanostructurale d'une suspension colloïdale à un composite d'élastomère

Mots clés : caoutchouc naturel, noir de carbone, silice, coagulation, mélange liquide

Résumé : Le latex de caoutchouc naturel (NR) extrait d'*Hevea brasiliensis* est connu pour être utilisé pour la préparation d'une variété de matériaux. L'ajout de charges renforçantes est une méthode bien établie pour augmenter les propriétés mécaniques de la matrice polymère et il est nécessaire pour obtenir la résistance requise par la plupart des applications. Plusieurs stratégies ont été proposées pour mélanger le caoutchouc avec des charges. Parmi les différentes méthodes, le procédé de mélange liquide semble intéressant et il est central dans le cadre de technologie d'innovation Michelin. Dans ce procédé, le latex NR est mélangé à une suspension aqueuse de charges (silice / noir de carbone) donnant lieu à un hétéro-coagulum, qui est ensuite soumis à un séchage. Si ce processus se développe rapidement au niveau de l'ingénierie, la connaissance structurale de l'hétéro-coagulum le long du processus ainsi que les

mécanismes de régulation de l'agrégation ne sont encore bien connus. Dans ce but, nous avons utilisé une approche de microscopie multimodale comprenant: la microscopie électronique à balayage à émission de champ (FESEM) (avec à la fois l'imagerie électronique à rétrodiffusion et des électrons secondaires), la microscopie à super résolution optique (d-STROM) et la microscopie à force atomique couplée à la spectroscopie infrarouge (AFM) -IR) pour étudier la nanostructure de l'hétéro-coagulum et son évolution vers un composite élastomère. Nous pensons que la compréhension micro / nanoscopiques des mécanismes survenant au cours du processus de mélange des liquides pourrait ouvrir de nouvelles voies pour l'amélioration et d'exploitation de cette technologie.

Title : Natural rubber latex- carbon black/silica coagulation: following the nanostructure evolution from a colloidal suspension to an elastomeric composite

Keywords : natural rubber, carbon black, silica, coagulation, liquid phase mixing

Abstract : Natural rubber (NR) latex extracted from *Hevea brasiliensis* is known to be used for the preparation of a variety of materials. Addition of reinforcing fillers is a well-established method to increase mechanical properties of the polymer matrix and it is necessary to achieve the required strength for most applications. Several strategies have been proposed to mix rubber with fillers. Among the different methods, the liquid mixing process seems interesting and it is central for Michelin innovation technology. In this process, NR latex is mixed with an aqueous suspension of fillers (silica/ carbon black) giving rise to a hetero-coagulum, which is further subjected to dehydration and drying. If this process is quickly developing at engineering level, the structural knowledge of the hetero-coagulum

along the process as well as the mechanisms regulating aggregation is still at its infancy. To this aim, we employed a multimodal microscopy approach comprising: Field Emission Scanning Electron Microscopy (FESEM) (with both backscattering electron imaging and secondary electron), optical super resolution microscopy (d-STROM) and atomic force microscopy coupled with infrared spectroscopy (AFM-IR) to investigate on the nanostructure of the hetero-coagulum and its evolution towards an elastomeric composite. We believe that understanding micro/nanoscale mechanisms occurring during the liquid mixing process might open up new ways of improvement and exploitation of this technology.